Maturation of the *Salmonella* containing vacuole is compromised in G1 arrested host cells

---

Die Reifung der *Salmonella*-enthaltenden Vakuole ist kompromittiert in G1-arretierten Wirtszellen

Doctoral thesis for a doctoral degree at the Graduate School of Life Sciences,

Julius-Maximilians-Universität Würzburg,

Section Infection and Immunity

submitted by

Clivia Lisowski

from

Berlin

Würzburg, 2019

Submitted on:……..

(office stamp)

Members of the Promotionskomitee:

Chairperson:

Primary Supervisor: Dr. Ana Eulalio

Second Supervisor: Dr. Daniel Lopez

Third Supervisor: Prof. Dr. Jörg Wischhusen

Date of Public Defense:

Date of Receipt of Certificates:

Summary

The interaction of bacterial pathogens and the human host is a complex process that has shaped both organisms on a molecular, cellular and population level. When pathogenic bacteria infect the human body, a battle ensues between the host immune system and the pathogen. In order to escape an immune response and to colonize the host, pathogenic bacteria have developed diverse virulence strategies and some pathogens even replicate within host cells. For survival and propagation within the dynamic environment of a host cell, these bacteria interfere with the regulation of host pathways, such as the cell cycle, for their own benefit.

The intracellular pathogen *Salmonella* Typhimurium invades eukaryotic cells and resides and replicates in a modified vacuolar compartment in which it is protected from the innate immune response. To this end, it employs a set of virulence factors that help to invade cells (SPI-1 effectors) and to hijack and modify the host endolysosomal system, in order to stabilize and mature its vacuolar niche (SPI-2 effectors). Previous studies have shown that *Salmonella* arrests host cells in G2/M phase and that *Salmonella* infected cells progress faster from G1 into S phase, suggesting that the G1 phase is disadvantageous for *Salmonella* infection. In fact, it has already been observed that *Salmonella* replication is impaired in G1 arrested cells. However, the reason for this impairment remained unclear.

The current study addressed this question for the first time and revealed that the highly adapted, intracellular lifestyle of *Salmonella* is drastically altered upon G1 arrest of the host cell. It is shown that proteasomal degradation in G1 arrested cells is delayed and endolysosomal and autophagosomal trafficking is compromised. Accordingly, processing of lysosomal proteins is insufficient and lysosomal activity is decreased; resulting in uneven distribution and accumulation of endolysosomes and autophagosomes, containing undegraded cargo. The deregulation of these cellular signaling pathways affects maturation of the *Salmonella* containing vacuole (SCV). For the first time it is shown that acidification of SCVs is impaired upon G1 arrest. Thus, an important environmental factor for the switch from SPI-1 to SPI-2 gene expression is

missing and the SPI-2 system is not activated. Consequently, targeting and modification of host cell structures by SPI-2 effectors e.g. recruitment of endolysosomal membrane proteins, like LAMP1, or exchange of endosomal cargo, is compromised.

In addition, degradation of *Salmonella* SPI-1 effectors by the host proteasome is delayed. Their prolonged presence sustained the recruitment of early endosomes and contributed to the SCV remaining in an early, vulnerable maturation stage. Finally, it was shown that SCV membrane integrity is compromised; the early SCV ruptures and bacteria are released into the cytoplasm. Depending on the host cell type, SPI-2 independent, cytoplasmic replication is promoted. This might favor bacterial spreading, dissemination into the tissue and provide an advantage in host colonization.

Overall, the present study establishes a link between host cell cycle regulation and the outcome of *Salmonella* infection. It fills the gap of knowledge as to why the host cell cycle stage is of critical importance for *Salmonella* infection and sheds light on a key aspect of host-pathogen interaction.

Zusammenfassung

Die Interaktion zwischen bakteriellen Krankheitserregern und dem menschlichen Wirt ist ein komplexer Prozess, der beide Organismen auf molekularer, zellulärer und Populationsebene geprägt hat. Wenn pathogene Bakterien den menschlichen Körper infizieren, kommt es zu einem Kampf zwischen dem Immunsystem des Wirtes und dem Krankheitserregers. Um einer Immunantwort zu entgehen und den Wirt zu besiedeln, haben pathogene Bakterien diverse Strategien entwickelt und einige Erreger vermehren sich sogar innerhalb von Wirtszellen. Zum Überleben und zur Vermehrung innerhalb der dynamischen Umgebung einer Wirtszelle, manipulieren diese Bakterien die Regulation zellulärer Netzwerke, wie zum Beispiel den Zellzyklus, zu ihrem eigenen Vorteil.

Salmonella Typhimurium, ein intrazelluläres Bakterium, dringt in eukaryotische Wirtszellen ein und vermehrt sich in einem modifizierten, vakuolären Kompartiment, welches gleichzeitig vor der angeboren Immunantwort des Wirtes schützt. Zu diesem Zweck entwickelten Salmonellen eine Reihe von Virulenzfaktoren. Diese sind zum einen für die Invasion von Zellen verantwortlich (SPI-1 Faktoren), zum anderen greifen sie das endolysosomale System der Wirtszelle an und modifizieren es, mit dem Ziel die intrazelluläre Salmonellen-enthaltende Vakuole (SCV) zu stabilisieren und reifen zu lassen (SPI-2 Faktoren). Frühere Studien haben gezeigt, dass Salmonellen ihre Wirtszellen in der G2/M Phase blockieren. Zudem gehen Salmonellen-infizierte Zellen schneller von der G1 in die S-Phase über, was auf einen Nachteil der G1-Phase für die Salmonelleninfektion hindeutet. In der Tat wurde bereits beobachtet, dass die Vermehrung von Salmonellen in G1-arretierten Zellen beeinträchtigt war. Der Grund für diese Beeinträchtigung blieb jedoch unklar.

Die vorliegende Studie befasst sich zum ersten Mal mit dieser Frage und zeigt auf, dass der hoch angepasste, intrazelluläre Lebensstil von Salmonellen während des G1-Arrest der Wirtszelle dramatisch verändert wird. Im Rahmen der hier vorgelegten Arbeit wurde gezeigt, dass der proteasomale Abbau in G1-arretierten Zellen verzögert und die endolysosomalen und autophagosomalen Transportnetzwerke beeinträchtigt sind.

Dementsprechend ist die Prozessierung lysosomaler Proteine unzulänglich und die lysosomale Aktivität herabgesetzt; was zu einer ungleichmäßigen Verteilung und Anreicherung von Endolysosomen und Autophagosomen führt, die nicht abgebaute Stoffwechselprodukte akkumulieren. Die Deregulierung der genannten zellulären Signalwege beeinflusst die Reifung der SCV. Es konnte hier zum ersten Mal gezeigt werden, dass die Ansäuerung der SCV in G1-arretierten Zellen inhibiert ist. Somit fehlt ein essentieller Faktor für den Wechsel von SPI-1 zu SPI-2-Genexpression und das SPI-2 System wird nicht aktiviert. Folglich findet keine Modifikation der Wirtszelle durch SPI-2-Effektoren, z.B. die Rekrutierung endolysosomaler Membranproteine, wie LAMP1 oder der Austausch endosomaler Fracht statt.

Zudem ist der Abbau von bakteriellen SPI-1-Effektoren durch das Wirtsproteasom verzögert. Die verlängerte Präsenz der SPI-1 Effektoren fördert eine anhaltende Rekrutierung von frühen Endosomen und trägt zum Verbleib der SCV in einem frühen, sehr instabilen Reifestadium bei. Schließlich wurde gezeigt, dass die Integrität der SCV Membran kompromittiert ist, die Vakuole aufbricht und die Bakterien ins Zytoplasma entlassen werden. In Abhängigkeit des Wirtszelltyps wird eine SPI-2 unabhängige, zytoplasmatische Vermehrung begünstigt, was möglicherweise die Ausbreitung der Bakterien ins Gewebe erleichtert und somit einen Vorteil bei der Besiedelung des Wirtes darstellt.

Insgesamt etabliert die vorliegende Studie einen Zusammenhang zwischen der Regulation des Wirtszellzyklus und dem Ergebnis einer Salmonelleninfektion. Es wird aufgezeigt, warum der Zellzyklus der Wirtszelle von entscheidender Bedeutung für den Verlauf der Salmonelleninfektion ist und beleuchtet somit einen essentiellen Aspekt der Wirt-Pathogen-Interaktion.

Acknowledgements

I would like to thank my primary supervisor Dr. Ana Eulalio for her supervision and her support throughout the years. Thank you for giving me the opportunity to work on this project, which initially started as a "back-up", but turned out to be fruitful and exciting. I am truly grateful for the time I spend in your lab as part of my journey of becoming a scientist; it let me grow professionally and personally and I really appreciate that.

I would like to thank my committee members Dr. Daniel Lopez and Prof. Jörg Wischhusen. Thank you for taking the time, your advice and your encouraging and cheerful words; sometimes that is all you need.

I would like to thank all the past and present members of the Eulalio lab. Thank you Claire for teaching me what being a scientist means to you in my first year of PhD. Carmen, thanks a lot for your help and advice and for just being a great postdoc. Usha, my fellow PhD-sister, we shared many moments of joy and frustration and I am immensely thankful to have had you as a companion on this journey. Caroline, thank you for reading the first draft of the thesis and for all the scientific and non-scientific discussions we had. The endless nights we spend together in the lab grew into an amazing friendship that will last beyond science.

I would like to thank all members of the Siegel and Vogel labs that made the time so memorable. Amelie, Carolin, Charlotte, Emmanuel, Falk, Gianluca, Jens, Laura, Malvika, Raul, Yanji, Youseff - you rock!!! Thank you to all technicians whose work is so essential, but always underestimated. Everyone at the IMIB - I learned from all of you and I feel lucky that you have shared your kindness and knowledge with me. A very special thank you to Hilde for the technical and moral support, for having an open ear and for making countless "small things" possible.

A heartfelt and infinite thank you to Philipp. Thank you for being there, for reminding me that there is a life outside the lab and for all the invaluable "Mattes MacGyver" skills that keep impressing me. Thank you so much for your patience throughout the years and your support, especially in the last phase of my PhD. It was my decision to go on that journey, but we went through all the ups and downs together and you deserve this as much as I do!

Last but not least, I would like to thank my mum and dad. Without your unconditional love and support, without your advice and your faith in me when I stopped believing, this would not have been possible. I am infinitely grateful to have you. You are my heroes and my anchor. I dedicate this work to you.

Abbreviations

% (v/v)	% (volume/volume)
% (w/v)	% (weight/volume)
°C	degree Celsius
AMP	ampicillin
BSA	bovine serum albumin
cDNA	complementary DNA
Cm	chloramphenicol
Da	Dalton
DMSO	dimethylsulfoxide
DNA	deoxyribonucleic acid
dNTP	deoxyribonucleotide
DTT	dithiothreitol
EDTA	ethylene diamine tetraacetic acid
EGTA	ethylene glycol tetraacetic acid
Fig	figure
GFP	green fluorescent protein
CDK	cyclin dependent kinase
PI(3)P	phosphatidylinositol 3-phosphate
CFU	colony forming unit

Figures and tables

Index

1 Introduction

1.1 The mammalian cell cycle

1.1.1 The different cell cycle phases

The mammalian cell cycle is divided into two main phases, interphase and mitosis. Mitosis describes the coordinated sequence of events by which a cell divides into two daughter cells. The phase between two cell divisions is called interphase and is again separated into 3 phases. First stage after mitosis is called gap or growth phase 1 (G1) followed by DNA synthesis (S) and a second gap or growth phase (G2). During G1 phase, cells are metabolically very active and break down a high number of macromolecules to gain energy for growth and the re-building of components like cytoplasm and organelles that are still missing after cell division. In S-phase, several enzymes and other proteins required for the upcoming DNA synthesis are produced, the DNA content is doubled (2n → 4n) and erroneous DNA is repaired. In G2 phase, cells prepare for the upcoming mitosis. Enzymes, produced in G1 are further processed and modified and cell-cell contacts are loosened, while the cells swell due to increased uptake of liquids (1). In addition, there is another phase called G_0. It is usually defined as a special variant or sub-phase of G1 or also as a temporary exit of the cell cycle. G_0 is a reversible silent or "quiescent" phase in which cells do not divide or grow. It is the characteristic state for some cell types like nerve, liver or hematopoietic cells that proliferate very slowly or stop proliferation once they are fully differentiated. Other, usually fast proliferating cells, e.g. gastrointestinal epithelial cells, might enter G_0 due to a lack of mitogens or growth factors. Once conditions have improved, they re-enter the cell cycle (2) (3) [Fig. 1].

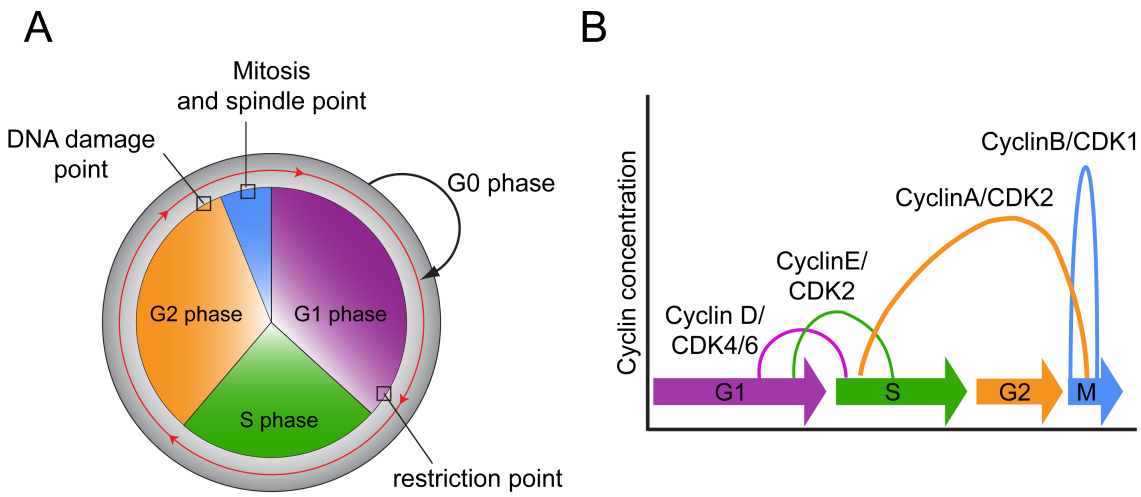

Fig. 1 Cell cycle regulation of mammalian cells

(A) The mammalian cell cycle is divided into four phases in which cells grow (G1 and G2), synthesize DNA (S) or divide (mitosis). Before entering the next phase, availability of nutrients, DNA integrity and proper processing of proteins is controlled at defined cell cycle checkpoints. G_0 is a resting or "quiescent" state that is entered once cells finished differentiation; do not proliferate further or in case of limited nutrient availability. (B) Transition from one phase of the cell cycle to the other is regulated by the coordinated activation and deactivation of CDK/cyclin complexes that are characteristic for each cell cycle phase.

1.1.2 Regulation of the cell cycle and G1-S transition

Transition through the cell cycle is tightly regulated by Cyclin-dependent-kinases (CDK), a family of serine/threonine protein kinases that are activated in an oscillatory manner. CDK protein levels remain stable during the cell cycle but their periodic activation depends on cyclins. Cyclins are the regulatory subunits of CDKs and throughout the cell cycle their levels rise and fall. Progression through the different cell cycle phases requires different cyclins and CDKs. Entry of quiescent cells into the cell cycle and transit through early G1 is regulated by D-type cyclins which bind to CDK4 and to CDK6. In contrast to other cyclins, Cyclin D is not expressed periodically but is continuously synthesized as long as growth factors are available. To promote progression from G1 into S, another (late) G1 cyclin, Cyclin E associates with CDK2. S-phase transit and early G2 are regulated by Cyclin A/CDK2 and Cyclin A/CDK1 complexes. Once Cyclin B binds to CDK1, progression into mitosis is promoted. Activity of CDKs is balanced by members of two families of CDK inhibitors (CKI). Members of the first family (INK4 family) specifically bind G1 CDKs (CDK4/CDK6) and thus block binding by Cyclin D. Members of

the second family (Cip/Kip family) inactivate Cyclin/CDK complexes (3)(4). Furthermore, microRNAs were shown to be involved in cell cycle regulation (cf. section about miRNAs), e.g. the miR-15 family were shown to downregulate Cyclin D1 levels in cells and thus counteracts proliferation from G1 into S phase, as well (5) (6).

Throughout the whole cell cycle so called checkpoint controls ensure that one cell cycle phase has properly finished before cells enter the next phase. Major checkpoints are the G1 (or restriction) checkpoint, the G2 (or DNA damage) checkpoint during interphase and the metaphase (or spindle) checkpoint during mitosis. Depending on internal and external stimuli, cells at the restriction point decide whether to delay G1, to enter G_0 or to progress into S-phase (7). Two protein classes are important for this step: the Retinoblastoma (Rb) family and the E2F-transcritption factor family. E2F transcription factors activate expression of genes required for DNA replication and cell cycle progression. Binding of Rb to E2F converts it into a repressor of the same genes and stalls the cells in G1/G_0. Mitogens and extracellular stimuli trigger activation of receptors and integrins that in turn activate Ras/MAP/ERK kinases (8). This cascade eventually activates transcription of Cyclin D, which accumulates inside the cell. Cyclin D binds CDK4/6 and initiates CDK activity, which leads to phosphorylation of Rb and releases it from E2F. Transcription of E2F target genes subsequently activate Cyclin E/CDK2 and Cyclin A/CDK2 complexes, and amplify activity of Cyclin D/CDK4/6. Formation of Cyclin E/CDK2 complexes is a signal for the cell to enter S-phase and marks a “point-of-no-return” from which the cells will continue to proliferate (3) (4) (9) [Fig. 1][Fig. 2]. After completion of S-phase, cells move on through G2 and prepare for mitosis. Before mitosis the cells have to pass a second important checkpoint, also called the ´DNA damage´ checkpoint. Here, the integrity of DNA is ensured and cells can only enter mitosis when all DNA damage has been repaired. Lastly, at the ‘spindle checkpoint’ during mitosis correct alignment and binding of chromosomes to the spindle apparatus and thus equal separation of DNA to both daughter cells is ensured (3) (4).

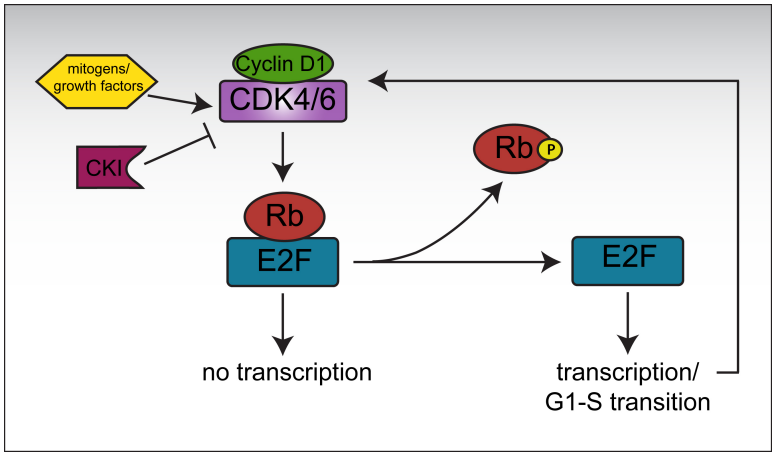

Fig. 2 Regulation of G1-S phase transition

Transcription of genes necessary for G1-S transition is under control of E2F transcription factors. E2F is repressed by Retinoblastoma protein (Rb). If sufficient growth factors or mitogenic signals are available, the cells synthesize Cyclin D1, which forms complexes with Cyclin dependent kinases 4 and 6. These complexes phosphorylate Rb and thereby release E2F. E2F activity leads to activation of further Cyclin/CDK complexes, amplification of Cyclin D1/CDK4/6 activity and subsequent transition into S phase. Endogenous inhibitors of CDKs (CKI) counteract formation of Cyclin/CDK complexes to balance CDK activity or stall cells in G1/G_0 phase.

1.1.3 Chemical inhibitors of cell cycle progression

Altered regulation and control of the cell cycle might cause unrestrained proliferation and accumulation of erroneous DNA. These dysfunctional cancer cells characteristically fail to undergo programmed cell death and will accumulate to form large tumors. Components of the CDK4/6–Cyclin D-RB pathway are commonly mutated in human cancers and CDK4 and CDK 6 are regular targets in cancer therapy (10) (11). CDK4/6 inhibitors mostly act downstream of mitogenic signaling cascades and eventually arrest cancer cells in G1/G_0 (3) (12). For research purposes several CDK4/6 inhibitors are available. In this study, a cell-permeable triaminopyrimidine compound that acts as a reversible and ATP-competitive inhibitor against Cyclin D1-complexed CDK4/6 was used (13) (14).

1.2 Endolysosomal trafficking and autophagy

The term endocytosis describes the internalization of fluids, solutes, macromolecules, plasma membrane components and particles by invagination of the plasma membrane and formation of vesicles or vacuoles, generally called endosomes. Eukaryotic cells ingest nutrients, receptor–ligand complexes, lipids, proteins and also bacteria or viruses. They sort, process, recycle, store, activate or silence and degrade their cargo. Therefore, endosomes play important roles for numerous pathways in the cell. The internalized vesicles undergo homotypic fusion with early or sorting endosomes, which usually have a tubular structure. A high proportion of cargo and membrane is recycled back to the plasma membrane via recycling endosomes ("recycling pathway"). Within one hour a mammalian cell can cycle the equivalent of 50–180% of the surface area of its plasma membrane in and out of the cell (15). Other cargo is sent to the trans-Golgi network (TGN) or traffics via late endosomes (also called multivesicular bodies, MVB) to lysosomes for degradation ("degradative pathway") (16).

1.2.1 Endosome maturation

Each endosomal compartment is characterized by a defined composition of membrane components e.g. various phospholipids and glycoproteins, its intracellular location, morphology and intraluminal pH. The gradual change of these characteristics is called endosomal maturation and is regulated by several factors that mutually influence each other. Maturation usually starts by fusion of incoming vesicles with early endosomes. If not sorted into recycling endosomes, they traffic along the degradative pathway. For this, early endosomes convert to late endosomes and move towards the perinuclear region. They undergo several heterotypic fusion events and often form so called multivesicular bodies containing intraluminal vesicles (ILV). Late endosomes or MVBs direct the incoming cargo to the TGN or to lysosomes and also mediate trafficking between both compartments. The resulting heterogeneous hybrid organelles, which carry endosomal cargo mixed with lysosomal hydrolases and membrane components, are also called endolysosomes. Further maturation leads to conversion of endolysosomes to smaller, compact and dense lysosomes (15) [Fig. 3][Fig. 5].

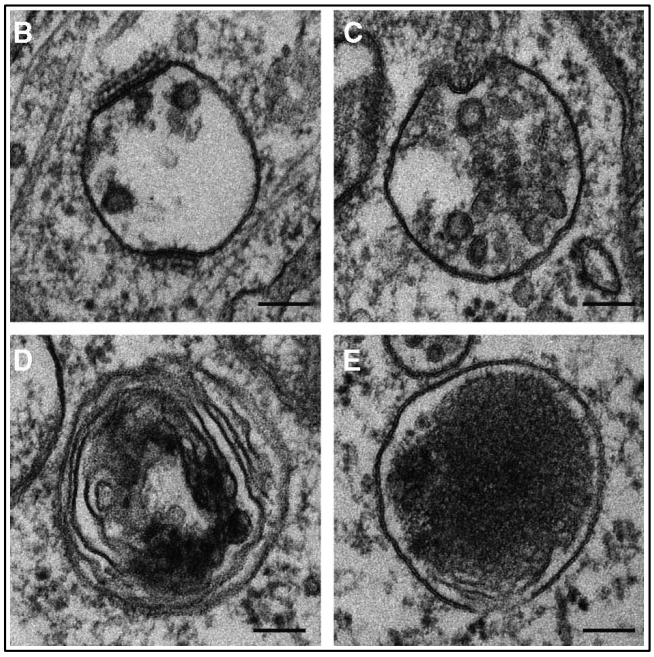

Fig. 3 Electron micrographs of endolysosomes at various stages (image taken from (15))
(B) Early endosomes with very little intraluminal vesicles (C) Late endosomes containing numerous ILVs; (D) endolysosome, with partial electron dense areas (E) Lysosomes with electron dense lumen. Images are all from HeLa cells that had been processed for thin section EM. Scale bars = 100 nm.

Early endosomes (EE) have a complex structure of tubules and vacuoles. They are mildly acidic (pH 6.5); have a low Ca^{2+} concentration and their membranes are rich in cholesterol and PI(3)P. The small GTPase Rab5 is a key membrane protein and its presence is used to define the early endosome as an early endosome. Interaction of Rab5 with two effector proteins, Vps34 and EEA1, is crucial for endosome maturation (15) (17). Vps34 (vacuolar sorting protein 34) is a phosphatidylinositol 3-kinase and converts PI to PI(3)P. Recruitment of Vps34 to the early endosome membrane results in increasing concentrations of the PI(3)P, which in turn recruits more Rab5 (18). EEA1 (early endosomal antigen-1) binds PI(3)P and has two binding sites for Rab5 and is therefore thought to bridge two Rab5 positive membranes in order to mediate fusion between early endosomes (19) [Fig. 4]. Increasing concentration of PI(3)P above a certain threshold eventually leads to recruitment of another protein complex (SAND/Mon1) that interrupts the positive feedback loop of Rab5 activation. In parallel, it recruits another GTPase, Rab7 onto the membrane and mediates conversion of an early to a late endosome (LE) (20).

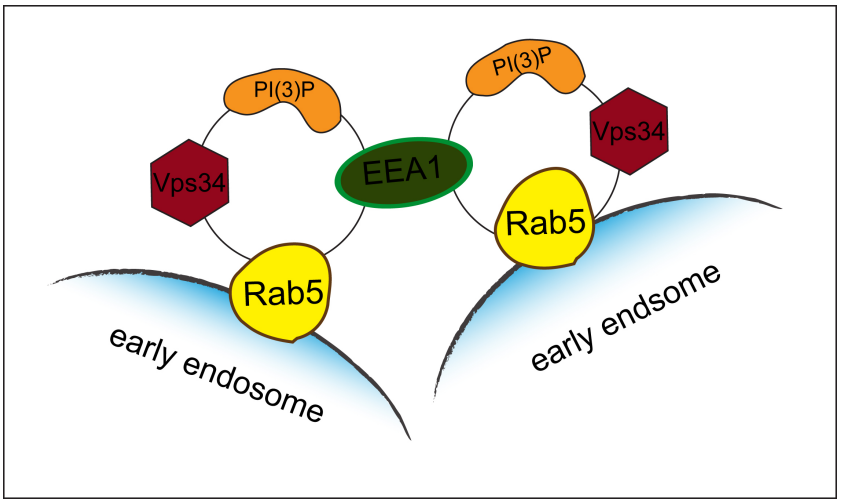

Fig. 4 Homotypic fusion between early endosomes
Fusion between early endosomes is mediated by Rab5, EEA1, and Vps34. EEA1 has two binding sites for Rab5 and bridges over to other early endosomes. Vps34 is a PI3K and converts PI to PI(3)P. Increasing concentration of PI(3)P recruits more Rab5 in turn.

The switch from Rab5 to Rab7 also induces changes in the composition of associated binding partners and their recruited effectors. In turn, this changes organization of membrane lipids and proteins, intraluminal pH and morphology. Most prominently, late endosomes are more round than tubular, their pH drops from 6.5 to 5 and PI(3)P is converted to $PI(3,5)P_2$. During maturation, they take up vesicles from different origins and continuous fission and fusion events ("kiss-and-run-model") with other early/late endosomes or lysosomes lead to formation of MVBs. At this stage, intraluminal cargo and membrane components still have a high turnover rate and sorting into different pathways occurs. With ongoing maturation, LEs contain only cargo that needs to be degraded or components necessary for functionality of lysosomes (e.g. still inactive lysosomal hydrolases or the membrane glycoprotein LAMP1) (15).

Important mediators of fusion between all kinds of intracellular vesicles are soluble N-ethylmaleimide-sensitive factor attachment protein receptors (SNAREs). SNAREs are protein complexes that reside on intracellular membranes. Once vesicles are brought in close proximity by tethering factors (like Rab-GTPases and their effector proteins), SNAREs of both compartments pair and form so-called SNAREpin complexes. Within these complexes they mediate the actual mixing of membrane bilayers and thus fusion of vesicles. Pairing of two SNAREs is less specific than previously thought and cannot be

used to explain fusion of particular vesicles. Most likely vesicle fusion is mediated by organelle specific tethering factors that enable membrane contact, while SNAREs can functionally replace each other (21).

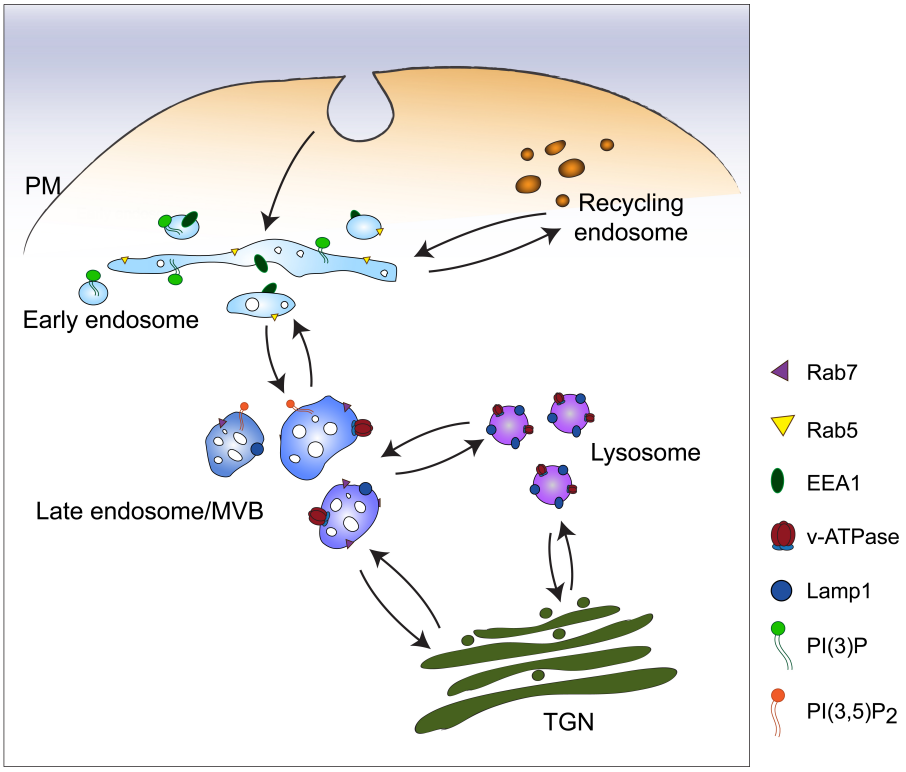

Fig. 5 Endosome maturation

Endocytic cargo is internalized by inward budding of the plasma membrane. The newly formed early endosomes usually form tubular structures that are positive for the small GTPase Rab5, its effector protein EEA1 and PI(3)P. Accumulation of PI(3)P recruits other protein complexes that induce exchange of Rab5 with Rab7 and conversion of PI(3)P to $PI(3,5)P_2$. At that stage, the endosome has accumulated several intraluminal vesicles and hence is also referred to as multivesicular body (MVB). Eventually, fusion with lysosomes leads to degradation of endocytic cargo. Maturation of endosomes is accompanied by gradual acidification from pH 6.5 in early endosomes to pH 4.6-5.0 in lysosomes due to the proton pumping activity of the v-ATPase. PM = plasma membrane, TGN = trans-Golgi-network

1.2.2 Autophagy

In contrast to endocytosis where cells take up and digest extracellular material, autophagy describes a process in which cells deliver cytoplasmic components to lysosomes for degradation (22). Autophagy serves to provide nutrients and to selectively discard unwanted, potentially harmful cytosolic material, such as damaged mitochondria or protein aggregates. This occurs in response to different forms of

stress, including nutrient deprivation, growth factor depletion, infection or hypoxia (23). Upon these stressors, formation of a cup-like structure, called phagophore, around the cytoplasmic substrates is initiated. The phagophore expands around its substrates and once completely closed, it is called autophagosome. Autophagosomes subsequently fuse with lysosomes to form autolysosomes in which their cargo is degraded [Fig. 6]. After breakdown of cargo, the resulting macromolecules as well as membrane components are released back into the cytosol and can be re-used for autophagosome formation. This dynamic cycling of autophagy specific proteins is called autophagy turnover or autophagy flux (24). Several proteins are involved in formation and function of the autophagocytic machinery. The microtubule-associated protein 1A/1B light chain 3B (LC-3B) is a soluble protein in the cytoplasm of mammalian cells. During phagophore formation the cytosolic form (LC-3B I) is conjugated to phosphatidylethanolamine on the phagophore membrane (LC-3B II) (25). After fusion with lysosomes, luminal content but also the autolysosomal membrane is degraded and LC-3B is released into the cytosol again. Therefore, LC-3B is used as a classic marker for autophagy but also for autophagosomal turnover (22).

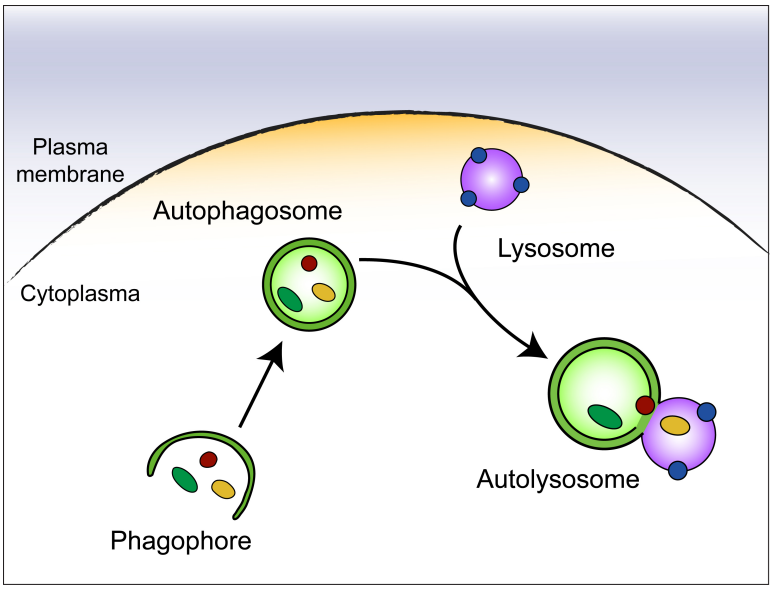

Fig. 6 Autophagy in mammalian cells

Autophagy is induced in response to different forms of stress e.g. nutrient deprivation, growth factor depletion, infection or hypoxia. Initiation starts with formation of a phagophore membrane that elongates around cytoplasmic content. After closure of the membrane, the newly formed autophagosome fuses with lysosomes to form autolysosomes. Eventually, degradation products and membrane components are released into the cytoplasm again.

1.2.3 Lysosomes

Lysosomes are membrane bound organelles that contain electron dense deposits and intraluminal membrane spirals or whorls. They differ in shape, size and number and mammalian cells might contain up to 100 lysosomes, constituting ca. 5% of the intracellular volume (26) (27). They differ from endosomes by the absence of the mannose-6-phosphate-receptor and their intraluminal pH, i.e. 4.6-5.0 (27). Lysosomes were merely considered to be the degradative "trash" factory of the cell for a long time. However, in recent years it has become clear that lysosomes are also important regulators of cellular energy metabolism (28). Beside their degradative function they mediate nutrient sensing, metabolic adaptation, and quality control of proteins and organelles (26) (29).

Lysosomes are composed of single phospholipid bilayers harboring transmembrane proteins like LAMP1 or LAMP2 (both decorating 80% of the lysosomal membrane). Lysosomal membrane proteins are heavily glycosylated on their luminal side and form the glycocalyx, protecting them from autodigestion by the 50-60 different hydrolases (lipases, proteases and glycosidases for catabolic degradation) (29) . Other important membrane proteins are various ion channels that balance ion homeostasis and maintain ionic gradients across the membrane and the membrane potential ($\Delta\Psi$) (26) . The v-ATPase, a proton pump, establishes and maintains an intraluminal pH of 4.6-5.0, which is the optimal range for hydrolytic activity (29).

Lysosomes receive cargo from endosomes, phagosomes (distinct form of endosomes after uptake of solid particles incl. pathogens) and autophagosomes. The end products of lysosomal digestion are either transported to the cytoplasm, where they are used in biosynthetic reactions, or are secreted over the plasma membrane to dispose of toxic compounds. Lysosomes also serve as intermediate storage sites and exchange macromolecules with the cytoplasm in response to cellular needs. Therefore, lysosomes act as nutrient sensors and depending on intraluminal accumulation of e.g. amino acids, their degradative activity is enhanced or reduced (26). The nutrient-sensing machinery comprises several protein complexes located in close proximity or on the lysosomal membrane, including the master regulator of growth complex 1,

mTORC1 (30). In case of nutrient starvation, mTORC1 inhibits cellular growth and activates the transcription factor EB (TFEB). TFEB then translocates from the cytoplasm to the nucleus and activates transcription of genes required for lysosomal degradation, resulting in (i) increased lysosomal function (acidification and delivery of hydrolases) and (ii) increased autophagosome formation (31) [Fig. 7].

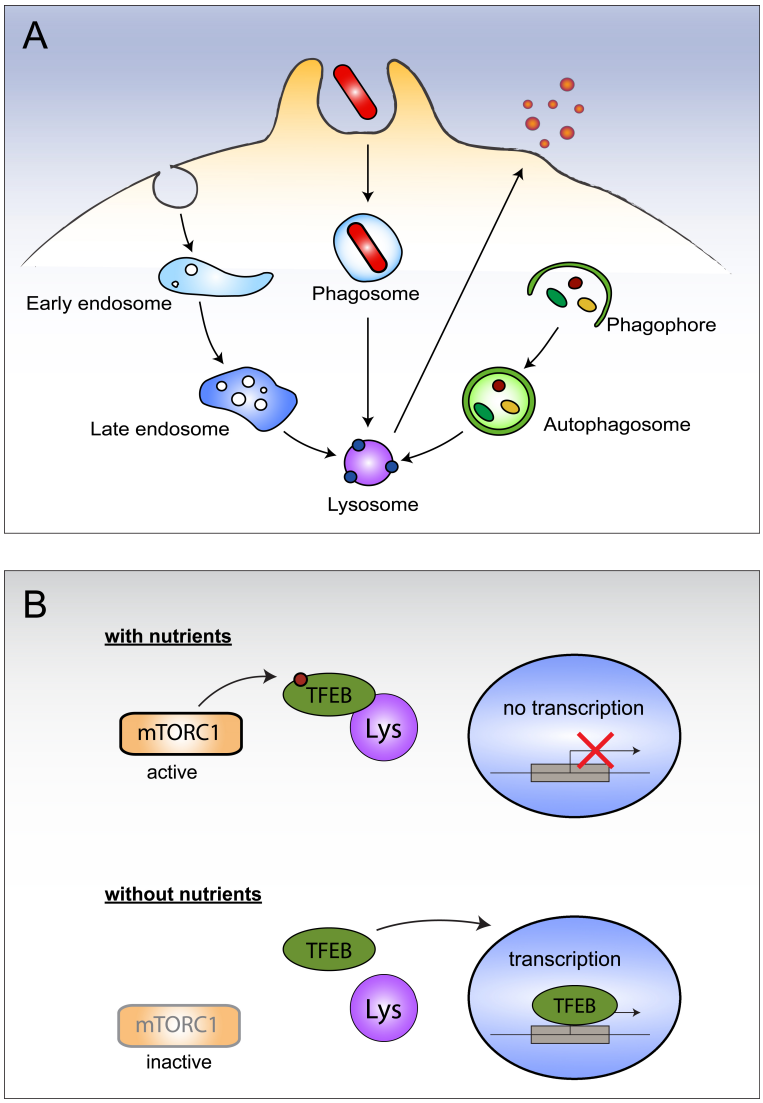

Fig. 7 Lysosomal trafficking and transcriptional activation via TFEB

(A) Lysosomes accept and process cargo via different intracellular trafficking pathways. Cells endocytose extracellular material, phagocytose pathogens or enclose intracellular material that might be toxic for cells or whose degradation is needed to yield macromolecules. (B) Under nutrient rich conditions, the master regulator of growth complex 1 (mTORC1) phosphorylates the transcription factor EB (TFEB), thereby inactivating it. Upon nutrient limitation or stress, TFEB is dephosphorylated and translocates from the cytoplasm into the nucleus. Here it activates transcription of genes responsible for lysosomal biogenesis and autophagosome formation.

Alterations in endocytic traffic, autophagy and lysosomal function result in metabolic dysfunction, cellular degeneration or impaired growth and are often caused by accumulation of lysosomal materials. Most of the "Lysosomal storage disorders (LSD)" are caused by mutations in lysosomal hydrolases, but can also occur if catabolite export or membrane trafficking is disturbed. Accumulation of undigested lipids slows down membrane traffic and sorting of hydrolases and in turn increase lysosomal disorders. Under physiological conditions, fusion of lysosomes with endo- or autophagosomes leads to formation of hybrid organelles (endolysosomes/ autolysosomes), which increase in size due to influx of water, hydrolases and the change in nutrient status. After digestion and export of materials, lysosomes shrink back to their original size. In LSDs, this reversion is often impaired and results in prolonged presence of these hybrid organelles that are filled with undigested materials. Eventually this will lead to complete arrest of endocytosis or autophagy (29) (32).

1.3 The proteasome

Eukaryotic cells need to breakdown macromolecules in order to yield energy for all cellular processes. Extracellular molecules are delivered to lysosomes via the endosomal pathway, whereas autophagosomes enclose cytoplasmic material and deliver it to lysosomes. Eventually, lysosomes degrade all kinds of bulk material, including proteins, lipids, carbohydrates and nucleic acids and thus were considered to be the only cellular system responsible for degradation and turnover. However, research on cells without lysosomes uncovered an additional protein-specific degradation pathway by which cells avoid accumulation of toxic proteins and re-gain protein components, the proteasome (33). The proteasome is a large protein complex with a regulatory and a proteolytic subunit and localizes to the nucleus as well as the cytoplasm of cells. It specifically cleaves peptide bonds and thus degrades only proteins. Proteasomal degradation was shown to be involved in the regulation of various cellular processes and several diseases are associated with malfunctioning of the proteasome (34). Proteasomal activity is an important growth factor of cells and contributes to proliferation and survival. Limited nutrient availability usually slows down proliferation, emphasizing the cross-talk between regulation of the cell cycle and

regulation of metabolic processes. If cells enter a quiescent state they go into a standby mode; just maintaining basic metabolic processes. For reasons not fully understood yet, cell cycle arrest or a quiescent cell state is accompanied by dissociation of proteolytic and regulatory subunits and formation of motile cytosolic clusters, called “proteasome storage granuli” (PSG) (35). PSGs are released, once cells re-enter the cell cycle. Nonetheless, quiescent cells have to avoid accumulation of toxic protein compounds and as a compensatory mechanism they increase lysosome biogenesis and autophagy (36). In contrast, cancer cells, which proliferate uncontrolled are found to have increased proteasomal activity, to yield energy and macromolecules for growth and proliferation (37) (38). For that reason, proteasomal inhibitors have been widely used as anti-cancer drugs in order to starve tumor cells and to slow down their proliferation (39). Yet, some slow proliferating tumors (as well as quiescent cells) were shown to be resistant against treatment with proteasomal inhibitors (40).

1.4 The intracellular pathogen *Salmonella* Typhimurium

Salmonella Typhimurium (*Salmonella enterica* ssp. *enterica* serovar Typhimurium, herein called *Salmonella*) is a motile, Gram-negative, intestinal pathogen. It belongs to the group of non-typhoidal *Salmonellae* and can infect a broad range of species, causing an acute self-limiting gastroenteritis associated with intestinal inflammation and diarrhea. *Salmonella*e are typically acquired by oral ingestion and can overcome the acidic pH of the stomach due to an adaptive acid-tolerance. In the small intestine, *Salmonella* crosses the intestinal mucous layer in order to escape first line innate immune defenses like digestive enzymes, bile salts or other antimicrobial peptides. Once they reach the underlying epithelium they enter by a trigger mechanism and induce an early local inflammatory response, which results in infiltration by polymorphonuclear leukocytes into the intestinal lumen and diarrhea (41) (42).

1.4.1 *Salmonella* entry into epithelial cells

Invasion of *Salmonella* into non-phagocytic cells is mediated by action of effectors of the type three secretion system-1, which is encoded on the *Salmonella* pathogenicity island 1 (T3SS-1 and SPI-1, respectively) (43). Upon translocation, the effectors induce actin cytoskeletal modifications and rearrangements in the host plasma membrane, leading to strong ruffling and entry of bacteria into a vacuolar compartment, the so-called *Salmonella*-containing-vacuole (SCV) (44) (45). Earlier studies claimed that entry of *Salmonella* occurs via macropinocytosis. Macropinosomes are heterogeneously sized vesicles that are positive for early endocytic markers like EEA1, Rab5 or PI(3)P, and that allow fluid-phase uptake into cells. More recent studies however, show that *Salmonella* is initially found in a distinct compartment in the vicinity of macropinosomes and propose a model in which the nascent SCV fuses with macropinosomes and early endosomes afterwards (46). It has been shown that *Salmonella* preferentially invades mitotic cells due to their high cholesterol content and also the SCV is characterized by high membrane cholesterol, which only gradually decreases during further maturation of the bacterial vacuole (47). Within the first hour, the early SCV is still unstable and easily damaged so that approx. 10-20% of bacteria are released from the vacuole.

Some of these bacteria replicate within in cytosol, while others are trapped by autophagy (48). Yet, the majority of *Salmonella* remains inside the vacuolar compartment and transiently fuses with early endosomes. This process is enhanced by SPI-1 effectors like SopE, which targets Rab5 and thus enforces fusion with early endosomes (49) (50). Other SPI-1 encoded effectors, like SptP, counteract the induced actin cytoskeleton or plasma membrane changes and thus help to re-establish cell morphology once *Salmonella* has invaded [Fig. 8]. The SPI-1 effector proteins are partially degraded by the host proteasome and *Salmonella* gene expression switches from SPI-1 to SPI-2 expression (51).

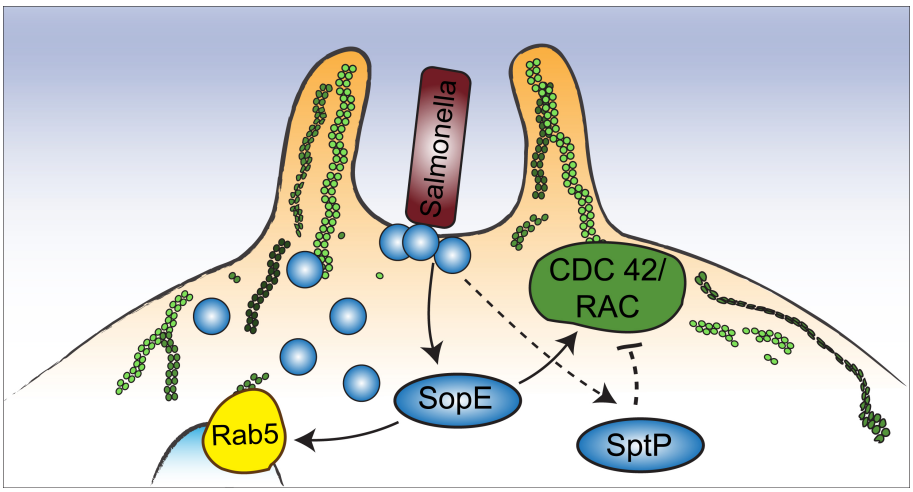

Fig. 8 Salmonella invasion of epithelial cells is mediated by SPI-1 encoded effectors.
Entry into host cells is mediated by the *Salmonella* pathogenicity island-1 (SPI-1) type III secretion system (T3SS) and its effectors. Adhesion of *Salmonella* and secretion of SPI-1 effectors induce rearrangement of the actin cytoskeleton and trigger formation of a cup-like structure. SopE enhances Cdc42 and Rac1 activity directly by acting as guanine-nucleotide-exchange factor. These cytoskeletal rearrangements are reverted by the GTPase-activating protein (GAP) activity of SptP, which inactivates Cdc42 and Rac once *Salmonella* is internalized. In addition, SopE targets Rab5 and thus enforces recruitment and fusion with early endosomes.

1.4.2 Intracellular lifestyle of *Salmonella*

Soon after invasion, the nascent SCV fuses with early endosomes and acquires markers like EEA1 or Rab5. These markers are quickly exchanged by late endosomal and lysosomal markers like Rab7 and Lamp1 (45) (52). This endosome-like maturation is accompanied by changes in membrane lipid composition and gradual acidification of the SCV, and results in fusion with lysosomes (53). However, digestive activity of these lysosomes is reduced due to alterations induced by *Salmonella* (54). Modifications of the SCV and its interaction with the host are mediated by a different set of bacterial effector proteins that target certain host structures (55). These effector proteins, mainly enzymes or enzyme adapters, are encoded on the pathogenicity island SPI-2 and reside on the SCV membrane or are released into the host cytoplasm. Secretion of SPI-2 effectors leads to coupling of the SCV to the host microtubule system and tethering to the Golgi, so that the SCV travels from the plasma membrane towards a perinuclear area. Other effectors induce formation of an actin meshwork around the SCV which improves its stability. Furthermore, host proteins involved in endolysosome maturation are either recruited onto or excluded from the SCV. Fusion of endolysosomes and the SCV provides *Salmonella* with membrane proteins and lipids or endosomal cargo (56). To increase the availability of nutrients, *Salmonella* induces the formation of so called *Salmonella*-induced-filaments (SIFs) or *Salmonella*-induced-tubules (SITs) that protrude throughout the whole cell (57). Like this, *Salmonella* protects itself inside a distinct compartment but simultaneously ensures that it has access to nutrients and membrane components [Fig. 9]. Moreover, it has been shown that *Salmonella* dampens the innate immune response of its host by inhibiting TNF-α induced NFκB signaling or IL-1β secretion (55).

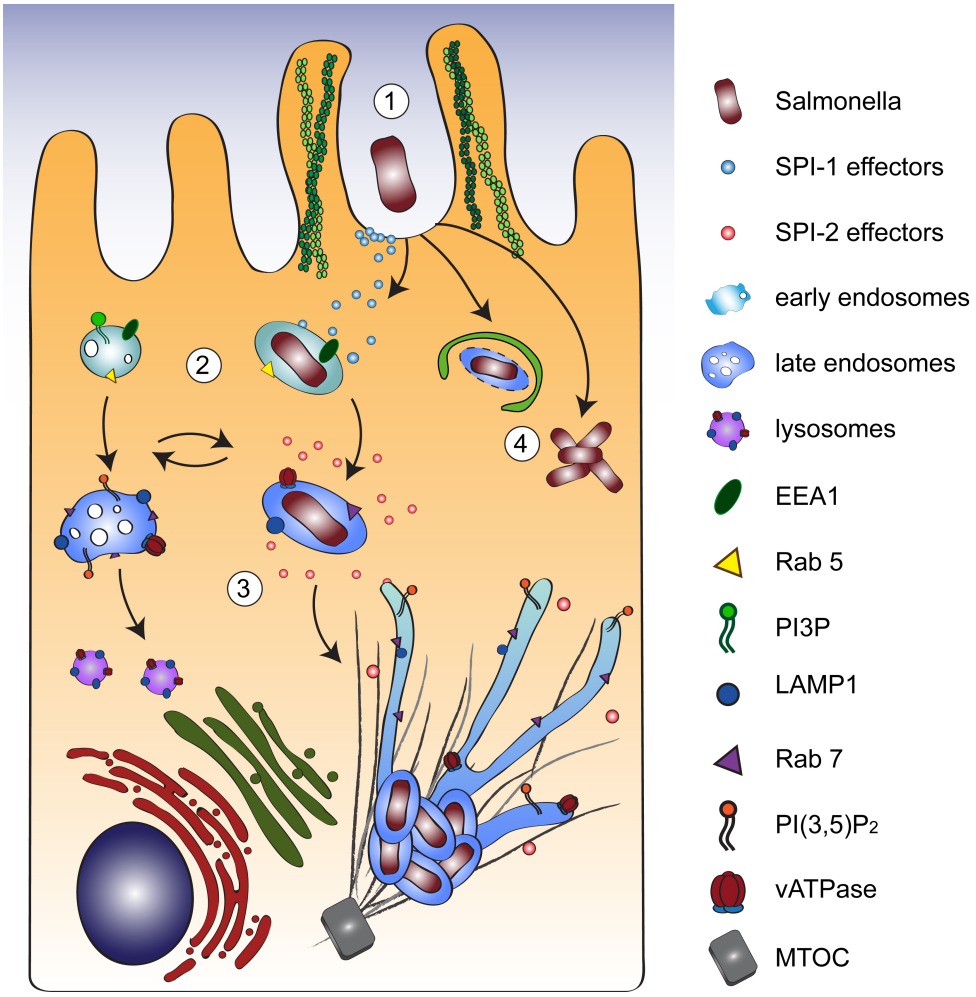

Fig. 9 *Salmonella* intracellular lifestyle

1. Salmonella adhesion and entry of epithelial cells is mediated by SPI-1 effector proteins that induce membrane ruffling and uptake into the nascent *Salmonella*-containing-vacuole (SCV). 2. The early SCV quickly fuses with early endosomes, a process enhanced by action of SPI-1 effectors. Subsequently, the SCV undergoes an endosome-like maturation process which is accompanied by shut down of the SPI-1 system and activation of the SPI-2 system. 3. SPI-2 effectors mediate stabilization of the vacuole, fusion with the endolysosomal system, protection from the innate immune system of the host and eventually allow intracellular replication of *Salmonella*. 4. Occasionally, the SCV is damaged and bacteria escape into the cytoplasm during the very early vulnerable period after invasion. Alternatively, the damaged SCV is recognized by the autophagy machinery and targeted for degradation. MTOC = microtubule organization center

1.4.3 Regulation of the SPI-2 system

Uptake of *Salmonella* from the extracellular space into an intracellular vacuolar compartment leads to nutrient limitation, low osmolarity, low Ca^{2+} or P_i concentrations and acidic pH (53) (58) (59). These sudden changes in environment are sensed by the two-component systems EnvZ/OmpR (60) (61) and SsrA/B (62) and eventually activate the SPI-2 system of *Salmonella*. The activated form of OmpR binds to the *ssrA/B* promoter and activates transcription of *ssrA* and *ssrB* genes. SsrA, the sensor kinase, senses the absence of $Ca^{2+,}$ acidic pH and low osmolarity inside the vacuole either directly or via another unknown sensor(s) (59). SsrA subsequently activates the response regulator SsrB, which in turn binds to the promotor regions for SPI-2 genes to induce their expression [Fig. 10].

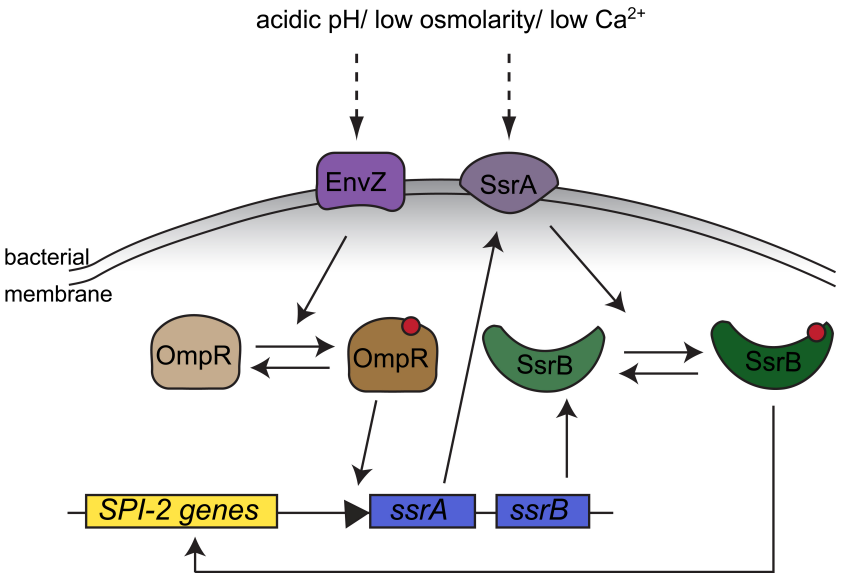

Fig. 10 Regulation of the SPI-2 T3SS of *Salmonella*
Inside SCVs *Salmonella* senses changes in the environment (decreasing osmolarity, pH and ion concentration) by the OmpR/EnvZ two component system. OmpR/EnvZ activate transcription of another two component system, SsrA/SsrB. Activation of SsrA/SsrB enhances sensitivity to the changing environment and induces transcription of SPI-2 genes.

1.5 Interplay between host cells and bacterial pathogens

1.5.1 MicroRNAs and bacterial infections

MicroRNAs (miRNAs) are a class of small non-coding RNAs (ca. 20-22 nt in length) that play an important role in post-transcriptional regulation of metazoan cells. Until today more than 2500 mature miRNAs are annotated in the human genome (mirBASE 22, 2018) and it is estimated that they regulate 60% of the human transcriptome (63). The biogenesis of miRNAs occurs in several steps, starting with primary miRNA transcripts (pri-miRNAs) in the nucleus. The long, capped and polyadenylated pri-miRNAs are transcribed by RNA polymerase II and form a hairpin structure. Further processing of pri-miRNAs into 60-100 nt long pre-miRNAs is accomplished by the Microprocessor complex. Subsequently the pre-miRNA is exported via Exportin-5 into the cytoplasm, where it is further processed by Dicer into a miRNA duplex. One of the strands is loaded onto the miRNA induced silencing complex (miRISC), which targets mRNAs. Base pairing of miRNAs and target mRNAs within the miRISC results in translational repression and/or mRNA degradation (64).

MiRNAs are involved in a broad range of biological functions and have been shown to regulate development, cellular differentiation and proliferation, apoptosis, autophagy and immune responses (65) (66) (67). Therefore, it is not surprising that dysregulation of miRNAs are implicated in a wide range of human diseases like cancer or cardiovascular disorders (68) (69). In addition, the role of miRNAs in bacterial infections has been intensively studied in recent years and it has become clear that they are an important part of the host response to infection, but are also exploited by bacterial pathogens in order to manipulate host cells for their own benefit (65) (66).

Infection of gastric epithelial cells with *Helicobacter pylori (H.pylori),* a Gram-negative microaerophilic bacterium which chronically infects the gastric mucosa and causes gastritis, peptic ulcer and gastric cancers (70), was shown to alter the expression of different miRNAs, which regulate cell proliferation and apoptosis and thus provided a link between *H. pylori* infection and development of gastric cancer (71) (72) (73). In addition, expression of miRNAs that regulate immune responses, like miR-155 or miR-

146a, are changed upon *H. pylori* infection (74) (75) (76) (77); and the expression of let-7 family members is strongly downregulated by CagA (cytotoxin-associated gene A), a major virulence factor of *H. pylori* (78) (79). Mir-155 was also shown to be regulated upon infection with *Mycobacterium tuberculosis (M. tuberculosis)* and due to its regulatory activity, it simultaneously promotes intracellular survival of *M. tuberculosis* and enhances the host immune response (80). In addition, miRNAs involved in autophagy are differentially expressed upon infection with *M. tuberculosis* and thus, intracellular survival of the bacteria is supported (81) (82) (83). Another bacterial pathogen that induces changes in host miRNA expression is *Staphylococcus aureus*. Besides up-regulation of miR-155 (84), it was shown that upon infection of wounds, DNA repair and an inflammatory response was compromised due to upregulation of mir-152-5p (85). A functional high throughput screen identified mir-29b-2-5p to increase binding of *Shigella flexneri (S. flexneri)* to host cells and its intracellular replication. Concurrently, expression of mir-29b-2-5p was decreased upon infection with *S. flexneri* (86). During infection with *Listeria monocytogenes (L. monocytogenes)* several miRNAs were upregulated in bone marrow derived macrophages but also in Caco-2 cells (87) (88). Interestingly upregulation of mir-155 was also induced by incubation with purified Listeriolysin O, a secreted toxin required for vacuolar escape of *L. monocytogenes* (88).

Infection with *Salmonella* Typhimurium induces changes in the host miRNome of macrophages and epithelial cells and it was shown that miRNAs regulating immune function like miR-155, miR-146a or the let-7 miRNA family were deregulated (89). Interestingly, upregulation of miR-155 was induced by LPS alone and did not depend on the *Salmonella* pathogenicity islands SPI-1 or SPI-2 (90). Let-7 family members were shown to target IL-6 and IL-10, two cytokines with opposing functions, which shows that miRNAs contribute to balance the inflammatory response of *Salmonella* infection (89). Other miRNAs, like miR-30c or miR-30e, target cellular pathways and are upregulated during *Salmonella* infection. Eventually, repression of their targets promotes intracellular survival of *Salmonella* (91).

In vivo experiments in chicken and piglets revealed deregulation of more than 100 miRNAs upon *Salmonella* infection (92) (93). Validation of some of these miRNAs reveal that not only the immune response, but also other cellular pathways and activities are targeted, e.g. activity of Rho GTPases that are involved in *Salmonella* invasion (94).

Additionally, the mir-15 family, known to target Cyclin D1 (6), and thereby blocking host cell transition from G1 into S phase, was identified to inhibit intracellular replication of *Salmonella*. Concomitantly, *Salmonella* infection leads to downregulation of the transcription factor E2F1 and consequently of the miR-15 family, resulting in faster progression of infected host cells from G1 into S phase (5). Together, these studies show the pivotal role of miRNAs in infection and demonstrate that they are part of the host response to infection, but can also be targeted by bacterial pathogens in order to modify their host environment for their own benefit.

1.5.2 Bacterial infections and the host cell cycle

Many intracellular bacteria have evolved sophisticated mechanisms in order to escape the innate immune response of their host cell, to modify their environment for their own benefit and to eventually colonize and invade host tissue. Therefore, they target the host cell architecture, vesicular trafficking pathways or interfere with the cell cycle of their host (95). For the latter, bacterial pathogens deliver cyclomodulins, molecules that modulate the eukaryotic cell cycle, into the cell (96). The family of cyclomodulins comprises bacterial proteins or peptides, some with enzymatic activity. One non-proteinaceous cyclomodulin was found in *Mycobacterium ulcerans (M. ulcerans)*, which produces mycolactone, a macrolide, causing G_0/G1 delay (95). A large group of cyclomodulins are cytolethal distending toxins (CDTs), which were the first bacterial toxins shown to block the host cell cycle at the G2/M transition in *E. coli* (97). Later CDTs, which induce DNA single and double strand breaks and thus block the cell cycle, were found in other bacteria as well. A second group of cyclomodulins are cycle inhibiting factors (Cifs), which do not induce DNA damage but cause cell cycle arrest by accumulation of CDK inhibitors (95) (96).

The cell cycle phase in which host cells are delayed or arrested varies, depending on the bacterial pathogen, but also on the host cell type. *Mycobacterium tuberculosis (M. tuberculosis),* a slow-growing, facultative intracellular bacterium, which avoids host cell clearance by arrest of macrophage maturation (98), secretes poliketides that arrest host cells in G_0/G1 phase and thus inhibits G1/S transition (99). Studies on *M. ulcerans* infected fibroblasts, lymphocytes and macrophages revealed cell rounding, inhibition of protein synthesis, cell-cycle arrest in G_0/G1 and eventually cell death (100). *Helicobacter pylori (H.pylori)* was first shown to delay transition from G2/M into G1 phase in AGS cells, a gastric adenocarcinoma cell line (101). Further studies observed a *H. pylori*-induced transient pre-mitotic arrest that caused changes in the activity of mitotic histone kinase modifications (102). CagA, a secreted bacterial effector of *H. pylori*, causes downregulation of miRNAs involved in cell cycle regulation (cf. section about miRNAs) and thus induces cell cycle arrest at the G1/S transition in embryonic stem cells (70). Another *H. pylori* virulence factor, the vacuolating cytotoxin VacA, induces G1 arrest in a p53-dependent manner (100). Recently, it was shown that *H. pylori* infection promoted PI3K/mTOR-dependent hypoxia-induced factor-1α (HIF-1α) induction, which subsequently causes G_0/G1 cell cycle arrest in a Cyclin D1-dependent mechanism (103). Infection with *Neisseria gonorrhoeae* caused DNA damage in a non-tumor epithelial cell line and consequently delayed progression through G2 phase (104), while *Neisseria meningitides* arrests host cells in different cell cycle phases, depending on the host cell type. Human pharyngeal and nasopharyngeal epithelial cells, infected with *N. meningitides,* are arrested in G1 (105), while infection of brain endothelial cell lines and primary brain endothelial cells causes an arrest in S-phase (106). Another intracellular bacterium that delays S-phase of its host cell, accompanied with increased double strand breaks and DNA damage, is *Listeria monocytogenes*. *L. monocytogenes* compromises the host DNA damage repair machinery by activity of the bacterial toxin ListeriolysinO and thus causes S-phase delay without fully blocking cell cycle progression (107) (108). *Staphylococcus aureus* was shown to induce a delay of G2/M transition, accompanied by accumulation of inactive CDK1 and unphosphorylated histone H3 (109). More recently, the *S. aureus* lipoprotein Lpl1 was shown to be the causative agent for the delay of G2/M transition (110). Another

pathogen that blocks host cells in G2/M is *Shigella flexneri*. The *Shigella* effector IpaB targets Mad2L2, an anaphase-promoting complex/cyclosome (APC) inhibitor. Consequently, *Shigella* infected cells fail to accumulate Cyclin B1, Cdc20 and Plk1 and are arrested in G2/M phase (111).

In addition to the above mentioned proteinaceous CDTs (97), *E. coli* also produces hybrid peptide-polyketide genotoxins, that induce DNA damage and thus cell cycle arrest (112). Enteropathogenic *E. coli* (EPEC) produce Cifs and thereby arrest host cells in G2/M, without causing DNA damage (113) (114). Interestingly, enterohemorrhagic *E. coli* (EHEC) produce outer membrane vesicles (OMVs) containing various substances, e.g. CdtV-B (cytolethal distending toxin V-B). Upon endocytosis of CdtV-B containing OMVs, cellular DNA is damaged and the subsequently induced DNA damage repair system causes G2/M arrest (115). In *Yersinia pseudotuberculosis* and *Burkholderia pseudomallei* homologs of E. coli Cifs were found, suggesting that these pathogens also target the cell cycle machinery of their host cells (116) (117) (118). CDTs that induce DNA damage and thus G2/M arrest, are also produced by *Campylobacter jejuni* (119), while infection with *Chlamydia trachomatis* was shown to causes a reduction in CDK1 levels and cleavage of Cyclin B1, ultimately delaying G2/M transition as well (120).

Isberg and co-workers showed that G1 phase and G2/M phase are permissive for intracellular growth of *Legionella pneumophila*, an intracellular pathogen infecting macrophages and amebae, whereas replication is strongly inhibited in S-phase (121). The same study revealed that the inability of *Legionella* to replicate in S-phase is due to its failure to control the integrity of the Legionella-containing-vacuole (LCV), leading to cytosolic exposure of the bacteria and eventual degradation. Following up on these results, it was recently shown that *Legionella* blocks its host cell from progression into S-phase with translation inhibitors, translocated via the Icm/Dot secretion system. Presence of these inhibitors in the host cells cause degradation of Cyclin D1 and thus block transition of host cells from G1 into S-phase (122).

Like many other pathogens, *Salmonella* Typhimurium also manipulates the cell cycle of its host and early studies already revealed that it arrests cells in G2/M by activity of the SPI-2 effector SpvB, an ADP-ribosyl transferase enzyme that induces F-actin

depolymerization (123). In addition, the *Salmonella* SPI-2 effectors SseF and SseG target the chromosomal passenger complex and mitotic kinesin-like protein 1 and consequently prevent cytokinesis, causing tetraploidy and binucleation (124). Interestingly, though mitotic cells were much more efficiently targeted for invasion by *Salmonella* due to a high surface cholesterol content (47), it was shown that upon *Salmonella* infection, host cells progress faster from G1 into S-phase, suggesting a certain preference for G2/M (5). Moreover, the same study showed that host cell cycle arrest in G1 was detrimental for *Salmonella* long-term infection, suggesting that exit of G1 phase is not only preferred, but absolutely essential for *Salmonella* infection.

1.6 Aim of the study

Several intracellular bacteria modulate the cell cycle of their host by enhancing or delaying proliferation or even arresting cells in a certain cell cycle stage. So far it has been shown that (i) *Salmonella* preferentially invades mitotic cells, (ii) infection with *Salmonella* induces a faster transition of host cells from G1 into S-phase and (iii) *Salmonella*, like other pathogens, blocks host cells in G2/M. In addition, it was found that *Salmonella* cannot establish a long term infection in G1 arrested cells. However, it is not yet clear why. The aim of the current study was to investigate what distinguishes G1 arrested host cells from cells in another cell cycle phase. More particularly, which factor(s)/pathways, required for intracellular *Salmonella* replication, are missing in G1 arrested cells. Since it is known that *Salmonella* modulates the host cell cycle to ensure intracellular replication, it is unclear why *Salmonella* cannot modulate G1 arrested cells to establish a long term infection. Results of the study will fill this gap of knowledge; shed more light on the aspect of host cell cycle regulation by *Salmonella* and contribute to the understanding of intracellular population dynamics in different host cell types.

2 Results

2.1 *Salmonella* vacuolar replication is inhibited in G1 arrested host cells

Salmonella intracellular replication is adapted and depends on the host cell metabolism and cell cycle. Previous studies suggested a preference of *Salmonella* for G2/M phase of the host cells (5) (123), raising the question why G1 phase is less permissive for intracellular replication. In order to determine to which extent *Salmonella* intracellular replication is affected by arresting host cells in G1 phase, the cells were treated with an inhibitor of CDK4/6 kinases (CDK 4/6i), or DMSO as control, for 16 hours prior to infection in all upcoming experiments. To continuously arrest the cells in G1, the treatment was maintained throughout the time course of infection.

2.1.1 Salmonella replication is impaired in G1 arrested HeLa 229 cells

Efficiency of G1 arrest was monitored by cell cycle measurements after staining of nuclei with propidium iodine at 0 hpi. CDK 4/6i treatment led to an increase of cells in G1 phase [Fig. 11 A, B]. Intracellular replication of *Salmonella* was quantified by microscopy [Fig. 11 C] and colony forming units [Fig. 11 D], and monitored over the time course of 20 hours to cover early, intermediate and late stages of infection. The bacterial load at 1 hpi was similar in DMSO treated and G1 arrested cells, suggesting that early stages of infection, comprising adhesion and invasion, were not significantly affected by G1 arrest. In control HeLa 229 cells, *Salmonella* began to replicate between 4-6 hpi and the intracellular bacterial load increased by 10-fold from 1 hpi to 20 hpi. In G1 arrested cells, the bacterial load continuously decreased over time, so that at 20 hpi the difference in intracellular bacterial load between DMSO and CDK4/6i treated cells was 55-fold [Fig. 11 D]. This shows that *Salmonella* is not able to replicate in G1 arrested HeLa 229 cells.

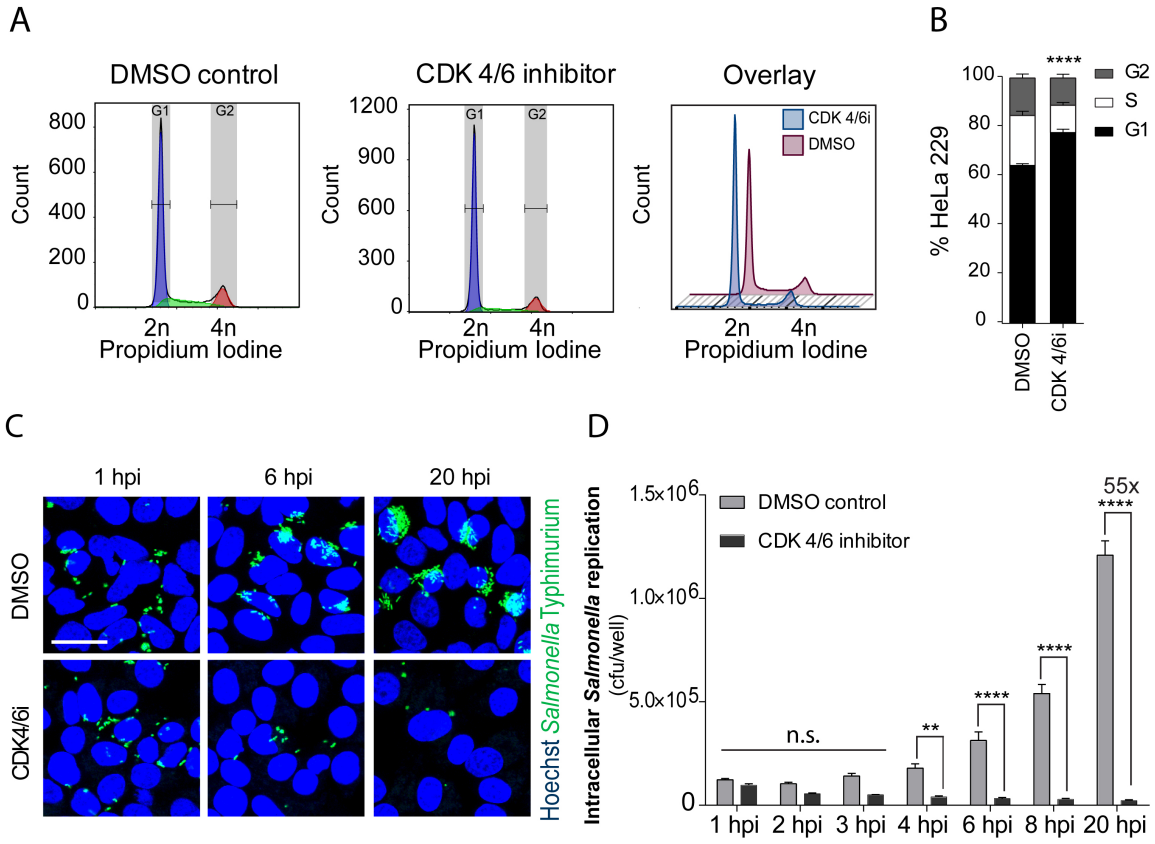

Fig. 11 *Salmonella* replication is inhibited in G1 arrested HeLa 229 cells.

(A) Example of individual and comparative cell cycle profiles of HeLa 229 cells treated with CDK4/6 inhibitor or DMSO for 16 hrs. DNA content of cells was determined by flow cytometry after staining with propidium iodine. (B) Quantification of cells in various cell cycle phases upon DMSO or CDK4/6i treatment. (C) Representative microscopy images of HeLa 229 cells infected with GFP-labelled *Salmonella* Typhimurium (MOI 25). (D) CFU quantification of intracellular *Salmonella* in G1 arrested or control cells. Results are shown as mean ± s.e.m. of at least 5 individual experiments; two-way ANOVA: *p≤0.05, **p≤0.01, ***p≤0.001, ****p≤0.0001, n.s. = non-significant. Scale bar = 50 µm.

2.1.2 G1 arrest of HCT8 cells leads to a temporary formation of large bacterial clusters while long-term replication is impaired

Treatment of HCT-8 cell with the CDK 4/6 inhibitor led to a significant increase of cells in G1 phase [Fig. 12 A, B]. Interestingly, in G1 arrested HCT8 cells, intracellular *Salmonella* replication peaks at 6 hpi and even exceeds replication in control cells at this intermediate stage of infection. Microscopy images show the formation of remarkable cluster of intracellular *Salmonella* at 6 hpi [Fig. 12C]. Nevertheless, at 20 hpi

the intracellular bacterial load was 30-fold lower in G1 arrested cells compared to the control situation [Fig. 12D].

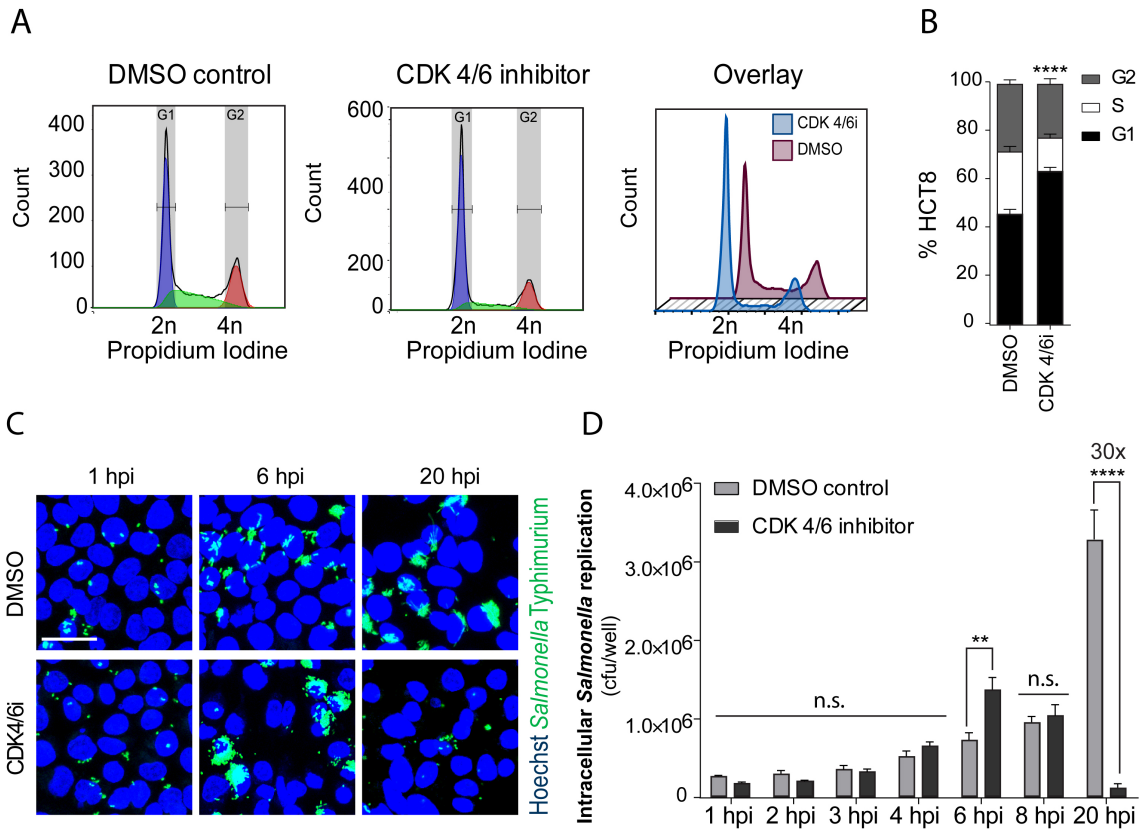

Fig. 12 *Salmonella* replication is compromised in G1 arrested HCT8 cells.

(A) Example of individual and comparative cell cycle profiles of HCT8 treated with CDK4/6 inhibitor or DMSO for 16 hrs. DNA content of cells was determined by flow cytometry after staining with propidium iodine. (B) Quantification of cells in various cell cycle phases upon CDK4/6i treatment. (C) Representative microscopy images of HCT8 cells infected with GFP-labelled *Salmonella* Typhimurium (MOI 25). (D) CFU quantification of intracellular *Salmonella* in G1 arrested or DMSO-treated cells. Results are shown as mean ± s.e.m. of at least 5 individual experiments; two-way ANOVA: *p≤0.05, **p≤0.01, ***p≤0.001, ****p≤0.0001, n.s. = non-significant. Scale bar = 50 µm.

2.1.3 G1 arrest of HeLa CCL2 cells impairs vacuolar replication of *Salmonella*

Although *Salmonella* is mainly considered to have a vacuolar intracellular lifestyle, the formation of large intracellular clusters of *Salmonella* at an intermediate stage of infection has been described in some cell lines before and was shown to resemble cytoplasmic replication. If the cluster contained ≥100 bacteria it is referred to as hyperreplication (125). Bearing this in mind, the bacterial cluster observed at 6 hpi in HCT8 and the lack of replication at 20 hpi suggested that *Salmonella* was not able to establish its vacuolar niche for long-term replication in HCT8, while cytoplasmic replication seemed not to be compromised, but even promoted. The finding that these clusters were not observed in HeLa 229 is curious since HeLa cells have been used to study cytoplasmic replication of *Salmonella* (126). However, these studies used a different clone of HeLa cells, namely CCL2. To test whether cytoplasmic replication of *Salmonella* was still possible in a different HeLa clone, experiments were repeated in G1 arrested HeLa CCL2 cells. Addition of CDK4/6i to HeLa CCL2 led to a comparable G1 arrest as in HeLa 229 [compare Fig. 11 A, B with Fig. 13 A, B]. After infection with *Salmonella* the bacterial load in control cells increased continuously from 1 hpi to 20 hpi, whereas in G1 arrested cells the overall bacterial load was lowered, resulting in a 17-fold difference between control and G1 arrested cells at 20 hpi. Interestingly, though the bacterial load in G1 arrested HeLa CCL2 did significantly increase until 6 hpi, it never exceeded bacterial replication in control cells (as it did in HCT8 at 6 hpi) [Fig. 13 D]. Together with the microscopy images [Fig. 13], this showed that *Salmonella* was able to replicate at least temporally in HeLa CCL2.

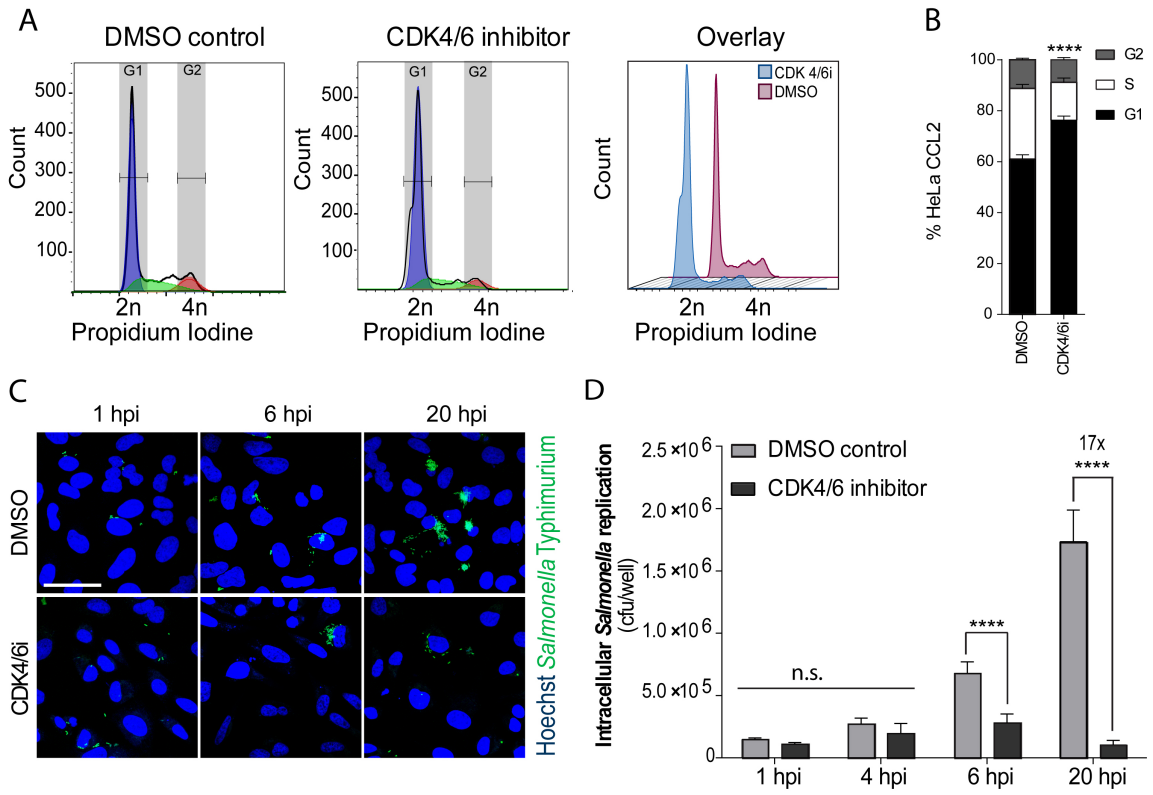

Fig. 13 *Salmonella* replication is compromised in G1 arrested HeLa CCL2

(A) Example of individual and comparative cell cycle profiles of HeLa CCL2 treated with CDK4/6 inhibitor or DMSO for 16 hrs. DNA content of cells was determined by flow cytometry after staining with propidium iodine. (B) Quantification of cells in different cell cycle phases upon CDK4/6i treatment. (C) Representative microscopy images of CCL2 infected with GFP-labelled *Salmonella* Typhimurium (MOI 25). (D) CFU quantification of intracellular *Salmonella* in G1 arrested or control cells. Results are shown as mean ± s.e.m. of at least 5 individual experiments; two-way ANOVA: *p≤0.05, **p≤0.01, ***p≤0.001, ****p≤0.0001, n.s. = non-significant. Scale bar = 50 µm.

2.1.4 G1 arrest promotes cytoplasmic replication of intracellular *Salmonella*

In order to confirm the finding of cytoplasmic *Salmonella*, a Chloroquine resistance assay was used to determine the proportion of intracellular vacuolar or cytoplasmic *Salmonella* in HeLa 229 and HCT8. Chloroquine (CHQ) is a weak base and can cross membranes by passive diffusion. It becomes protonated at low pH and hence is less membrane permeable. When entering an acidic compartment like a lysosome or phagosome it accumulates up to 1000-fold compared to the cytoplasmic concentration (127). Therefore, when CHQ is added to *Salmonella* infected cells it accumulates inside the SCV and kills intra-vacuolar bacteria (CHQ sensitive), while cytoplasmic bacteria (CHQ resistant) are not harmed and can be recovered in a CFU assay. In parallel, CFUs from untreated cells are quantified to determine the total population.

Results show that in DMSO-treated HeLa 229 only 4.9% of the total population was CHQ resistant (cytoplasmic) at 1 hpi and that this fraction slightly increased at 4 hpi, a time point where (vacuolar) replication had already led to an increase of the total bacterial population. Upon G1 arrest 74.6% of the total population was CHQ resistant at 1 hpi. Interestingly, the ratio between CHQ resistant and CHQ sensitive bacteria was the same at 4 hpi, however the total bacterial load had decreased [Fig. 14 A]. This confirms that *Salmonella* does not replicate in either compartment, cytoplasm or vacuole, in G1 arrested HeLa 229 cells.

In control HCT8 cells 10.5% of the total population was cytoplasmic at 1 hpi. At 4 hpi both, vacuolar and cytoplasmic bacteria had started to replicate, thereby maintaining the ratio between both fractions. Strikingly, in G1 arrested HCT8 the CHQ resistant fraction made up 98.4% of the total population at 1 hpi, indicating an early hindrance in SCV maturation. Until 4 hpi these cytoplasmic bacteria replicated further, forming the previously observed intracellular cluster [Fig. 12C]. In contrast to HeLa 229 cells, the small fraction of vacuolar bacteria (1.6%) was able to replicate until 4 hpi. In addition this fraction might contain bacteria that have been rescued and re-directed into a vacuolar pathway by autophagy, as described before (48). Nevertheless, they remained the minor fraction of intracellular *Salmonella* (25%) [Fig. 14 B]. These results confirm that upon G1 arrest vacuolar replication is delayed (HCT8) or completely abolished

(HeLa 229). Cytoplasmic replication however seemed to be even promoted, depending on the host cell type.

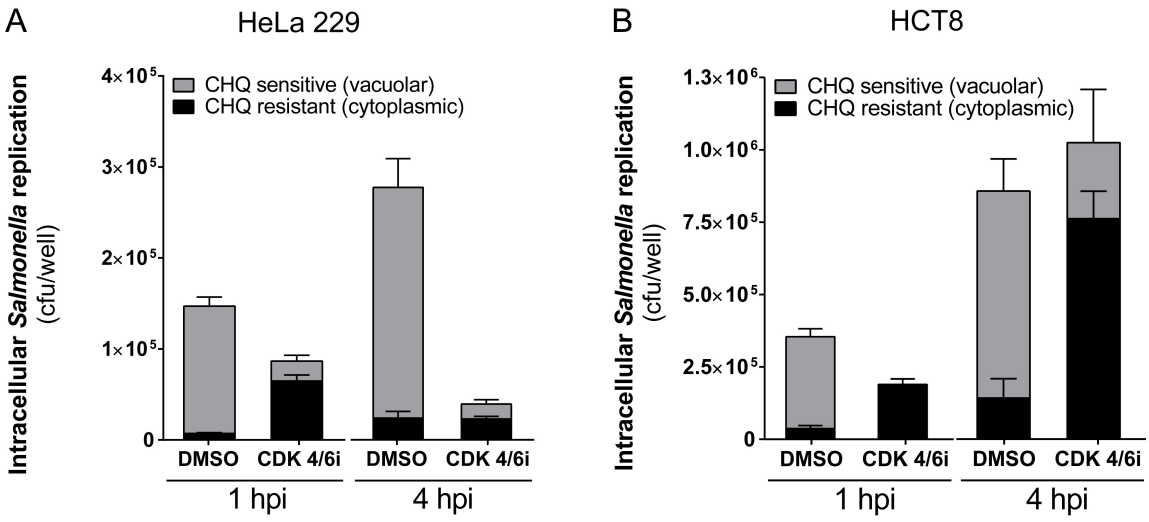

Fig. 14 G1 arrest of host cells renders intracellular *Salmonella* cytoplasmic

For (A) HeLa 229 and (B) HCT8 two wells per condition (DMSO or CDK4/6i) were infected with *Salmonella* (MOI 25). At 0 hpi or 3 hpi CHQ was added to one well each and incubated for an additional hour. At 1 hpi or 4 hpi untreated and CHQ treated cells were lysed and plated for CFU quantification. Results are shown as mean ± s.e.m. of at least 5 individual experiments.

2.1.5 G1 arrest does not interfere with *Shigella flexneri* replication

To test whether G1 arrest affects the cytoplasmic replication of other bacteria, the same approach was used for infection with *Shigella flexneri*. Similar to *Salmonella*, *Shigella* is initially taken up in a vacuole, which it escapes early in infection and then replicates in the cytoplasm of host cells before spreading to neighboring cells (128). To monitor intracellular replication of *Shigella*, microscopy images were taken at 0.5 hpi, 3 hpi and 6 hpi (early, intermediate, late stages of infection) and colony forming unit assays were used for quantification [Fig. 15]. Results show that intracellular replication of *Shigella* was not impaired in HeLa 229 and more importantly not changed upon G1 arrest.

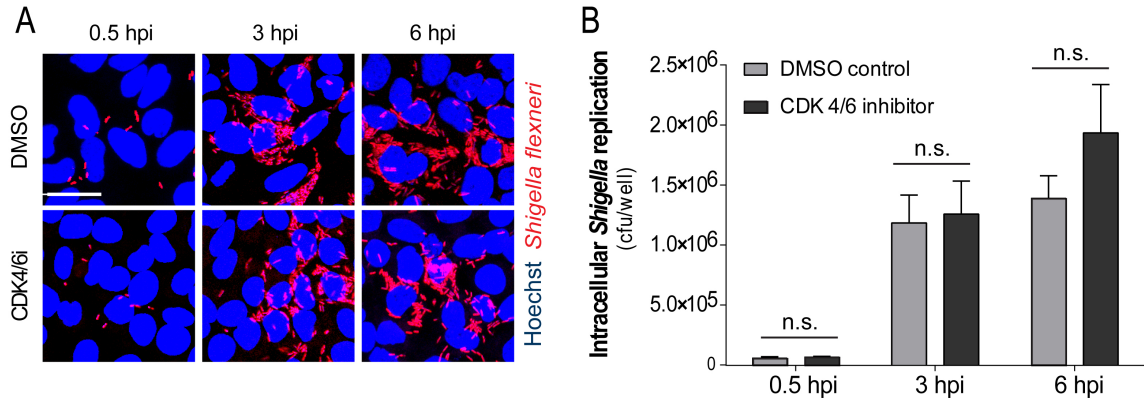

Fig. 15 *Shigella* intracellular replication is not affected upon G1 arrest

(A) Representative microscopy images of DMSO and CDK4/6i treated HeLa 229 cells, infected with *Shigella flexneri* (MOI 25).

(B) CFU quantification of intracellular *Shigella* in G1 arrested or control cells. Results are shown as mean ± s.e.m. of at least 5 individual experiments; n.s. = non-significant. Scale bar = 50 µm.

Taken together these results indicate that upon G1 arrest of HeLa 229, HeLa CCL2 and HCT8 cells, *Salmonella* was not able to establish a protective (vacuolar) niche in which it can replicate for a long-term infection. Additionally, G1 arrest of host cells led to a remarkable increase of cytosolic bacteria, resulting in the temporary formation of large bacterial cluster in HCT8 and CCL2, but not in HeLa 229. It is not clear why *Salmonella* replication is impaired in the latter. Replication of *Shigella*, a pathogen that escapes from the vacuole and replicates in the cytoplasm, is neither affected in control nor G1 arrested HeLa 229 cells.

2.1.6 CDK4/6i treatment does not inhibit bacterial growth *in vitro*

In order to exclude that the CDK4/6i treatment of cells might already interfere with bacterial replication, *Salmonella* and *Shigella* was grown in LB medium containing DMSO or CDK4/6i, respectively. Yet, addition of CDK4/6i did not interfere with *bacterial* growth [Fig. 16]

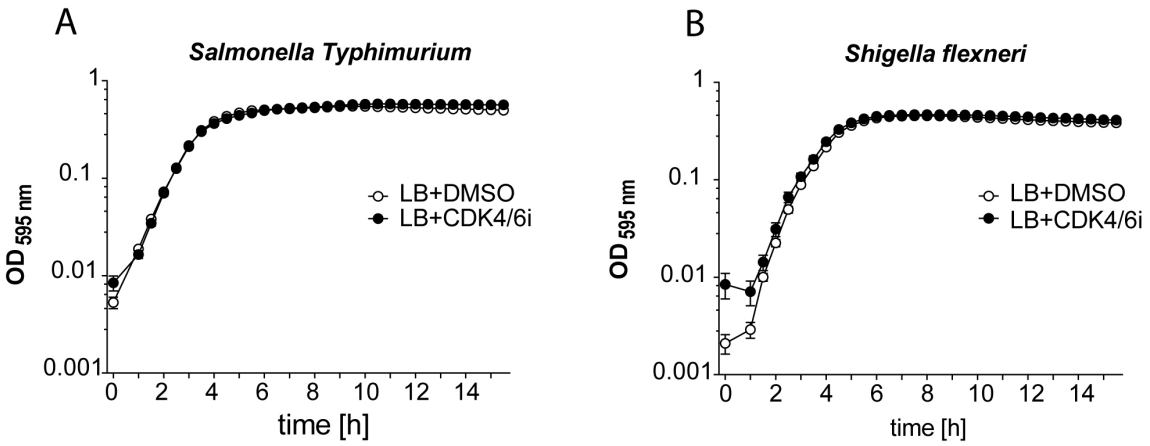

Fig. 16 Bacterial growth is not affected by CDK4/6 inhibitor treatment

Growth curves of (A) *Salmonella* Typhimurium and (B) *Shigella flexneri* in LB+DMSO and LB+CDK4/6i. Results are shown as mean ± s.e.m. of 5 individual experiments.

2.2 *Salmonella* SPI-2 activation is impaired, while SPI-1 activity is sustained in G1 arrested cells

2.2.1 SPI-2 reporter strain reveals impaired activation of SPI-2 in G1 arrested cells

Under physiological conditions, the majority of intracellular *Salmonella* replicate inside *Salmonella*-containing vacuoles (SCV). SCVs are initially formed when *Salmonella* invades host cells and subsequently modifies the vacuole for its own benefit. The modification of this protective niche depends on the secretion of bacterial effectors encoded on the SPI-2 island (55). In G1 arrested cells (vacuolar) replication was inhibited, pointing towards impaired activation of the SPI-2 system. In order to determine SPI-2 activation of *Salmonella* in G1 arrested cells, a reporter strain was constructed that constitutively expressed mCherry and had GFP under control of the SsaG promotor (a SPI-2 encoded effector).

Microscopy images of HeLa 299 cells showed that the *Salmonella* reporter strain equally invaded control and G1 arrested cells, but that GFP expression was hardly induced in G1 arrested cells throughout the time course [Fig. 17 A]. Instead, SPI-2 activation was slightly delayed and occurred only in a minor fraction of G1 arrested cells (max. 20% of infected cells) compared to control cells (ca. 75%), as confirmed by flow cytometry [Fig. 17 B, C]. In addition, the activation level (MFI GFP) within the SPI-2 positive fraction was significantly lower in G1 arrested cells. The SPI-2 negative fraction showed only minor replication at 4 and 6 hpi upon G1 arrest (MFI mCherry SPI-2 negative population) [Fig. 17 D].

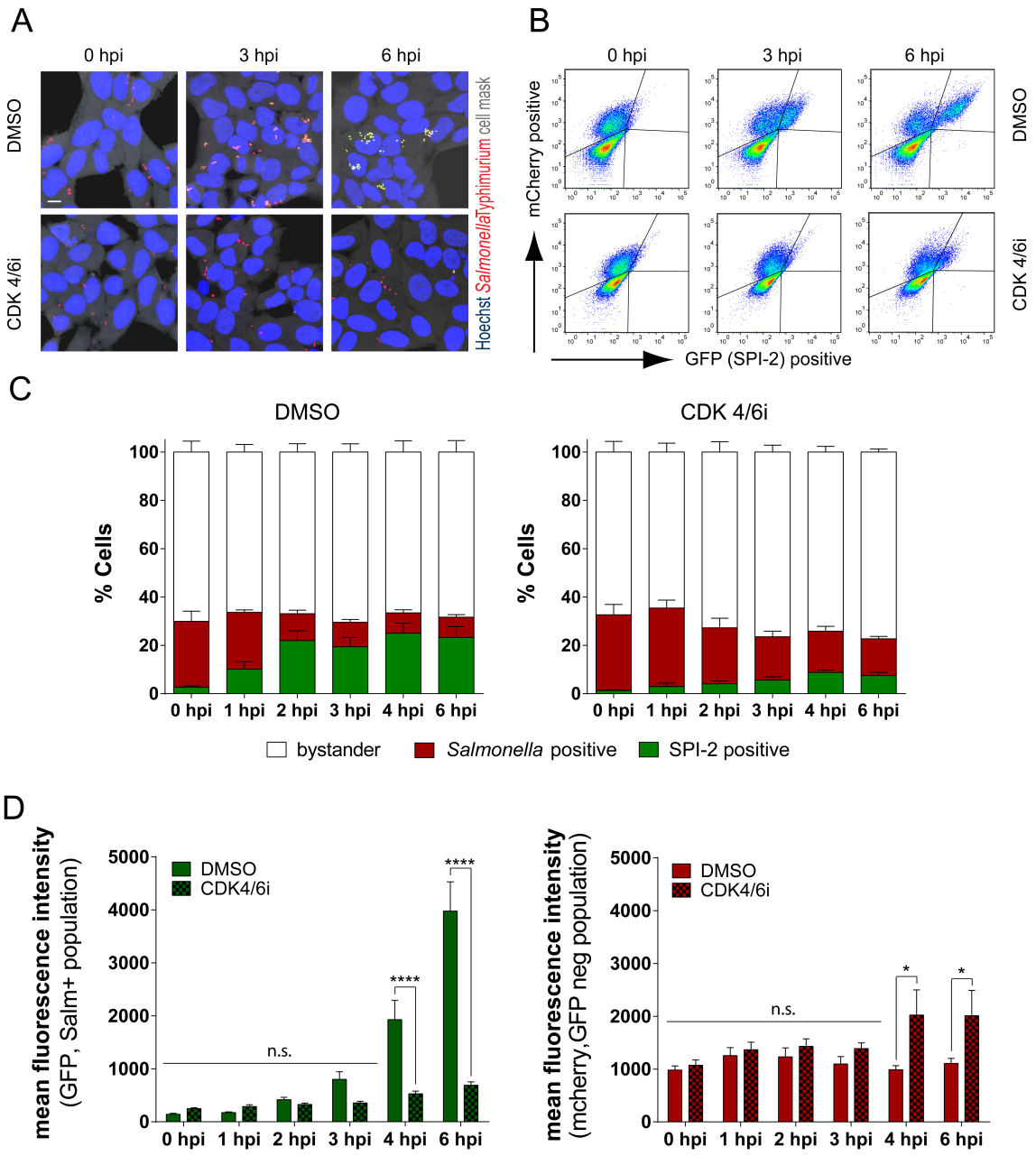

Fig. 17 SPI-2 is activated less in G1 arrested HeLa 229 cells.

(A) Representative microscopy images of HeLa 229 cells infected with a *Salmonella* reporter strain (mCherry is expressed constitutively; GFP is expressed upon SPI-2 activation), MOI 25. (B) Representative flow cytometry plots of HeLa 229 cells infected with the *Salmonella* reporter strain. Lower left quadrant = non infected bystander cells; upper left quadrant = mCherry pos/GFP neg cells; upper right quadrant = mCherry pos/GFP pos (C) Quantification of flow cytometry analysis of HeLa 229 cells infected with the *Salmonella* reporter strain. (D) Mean fluorescence intensity GFP of the SPI-2 positive fraction of cells, indicating the SPI-2 activation level and mean fluorescence intensity mCherry of the SPI-2 negative population. Results are shown as mean ± s.e.m. of 5 individual experiments; two-way ANOVA: *p≤0.05, **p≤0.01, ***p≤0.001, ****p≤0.0001, n.s. = non-significant. Scale bar = 10 µm

Infection of HCT8 cells with the same reporter strain revealed that SPI-2 activation in control cells also started at 1 hpi and reached a plateau at 3 hpi with ca. 76% of infected cells harboring SPI-2 positive bacteria. In G1 arrested cells, SPI-2 activation started later (ca. 2-3 hpi) and 60% of the infected cells were SPI-2 positive [Fig. 18 C]. This seemed to be only a minor difference compared to control cells; however, SPI-2 was activated to a much lower extent (MFI GFP). The MFI mCherry of the SPI-2 negative fraction significantly increased over time in G1 arrested HCT8 cells, showing that SPI-2 is inactive in the fraction of *Salmonella* that undergoes rapid cytoplasmic replication [Fig. 18 D]. Interestingly, microscopy images as well as FACS plots at 6 hpi revealed formation of a third heterogeneous bacterial population in G1 arrested cells. These cluster contained mainly SPI-2 negative bacteria and a small number of SPI-2 positive bacteria within the cluster [Fig. 18 A, B]. Overall, G1 arrest of HCT8 cells resulted in three distinct cell populations, cells harboring only SPI-2 positive bacteria, cells harboring only SPI-2 negative bacteria and cells harboring a population of *Salmonella* with heterogeneous SPI-2 activity. Nonetheless, the main population contributing to the increase in intracellular bacterial load at 6 hpi was SPI-2 negative *Salmonella* [Fig. 12].

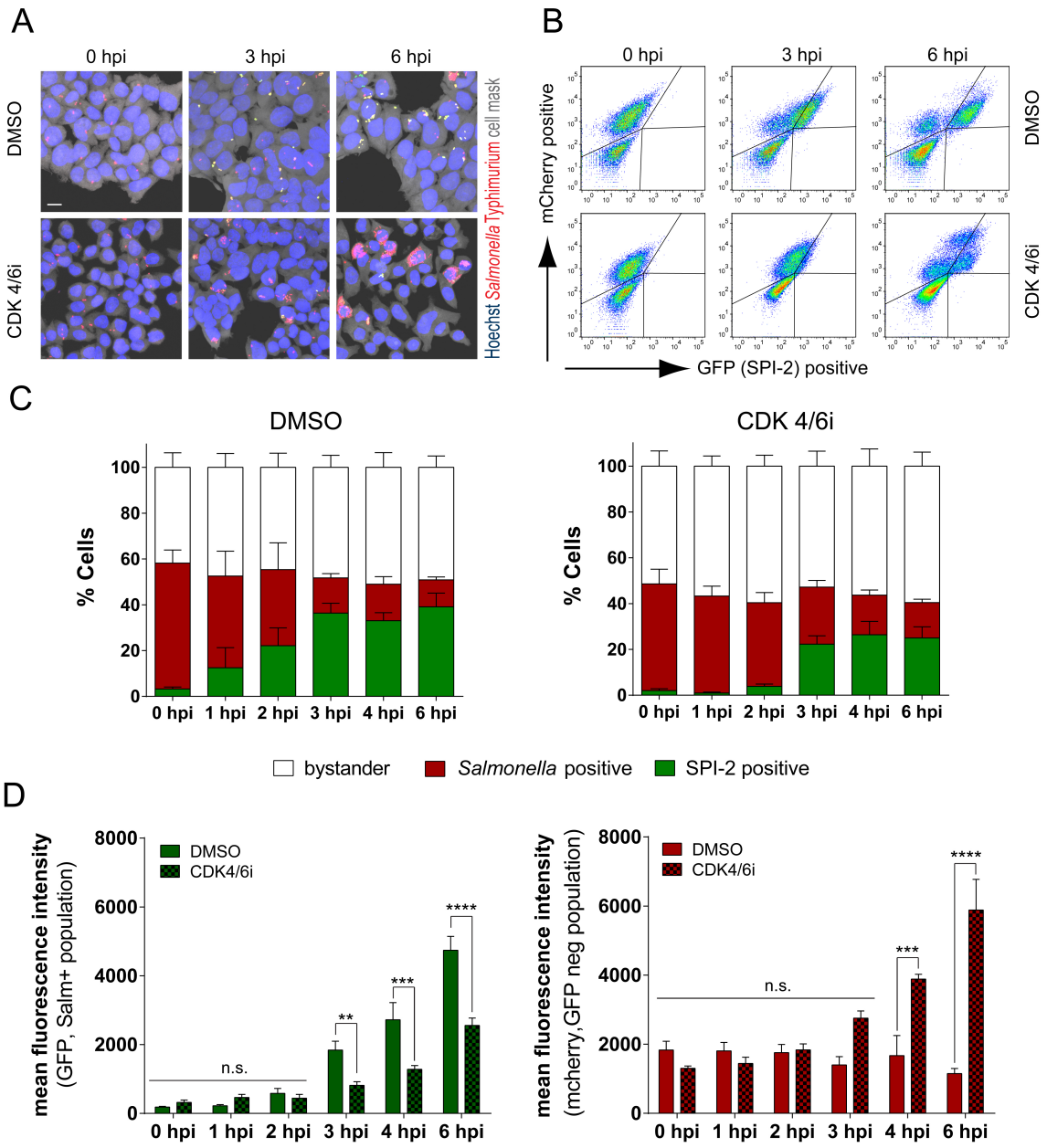

Fig. 18 SPI-2 is activated less in G1 arrested HCT8 cells.

(A) Representative microscopy images of HCT8 cells infected with a *Salmonella* reporter strain (mCherry is expressed constitutively; GFP is expressed upon SPI-2 activation), MOI 25. (B) Representative flow cytometry plots of HCT8 cells infected with the *Salmonella* reporter strain. Lower left quadrant = non infected bystander cells; upper left quadrant = mCherry pos/GFP neg cells; upper right quadrant = mCherry pos/GFP pos (C) Quantification of flow cytometry analysis of HCT8 cells infected with the *Salmonella* reporter strain. (D) Mean fluorescence intensity GFP of the SPI-2 positive fraction of cells, indicating the SPI-2 activation level and mean fluorescence intensity mCherry of the SPI-2 negative population. Results are shown as mean ± s.e.m. of 5 individual experiments; two-way ANOVA: *p≤0.05, **p≤0.01, ***p≤0.001, ****p≤0.0001, n.s. = non-significant. Scale bar = 10 µm

In order to test whether the mild replication observed in HeLa CCL2 was also SPI-2 independent, cells were infected with the reporter strain. As expected, the bacterial cluster observed in G1 arrested CCL2 cells were due to SPI-2 independent replication [Fig. 19 A, B]. Only 30% of G1 arrested CCL2 harbored SPI-2 positive bacteria compared to control cells (73.5%), which is similar to results obtained in HeLa 229 cells. The activation level of SPI-2 (MFI GFP) was significantly lower, while replication of SPI-2 negative bacteria was increased upon G1 arrest, though not to the same extent as in HCT8 [Fig. 19 C, D].

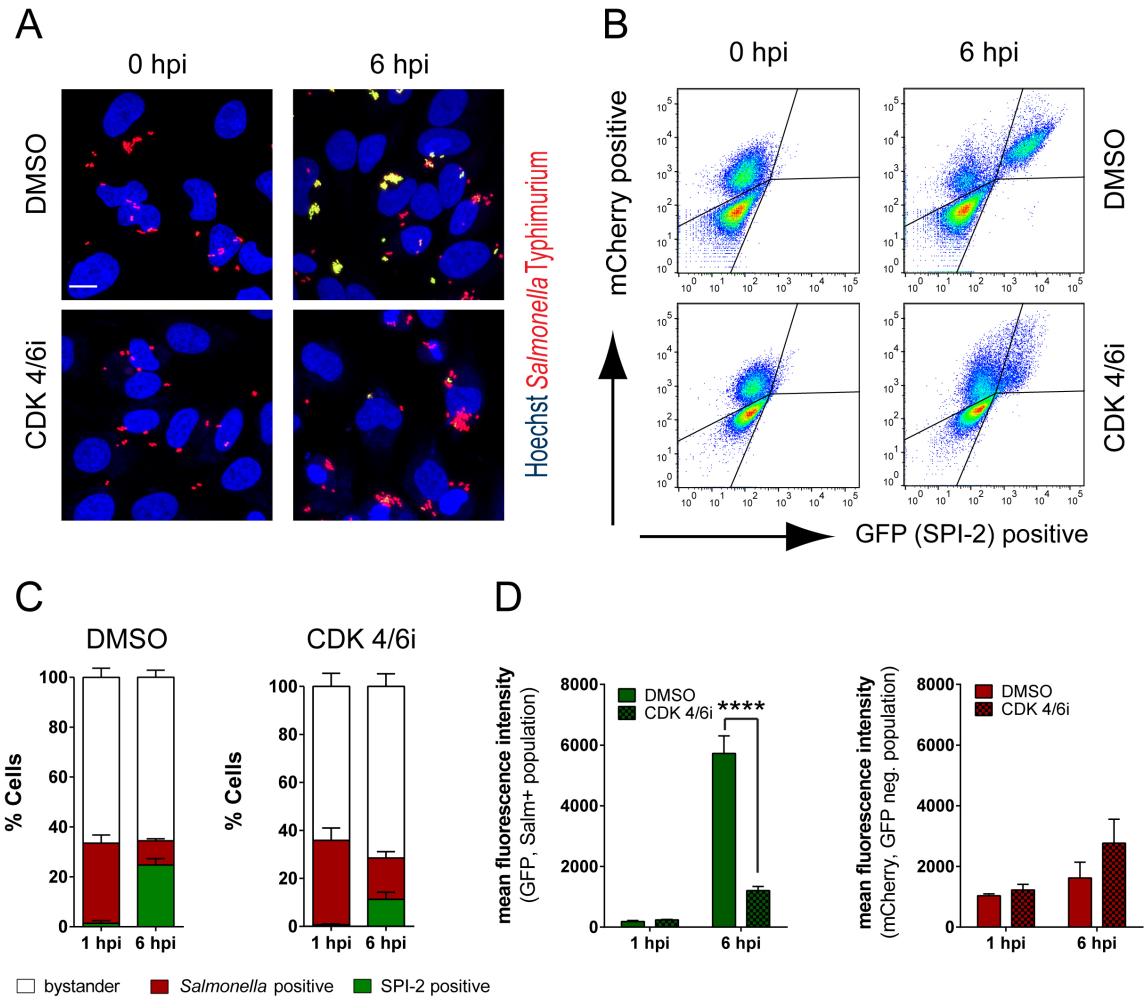

Fig. 19 SPI-2 is less activated in G1 arrested HeLa CCL2 cells.

(A) Representative microscopy images of CCL2 cells infected with a *Salmonella* reporter strain (mCherry is expressed constitutively; GFP is expressed upon SPI-2 activation), MOI 25. (B) Representative flow cytometry plots of HeLa CCL2 cells infected with the *Salmonella* reporter strain. Lower left quadrant = non infected bystander cells; upper left quadrant = mCherry pos/GFP neg cells; upper right quadrant = mCherry pos/GFP pos. (C) Quantification of flow

figure legend continues on next page

cytometry analysis of CCL2 cells infected with the *Salmonella* reporter strain. (D) Mean fluorescence intensity GFP of the SPI-2 positive fraction of cells, indicating the SPI-2 activation level and mean fluorescence intensity mCherry of the SPI-2 negative population. Results are shown as mean ± s.e.m. of 6 individual experiments; two-way ANOVA: *p≤0.05, **p≤0.01, ***p≤0.001, ****p≤0.0001. Scale bar = 10 µm

Altogether, the results show that in G1 arrested cells (i) SPI-2 activation was delayed (ii) fewer cells harbored SPI-2 positive bacteria, (iii) the SPI-2 activation level was significantly lower than in control cells and (iv) SPI-2 independent (cytoplasmic) replication was increased.

Further investigation of SPI-2 activity in G1 arrested cells focused on HeLa 229 (only SPI-2 dependent replication) and HCT8 (SPI-2 dependent and independent replication), based on the idea that HCT8 cells might represent a biologically more relevant phenotype of a heterogeneous intracellular *Salmonella* population, while HeLa 229 cells provided the advantage to investigate vacuolar maturation exclusively.

2.2.2 SPI-2 gene expression is impaired in G1 arrested cells

Since the reporter assays showed an impaired GFP (i.e. SPI-2) expression in G1 arrested cells, endogenous gene expression of SPI-2 effectors was measured by quantitative real time PCR (qRT-PCR). The SPI-2 effectors chosen [Table 1] are part of the secretion apparatus itself as well as secreted molecules. In addition, the expression level of s*srB*, the response regulator of the two component system inducing SPI-2 expression, was determined.

Table 1 T3SS-2 proteins

Effector	Name	Function	Reference
PipB2	*Salmonella* secreted effector protein PipB2	recruits kinesin-1 to the SCV	(55)
SteC	*Salmonella* translocated effector protein C	induces assembly of F-actin meshwork around SCV	(55)
SopD2	*Salmonella* outer protein D2	SIT formation, prevents accumulation of Rab32 on SCV and SITs	(55)
SseC	Secretion system effector protein C	integral part of translocon apparatus	(129)
SsaG	Secretion system apparatus protein G	integral part of T3SS needle	(130)
SsrB	Response regulator of SsrA/SsrB two component system	controls expression of T3SS-2 apparatus and translocation of its effectors	(60)

Prior the infection assays, it was confirmed that SPI-2 activation in *Salmonella* was not hampered by CDK4/6i treatment itself. Therefore, *Salmonella* was grown in defined minimal medium containing DMSO or CDK4/6i at pH 5.8 to mimic the early stages of the infection of a host cell in vitro and to induce expression of SPI-2 genes as described before (131) (132). Levels of SsrB and SPI-2 effector mRNA were quantified by qRT-PCR. This analysis verified that addition of CDK4/6i did not interfere with *Salmonella* SPI-2 expression [Fig. 20].

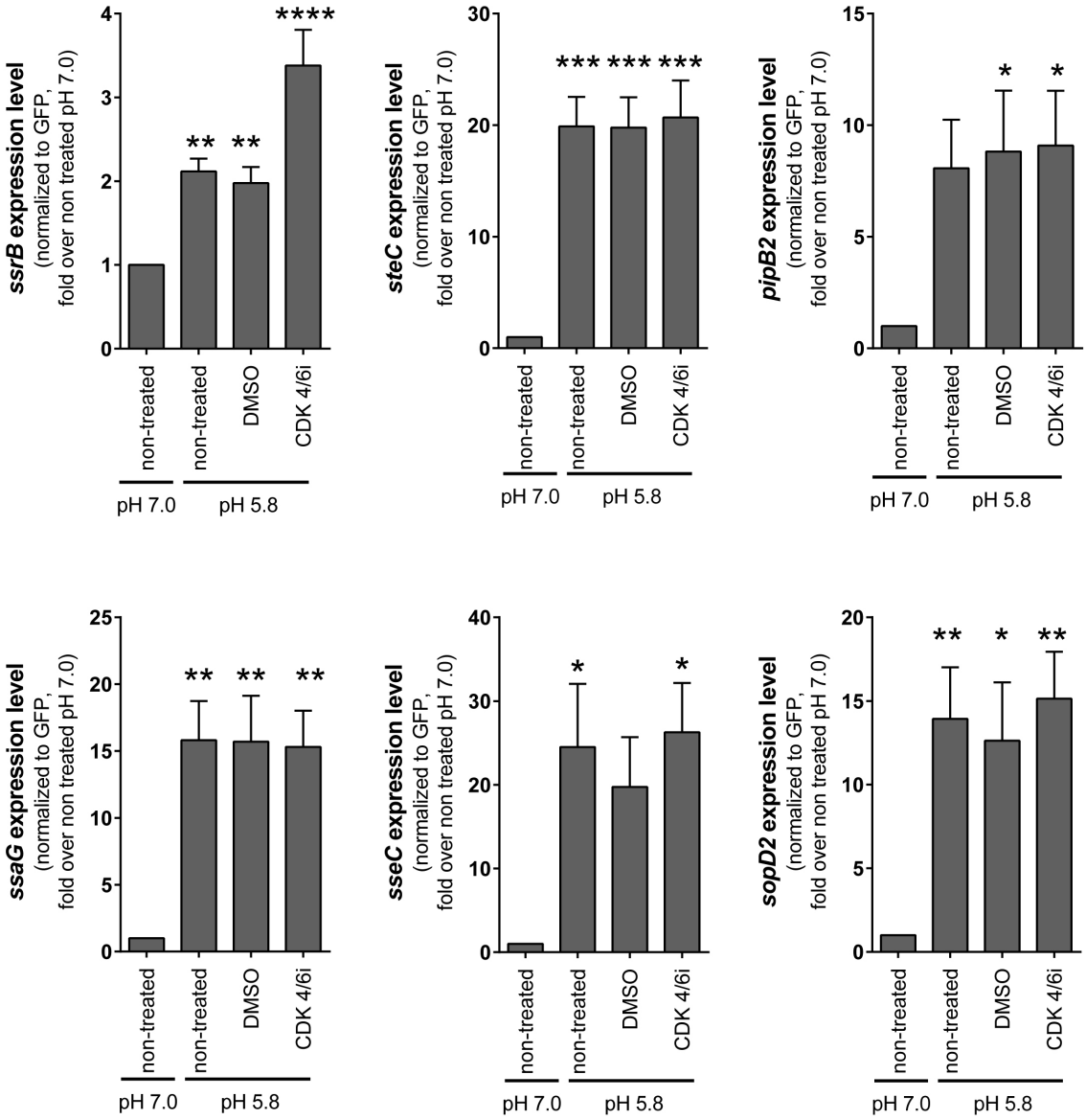

Fig. 20 SPI-2 gene expression in *Salmonella* is not affected by CDK4/6 inhibitor treatment

To induce expression of SPI-2 genes, *Salmonella* was grown in minimal medium at pH 7.0 or pH 5.8 containing DMSO or CDK4/6i. Expression in minimal medium at pH 5.8 was normalized to expression at pH 7.0. Results are shown as mean ± s.e.m. of 3-6 individual experiments, one-way ANOVA: *p≤0.05, **p≤0.01, ***p≤0.001, ****p≤0.0001.

Infection of control HeLa 229 cells with *Salmonella* resulted in an early increase of *ssrB* mRNA levels. After reaching a peak at 2 hpi, it decreased to an intermediate level that was kept constant until the end of the time course. In contrast, expression of *ssrB* in G1 arrested cells did not increase significantly and barely reached the level of control cells at 0.5 hpi. As expected for control cells, expression levels of the other SPI-2 genes started to increase at approx. 0.5 hpi until 2 hpi and remained approximately on the same level afterwards. In G1 arrested cells, mRNA expression of the other SPI-2 genes remained at a significantly lower level compared to the control [Fig. 21].

CDK4/6i induced G1 arrest of HCT8 cells had a comparable effect on SPI-2 gene expression. In control cells, expression of *ssrB* started already early, peaked at 2 hpi and slightly decreased afterwards. In G1 arrested cells, *ssrB* expression was only slightly induced and remained below the level of control cells. MRNA levels of other SPI-2 genes began to increase at 0.5 hpi and remained constant for the rest of the time course. In G1 arrested cells however, expression of other SPI-2 genes maintained a low level and only began to increase slightly at ≥6 hpi [Fig. 22]. These results suggest that ssrB was not activated and thus downstream SPI-2 genes remain equally inactive.

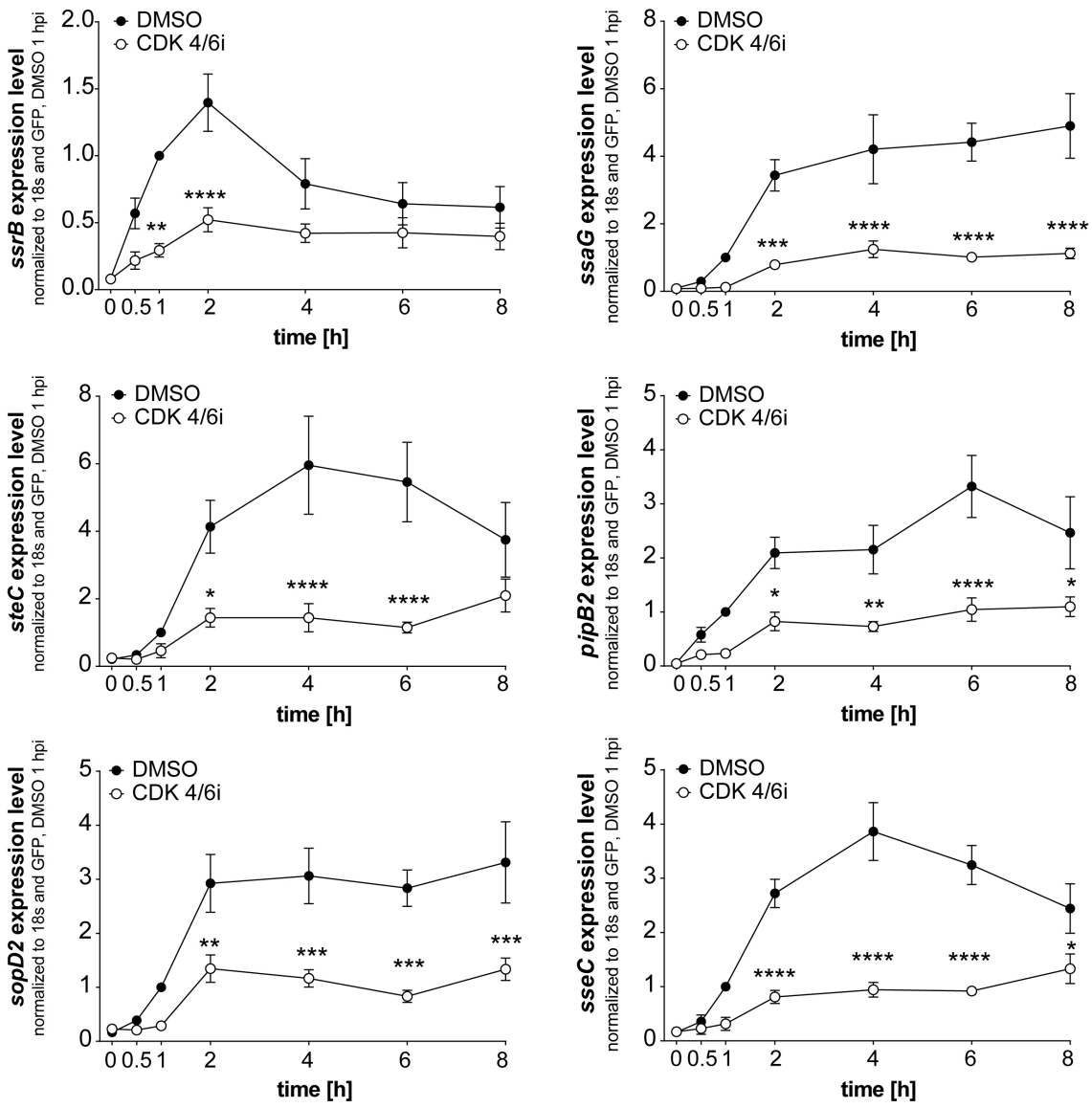

Fig. 21 Endogenous expression levels of SPI-2 genes in G1 arrested HeLa 229 cells are reduced

HeLa 229 cells were infected with *Salmonella*-GFP (MOI 25) and samples were prepared for qRT-PCR. Data were normalized to 18s and *Salmonella* GFP at 1 hpi DMSO. Results are shown as mean ± s.e.m. of 5 individual experiments; two-way ANOVA between DMSO and CDK 4/6i for each time point: *p≤0.05, **p≤0.01, ***p≤0.001, ****p≤0.0001.

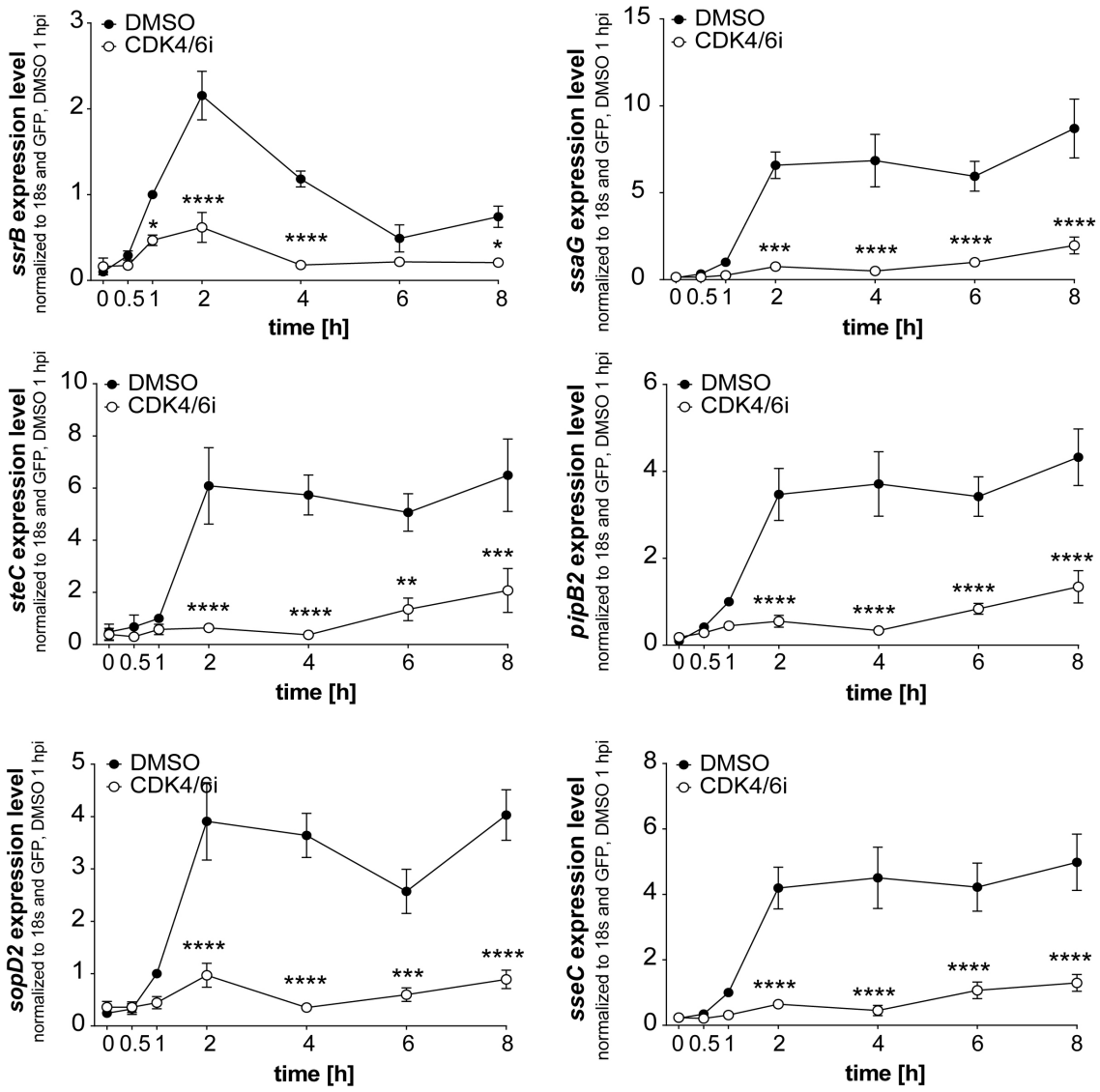

Fig. 22 Endogenous expression levels of SPI-2 genes in G1 arrested HCT8 cells are reduced

HCT8 cells were infected with *Salmonella*-GFP (MOI 25) and samples were prepared for qRT-PCR. Data were normalized to 18s and *Salmonella* GFP at 1 hpi DMSO. Results are shown as mean ± s.e.m. of at least 4 individual experiments; two-way ANOVA between DMSO and CDK 4/6i for each time point: *p≤0.05, **p≤0.01, ***p≤0.001, ****p≤0.0001.

2.2.3 SPI-2 effectors proteins are not expressed in G1 arrested cells

Quantitative RT-PCR results showed that the mRNA expression of SPI-2 effectors is considerably reduced in G1 arrested cells. Consequently, the amount of SPI-2 effector proteins should be reduced as well. In order to test this, HeLa 229 cells were infected with *Salmonella* strains harboring Flag-tagged SsrB, SteC or PipB2 for Western blot analysis. At 2 hpi, SsrB was already detected in control cells and its levels increased continuously until 6 hpi. However, in G1 arrested cells, levels of SsrB at 2 hpi were 5-fold lower and did not increase during the time course [Fig. 23 A, B], which is in agreement with the reduced gene expression level [Fig. 21]. In control cells, protein levels of the SPI-2 effectors, SteC and PipB2 were hardly detectable at 2 hpi but increased considerably, while protein levels in G1 arrested cells were 2 to 7-fold lower at 2 hpi and remained low throughout the time course [Fig. 23 C-F].

Western blot analysis of infected HCT8 cells showed a similar result. In control cells, SsrB, SteC and PipB2 were already detectable at 2 hpi and increased steadily (except for SsrB, which decreased again after 4 hpi). In G1 arrested cells, SsrB was reduced 1.6-fold at 2 hpi and remained low. SteC and PipB2 were reduced by 3.5 or 9-fold at 2 hpi. Protein levels for both effectors increased more than in G1 arrested HeLa 229 [Fig. 23], resulting in a protein band almost as strong as in control cells [Fig. 24 A-F]. However, intracellular replication of *Salmonella*, particularly at 4-6 hpi in G1 arrested HCT8, has to be taken into account and thus GroEL was used to normalize *Salmonella* replication levels in the different conditions. Quantitative analysis eventually showed that SPI-2 protein levels in G1 arrested HCT8 cells are decreased to a similar extent as in HeLa 229 cells.

Taken together, Western blot analysis of SsrB, SteC and PipB2 showed reduced protein levels in G1 arrested HeLa 229 and HCT8 cells, which is in agreement with their transcript levels, analyzed by qRT-PCR. Overall, microscopy, flow cytometry, qRT-PCR and Western blot analysis conclusively reveal that SPI-2 activation is significantly impaired upon G1 arrest.

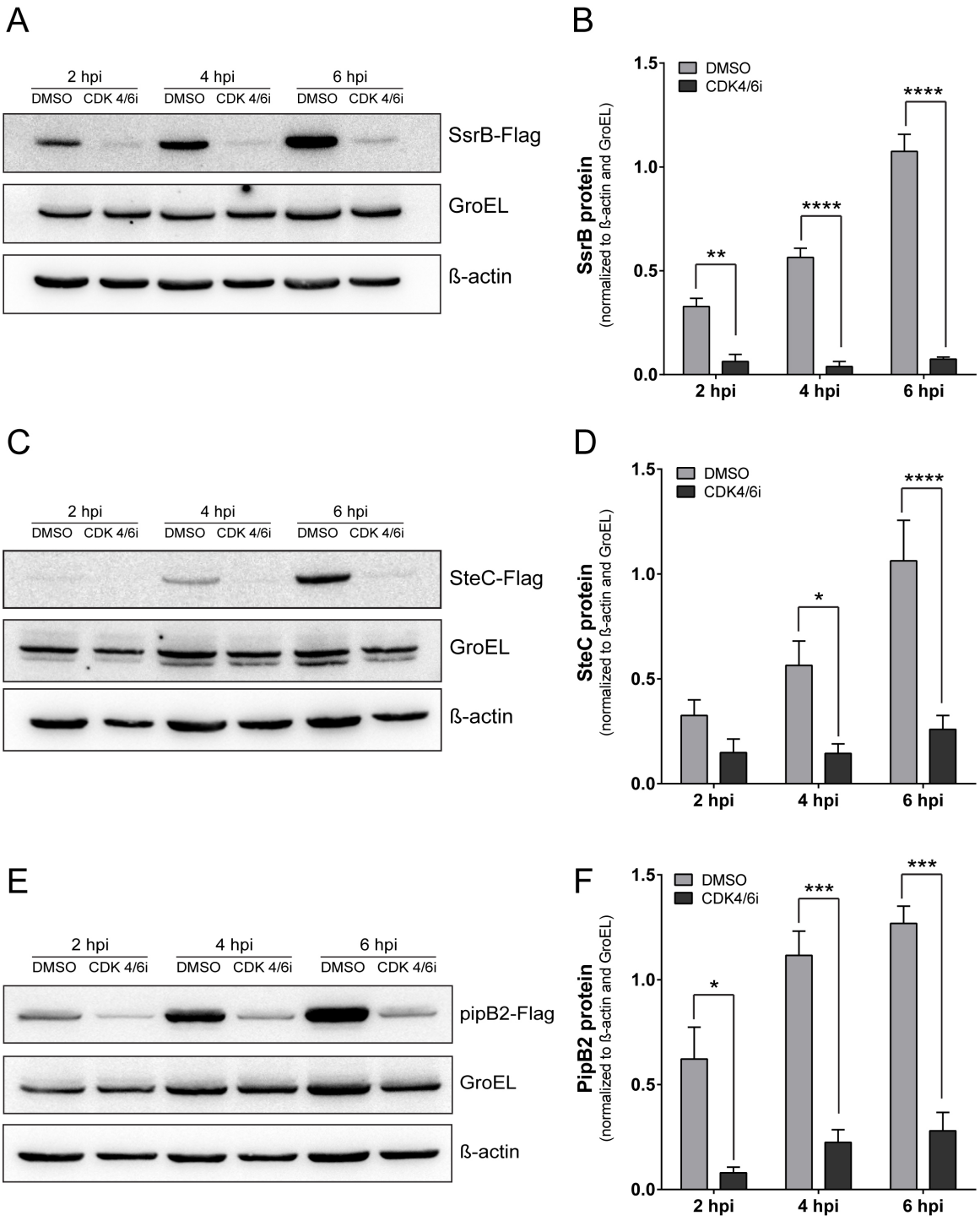

Fig. 23 SPI-2 proteins are not expressed in G1 arrested HeLa 229

HeLa 229 cells were infected with *Salmonella* strains harboring Flag-tagged (A) ssrB, (C) steC or (E) pipB2 (MOI 100) and samples were processed for Western blot at 2, 4 and 6 hpi. (B, D, F) Quantification of Western blot analysis, normalized to GroEL and ß-actin. Results are shown as mean ± s.e.m. of 3 (SsrB) or 5 (SteC and PipB2) individual experiments; two-way ANOVA: *p≤0.05, **p≤0.01, ***p≤0.001, ****p≤0.0001.

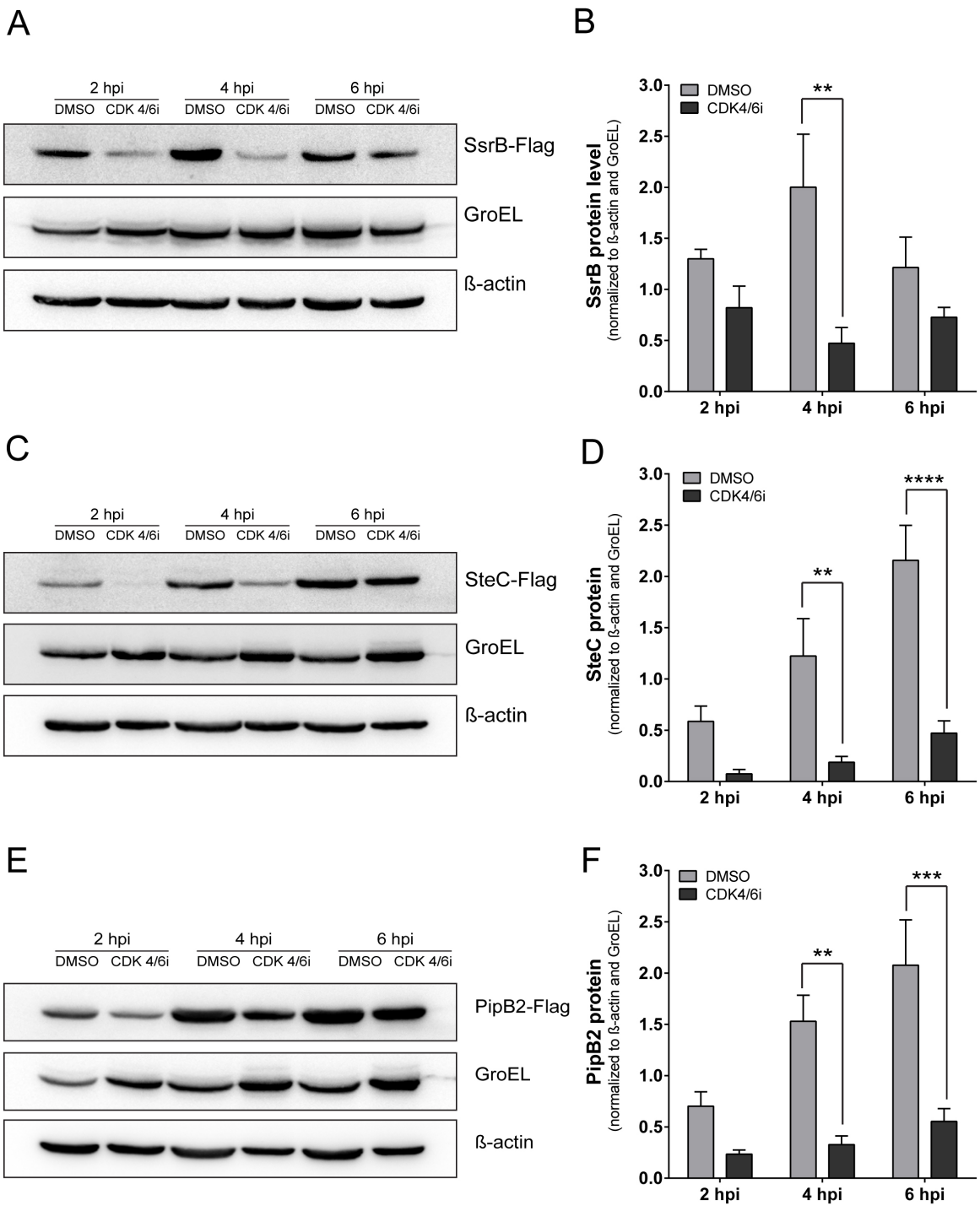

Fig. 24 SPI-2 proteins are not expressed in G1 arrested HCT8

HCT8 cells were infected with *Salmonella* strains harboring Flag-tagged (A) ssrB, (C) steC or (E) pipB2 (MOI 100) and samples were processed for Western blot at 2, 4 and 6 hpi. (B, D, F) Quantification of Western blot analysis, normalized to GroEL and ß-actin. Results are shown as mean ± s.e.m. of 3 (SsrB) or 5 (SteC and PipB2) individual experiments; two-way ANOVA: *p≤0.05, **p≤0.01, ***p≤0.001, ****p≤0.0001.

2.2.4 SPI-1 activity is sustained in G1 arrested cells

Salmonella infection is characterized by the sequential activity of two pathogenicity islands, SPI-1 and SPI-2. The SPI-1 system is required for host cell invasion by inducing the formation of actin ruffles and uptake of bacteria into phagosomal vacuoles. Once inside, *Salmonella* shuts off SPI-1 and concurrently activates SPI-2 (45)(133)(134). Results so far revealed that *Salmonella* did not activate SPI-2 in G1 arrested cells, which raised the question whether SPI-1 was still activated. To answer that question, two SPI-1 effectors, SopE and SptP were investigated exemplarily. SopE is a guanine nucleotide exchange factor, that activates CDC42 and RAC1 leading to actin cytoskeleton rearrangements and membrane ruffling (135), and also targets Rab5 to recruit early endosomes to the SCV (49). SptP is a tyrosine phosphatase and has GTPase activating protein (GAP) activities. After bacterial internalization, it reverts cytoskeletal changes induced by SopE. Both secreted effectors are rapidly degraded by the host proteasome, with SopE being degraded faster than SptP (51).

HeLa 229 cells were infected with *Salmonella* and mRNA levels of *sopE* and *sptP* were determined by qRT-PCR. In G1 arrested cells, *sopE* expression levels were slightly higher than in control cells at the earliest measured time point (0 hpi, which is 30 min after the first contact of bacteria and host cells). In both, G1 arrested and control cells, *sopE* expression decreased over time [Fig. 25 A]. *SptP* expression was equal in G1 arrested and control cells at 0 hpi and remained constant for additional 30 min in G1 arrested cells, before it decreased. At later stages of infection (6-8 hpi) a slight increase was observed, while expression in control cells was shut off [Fig. 25 B].

In order to determine the corresponding SPI-1 protein levels, HeLa 229 cells were infected with SopE- or SptP-flag tagged *Salmonella*. Interestingly, protein levels for both effectors were higher in G1 arrested cells at all times. However, taking into consideration that both effectors should be rapidly degraded by the host proteasome (51), and that gene expression levels equally decreased in G1 arrested and control cells, one would expect SopE or SptP proteins to equally decline, too. Yet surprisingly, SopE levels in G1 arrested cells even increased until 2 hpi, before they dropped again to their initial levels. This finding indicates that besides increased bacterial expression an

additional factor, e.g. reduced degradation, leads to a higher protein level of SopE. SptP levels in G1 arrested cells declined gradually, but always remained higher than in control cells [Fig. 25 C, D].

Infection of G1 arrested HCT8 cells revealed a 2-fold higher gene expression of *sopE* and *sptP* at 0 hpi and levels increased even more at 0.5 hpi. Afterwards expression dropped drastically approaching levels in control cells [Fig. 26 A, B]. Western blot analysis for SopE and SptP resulted in much higher protein levels in G1 arrested cells at all time points. But while SptP decreased gradually, SopE increased until 2 hpi [Fig. 26 C, D]. Again, this indicates possible reduced degradation of the effector molecules by the host proteasome and/or higher bacterial SPI-1 expression in G1 arrested cells.

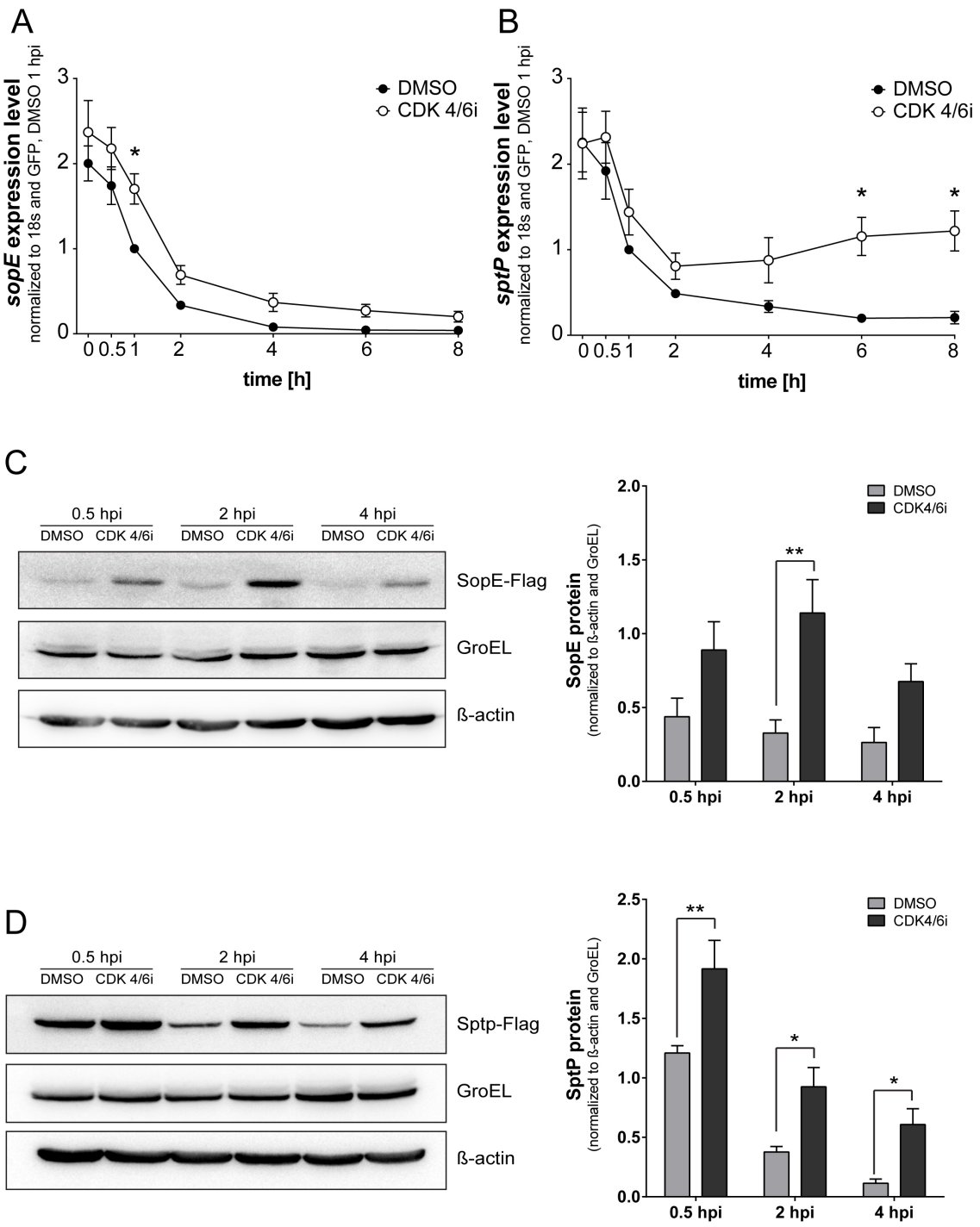

Fig. 25 SPI-1 effector levels are sustained in G1 arrested HeLa 229

(A) *sopE* or (B) *sptP* expression determined after infection of HeLa 229 (MOI 25), data were normalized to 18s and *Salmonella* GFP at 1 hpi DMSO. (C) Western blot and quantification of HeLa 229 infected with *Salmonella* SopE-Flag (MOI 100). (D) Western blot and quantification of HeLa 229 infected with *Salmonella* SptP-Flag (MOI 100). Protein levels were normalized to GroEL and ß-actin. Results are shown as mean ± s.e.m. of at least 5 individual experiments; two-way ANOVA: *p≤0.05, **p≤0.01.

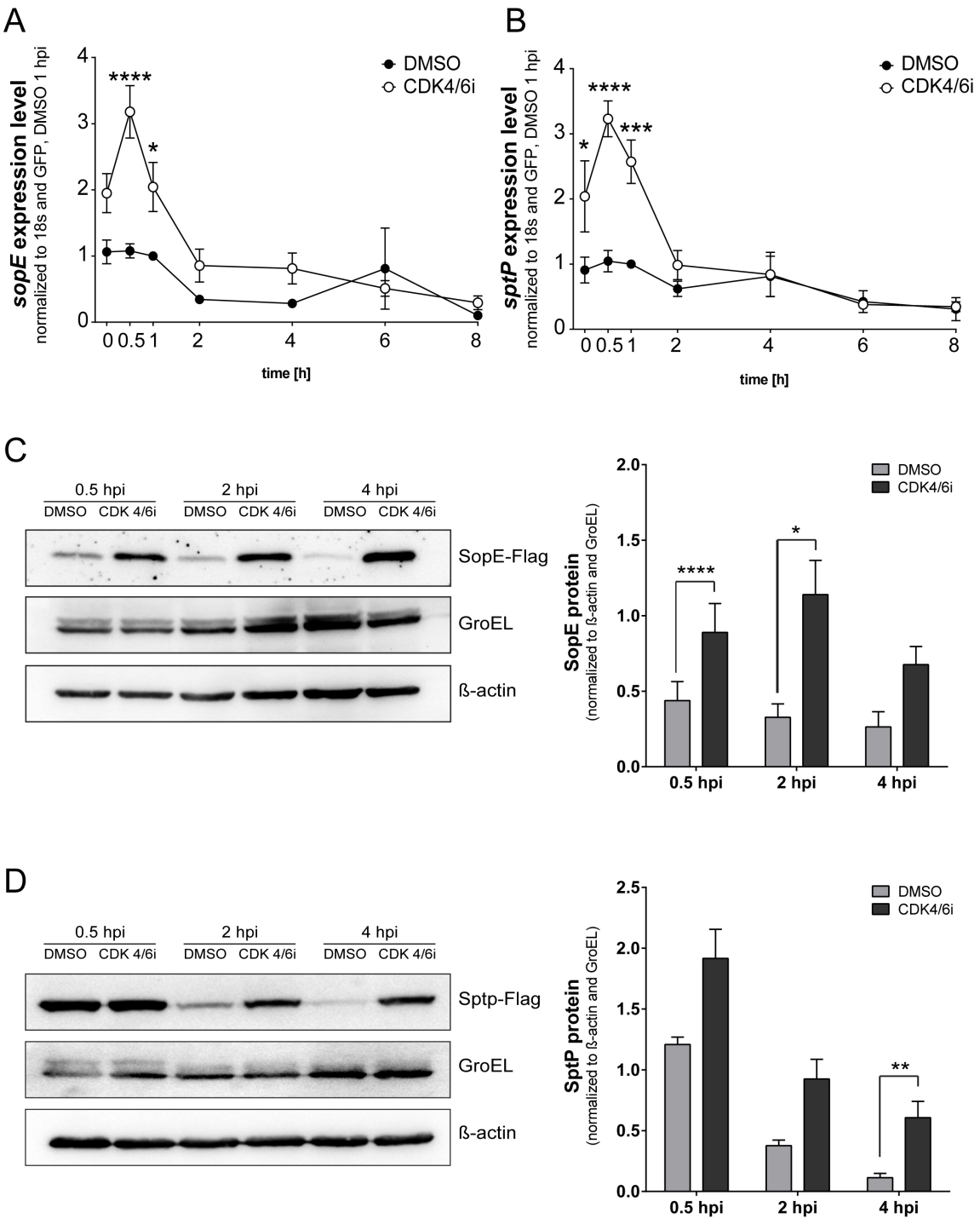

Fig. 26 SPI-1 effectors levels are sustained in G1 arrested HCT8

(A) *sopE* or (B) *sptP* expression determined after infection of HCT8 (MOI 25), data were normalized to 18s and *Salmonella* GFP at 1 hpi DMSO. (C) Western blot and quantification of HCT8 infected with *Salmonella* SopE-Flag (MOI 100). (D) Western blot and quantification of HCT8 infected with *Salmonella* SptP-Flag (MOI 100). Protein levels were normalized to GroEL and ß-actin. Results are shown as mean ± s.e.m. of at least 5 individual experiments; two-way ANOVA: *p≤0.05, **p≤0.01, ***p≤0.001, ****p≤0.0001.

2.2.5 Proteasomal degradation of SPI-1 effectors is delayed in G1 arrested cells

Results so far show that SopE levels remain increased in G1 arrested cells compared to control cells, which could be caused by increased or prolonged bacterial synthesis or impaired degradation by the host, or both. In order to further address this question another approach was taken and proteasomal degradation of SopE was inhibited in control and G1 arrested cells, by the proteasomal inhibitor MG132.

If bacterial synthesis of SopE was the same in control and G1 arrested cells, and the variation of protein levels were caused by different proteasome activities, treatment with MG132 should eliminate this effect and result in equal protein levels in G1 arrested and control cells. However, upon MG132 treatment, SopE protein levels remained higher in G1 arrested HeLa 229 cells compared to the control, hinting towards increased or prolonged bacterial SopE synthesis [Fig. 27 A]. At 0.5 hpi SopE protein levels were equally different between G1 arrested and control cells with or without MG132 treatment (compare DMSO vs. CDK4/6i = 1.9-fold and DMSO+MG132 vs. CDK4/6i+MG132 = 1.8-fold) [Fig. 27 B]. In MG132 treated cells, this ratio remained similar at 2 hpi and 4 hpi (1.5 or 1.7-fold, respectively), which is also shown by graphs in [Fig. 27 C], where SopE protein levels follow a parallel course in control and G1 arrested cells (open triangle and circle). In addition, the data also reveal that the degradative capacity of the host proteasome in G1 arrested HeLa 229 cells must be reduced as well. Because, if proteasomal degradation was equally efficient in control and G1 arrested cells, then SopE protein levels should decline similarly. However, they did not. Proteasomal degradation of SopE in control cells occurred rapidly, so that SopE levels were already very low at 0.5 hpi and hardly detectable at later time points [Fig. 27 A-C]. In contrast, SopE levels in G1 arrested cells were not only higher at 0.5 hpi, but even increased at 2 and 4 hpi (filled triangle). If proteasomal degradation would be equally efficient in G1 arrested cells and in control cells, SopE levels would follow a parallel, decreasing course. Overall, this shows that the prolonged presence of SopE in G1 arrested cells is presumably caused by a combination of (i) increased bacterial expression and (ii) reduced proteasomal degradation.

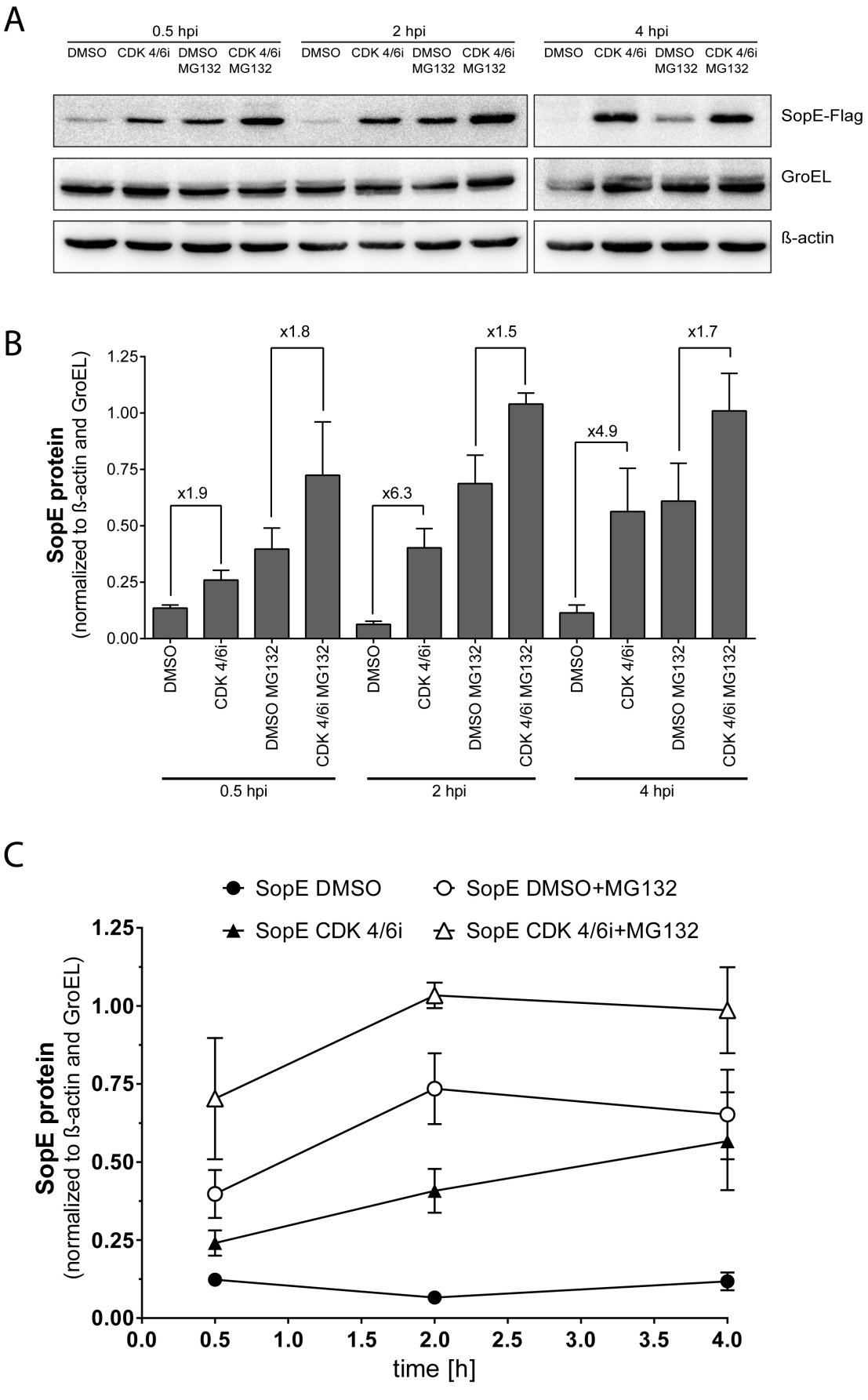

figure legend on next page

Fig. 27 Proteasomal degradation of bacterial SPI-1 effector SopE is reduced in G1 arrested HeLa 229

(A) Western blot of HeLa 229 infected with *Salmonella* SopE-Flag (MOI 100). MG132 was applied 3 hrs prior and during infection (B) Quantification of SopE Protein levels (C) SopE protein levels. Results are shown as mean ± s.e.m. of 5 individual experiments.

The same approach was applied to HCT8 cells [Fig. 28 A]. At 0.5 hpi approximately 4 times more SopE protein was detected in G1 arrested cells, independent of proteasomal activity (DMSO vs. CDK4/6i = 3.6-fold and DMSO+MG132 vs. CDK4/6i+MG132 = 4.3-fold) [Fig. 28 B]. In control cells treated with MG132 (open circles), SopE levels were constantly increasing, indicating ongoing bacterial synthesis. In G1 arrested cells, the SopE protein levels were almost at the maximum already at 0.5 hpi and increased only slightly at 2 hpi and 4 hpi [Fig. 27 C]. Again, if bacterial synthesis would be the same in G1 arrested and control cells, SopE levels should be on an equal level after blocking degradation by MG132. Together with the increased *sopE* mRNA expression level [Fig. 26] it indicates increased bacterial expression in G1 arrested HCT8 cells.

Additionally, the data also confirmed that proteasomal degradation must be impaired in HCT8 cells. As mentioned above, SopE protein levels were constantly increasing when proteasomal degradation was blocked in control cells. In contrast, without inhibition of proteasomal activity, SopE was degraded so efficiently, that it was hardly detectable, despite the ongoing synthesis (filled circles). Upon G1 arrest, degradation was less efficient, though not completely impaired, so that SopE levels did not decrease as fast as in control cells, but also did not reach the level of G1 arrested cells after MG132 treatment [Fig. 28 C]. This shows that proteasomal degradation in G1 arrested HCT8 is also reduced but not completely abolished.

Together, protein levels of SopE, a SPI-1 effector, is higher in HeLa 229 and HCT8 upon G1 arrest, presumably resulting from a combination of increased bacterial synthesis and reduced proteasomal degradation.

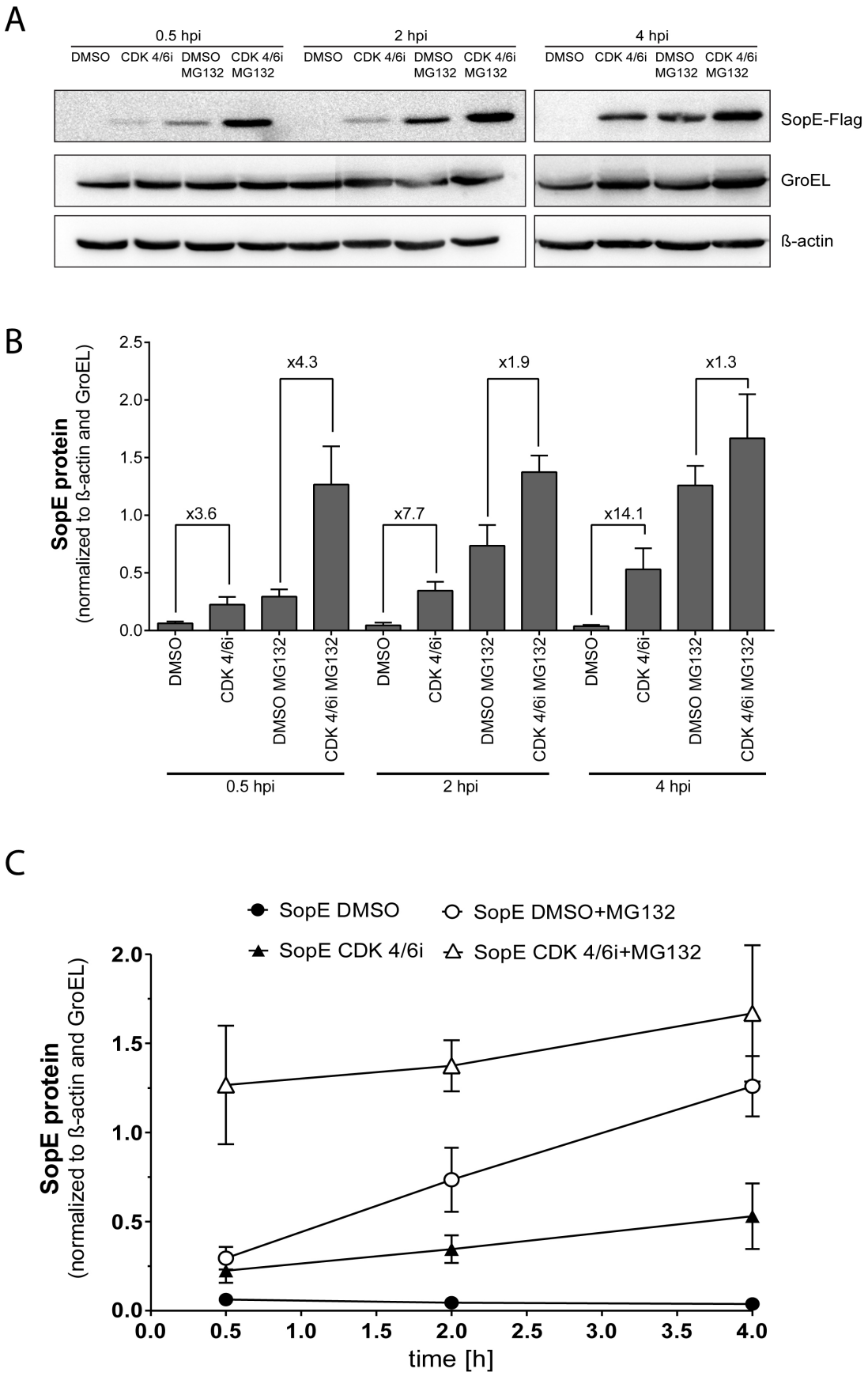

figure legend on next page

Fig. 28 Proteasomal degradation of bacterial SPI-1 effector SopE is delayed in G1 arrested HCT8

(A) Western blot of HCT8 infected with *Salmonella* SopE-Flag (MOI 100). MG132 was applied 3 hrs prior and during infection (B) Quantification of SopE Protein levels (C) Quantification of SopE Protein levels. Results are shown as mean ± s.e.m. of 6 individual experiments.

2.2.6 Lovastatin-induced G1 arrest impairs SPI-2 activation

Arresting host cells in G1 phase of the cell cycle by inhibiting the cyclin dependent kinases 4 and 6 affected maturation of the *Salmonella* containing vacuole, with detrimental effects for the bacteria. In order to confirm that maturation of the SCV depends on the cell cycle state of host, the cells were arrested indirectly in G1 phase by lovastatin. Lovastatin, an inhibitor of 3-hydroxy-3-methylglutaryl-CoA (HMG-CoA) reductase is usually used to treat hypercholesterolemia, because it prevents the reduction of HMG-CoA to mevalonate and thus becomes the rate limiting step in cholesterol biosynthesis (136)(137). Several studies have shown that lovastatin treatment does not only reduce the cholesterol content of cells, but also arrests them in G1 phase (138)(139). The full mechanism of G1 arrest by lovastatin is still not fully resolved, but it was shown that addition of mevalonate released cells from lovastatin-induced G1 arrest (140).

Addition of lovastatin to HeLa 229 cells resulted in an arrest in the G1 phase [Fig. 29 A]; comparable to what was observed after CDK4/6i treatment [Fig. 11 A]. Infection of lovastatin treated cells with *Salmonella* revealed that intracellular replication was reduced [Fig. 41 B]. This reduction is explained by less SPI-2 positive bacteria (DMSO=64% vs. lovastatin = 33%) and a lower SPI-2 activation level within this population (MFI GFP) [Fig. 29 C]. These results clearly showed that SPI-2 activation and subsequent intravacuolar replication of *Salmonella* was impaired upon lovastatin induced G1 arrest.

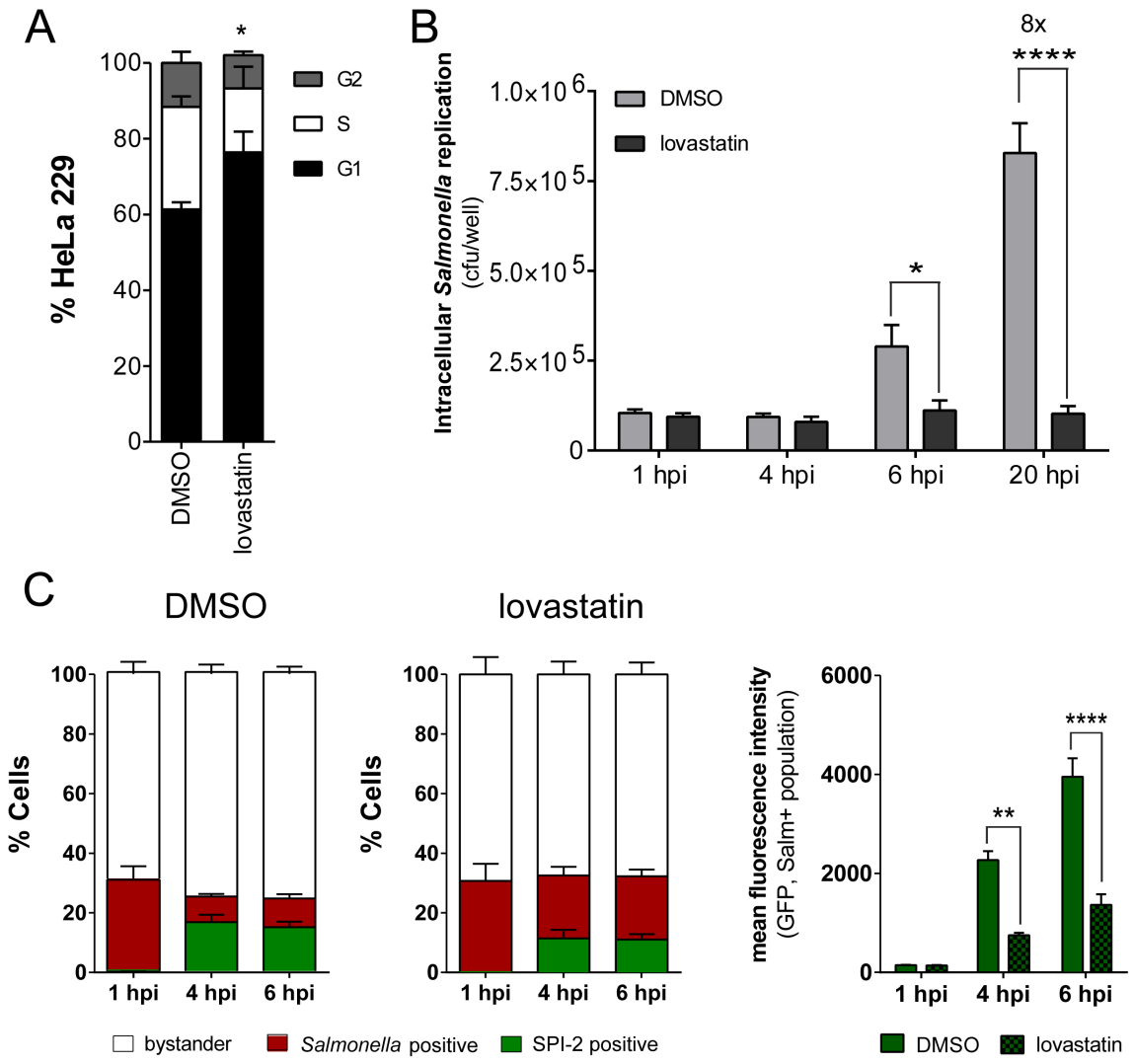

Fig. 29 Lovastatin induced G1 arrest impairs intracellular *Salmonella* replication in HeLa 229 cells

(A) Quantification of various cell cycle stages in control cells or after treatment with lovastatin (20µM) for 20 hrs (B) CFU quantification after infection with *Salmonella* (MOI 25). (C) Quantification of flow cytometry analysis of lovastatin treated cells infected with the *Salmonella* reporter strain and mean fluorescence intensity (MFI GFP) of the SPI-2 positive fraction of cells, indicating the SPI-2 activation level. Results are shown as mean ± s.e.m. of 5 individual experiments; two-way ANOVA: *p≤0.05, **p≤0.01, ***p≤0.001, ****p≤0.0001.

Taken together, results so far demonstrated that after invasion of mock-treated host cells *Salmonella* switched "off" SPI-1 expression and activated SPI-2 expression (ca. 0.5 hpi). Subsequently, SPI-2 effector proteins were synthesized and levels increased significantly (1 hpi - 2 hpi). In parallel, bacterial SPI-1 effectors were efficiently degraded by the host proteasome leading to a rapid reduction of overall SPI-1 protein levels. In contrast, upon G1 arrest of host cells, *Salmonella* SPI-1 mRNA levels were initially higher but otherwise decreased in the same way as in non-arrested cells. Proteasomal degradation of the SPI-1 effector SopE was reduced. Both contributed to prolonged presence of SPI-1 proteins in host cells. Simultaneously, SPI-2 activation was impaired and thus effectors, required to stabilize and modify the SCV were not secreted. Without the necessary modifications, *Salmonella* could not establish a protective niche to replicate inside host cells for a longer time course of infection. As consequence of prolonged SPI-1 activity and reduced SPI-2 activity, cytoplasmic replication of *Salmonella*, which usually comprises only 5-10% of the total population, was significantly promoted in a cell specific manner.

2.3 Endolysosomal trafficking is dysregulated in G1 arrested cells

Maturation of the SCV is closely connected to the endolysosomal trafficking pathway in host cells. After invasion, the newly formed vacuole fuses with early endosomes and undergoes endosome-like maturation steps in which it acquires late endosomal and lysosomal markers (15). In G1 arrested cells, long-term replication of *Salmonella* was impaired, raising the question of whether the endosomal pathway of host cells was functional. To answer this, endolysosomal trafficking of G1 arrested cells was analyzed.

2.3.1 G1 arrested mammalian cells accumulate endolysosomal vesicles

Arresting mammalian cells in G1 phase of the cell cycle led to a remarkable accumulation of intracellular vesicles. These vesicles were visible in brightfield microscopy, and transmission electron microscopy revealed the electron dense nature of the vesicles [Fig. 30 A, B]. The observed multivesicular and multilamellar structure of these organelles is characteristic for late endosomes (LE) and lysosomes (Lys) (15). Thus, to characterize the vesicles in more detail, typical membrane proteins of endosomes and lysosomes were analyzed by immunofluorescence. Early endosomal antigen 1 (EEA1) is a marker protein for early endosomes, Ras-related protein Rab-7 (Rab7) is found on late endosomes and lysosomal associated protein 1 (Lamp1) was used as a maker for lysosomes. Interestingly, distribution of vesicles labelled for the different markers was different in G1 arrested cells when compared to control cells. While early endosomes usually distribute homogenously all over the cytoplasm, they accumulated to large and distinct areas in G1 arrested cells. LE and Lys usually locate closer to the nucleus but are also finely dispersed (15). In G1 arrested cells however, their number seemed to be increased and they accumulated in the perinuclear region [Fig. 31 A]. The increase of vesicles with endolysosomal markers hinted at an increased production of these organelles in G1 arrested cells, which was addressed by Western blot quantification. Surprisingly, the total amount of protein (EEA1, Rab7 and Lamp1) was not significantly different in G1 arrested or control cells [Fig. 31 B], even though Lamp1 levels were slightly higher than in control cells. This clearly showed that instead

of forming a higher number of small evenly dispersed structures, these organelles were rather merged and “swollen” as has been described before (141). Collectively, this indicated that fusion and fission events of endosomal structures in G1 arrested cells were impaired, but there was not an overall increase of endolysosomal membrane proteins.

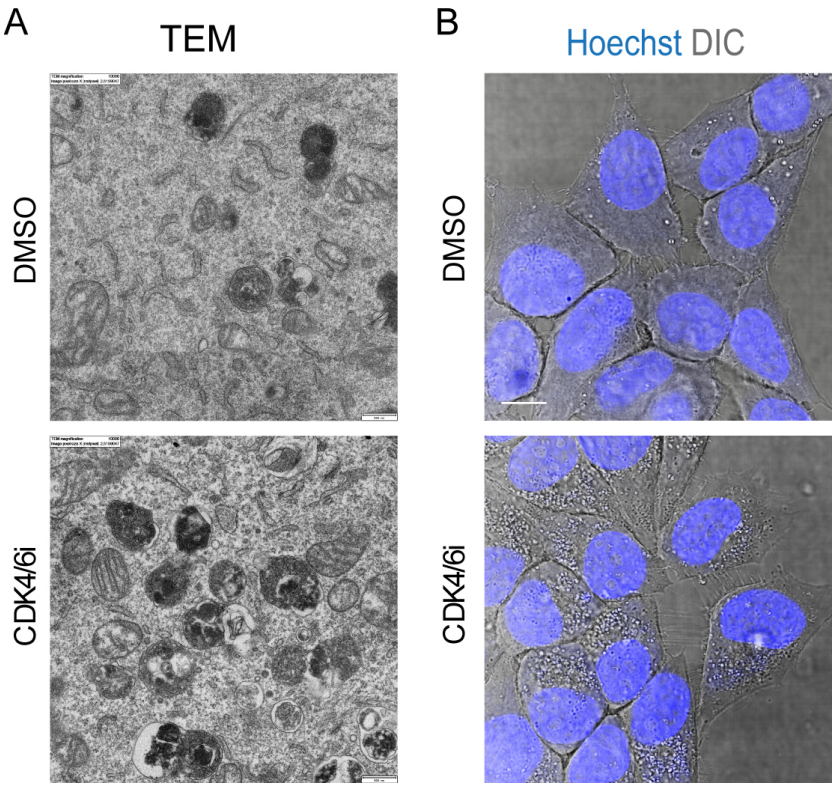

Fig. 30 G1 arrested HeLa 229 cells accumulate intracellular vesicles

(A) Representative transmission electron microscopy images of HeLa 229 cells treated with DMSO or CDK4/6i (sample preparation by EM facility University Würzburg, images acquired by A. Eulalio in a Zeiss EM10 TEM). Scale bar = 0.5 µm (B) Differential interference contrast microscopy (DIC) of HeLa 229 cells, nuclei are stained with Hoechst. Scale bar = 10 µm.

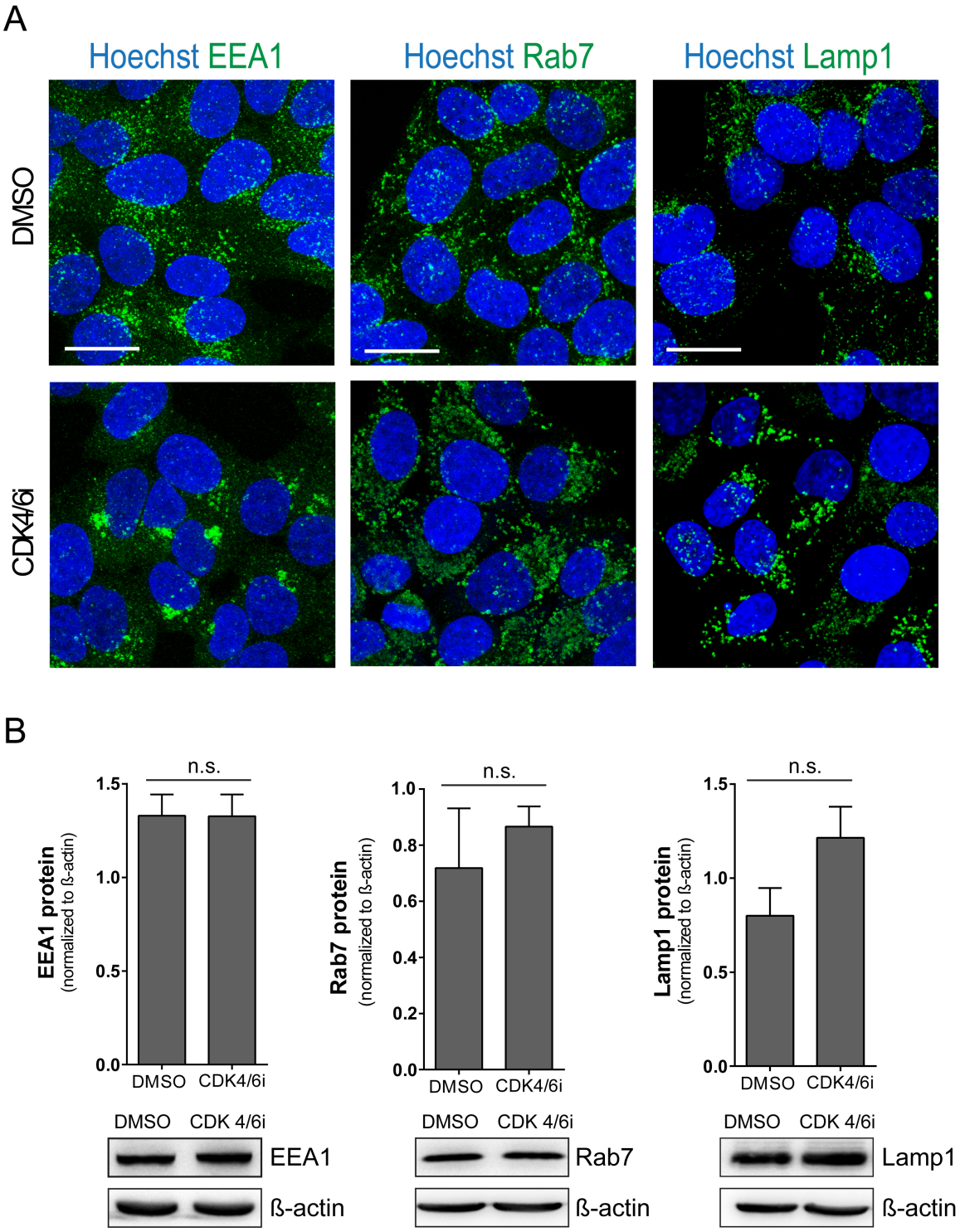

Fig. 31 Endolysosomal vesicles are abnormally distributed in G1 arrested HeLa 229 cells

(A) Representative images of HeLa229 cells labeled for endolysosomal marker proteins. EEA1, early endosomes; Rab7, late endosomes; Lamp1, lysosomes. (B) Western blot quantification of EEA1, Rab7 and Lamp1 in G1 arrested HeLa 229 cells. Results are shown as mean ± s.e.m. of 3-5 individual experiments. n.s. = non-significant. Scale bar = 10 µm

2.3.2 Lysosomal activity is impaired in G1 arrested HeLa 229 cells

Since the distribution and location of endolysosomes is indistinguishable from their functionality (15) (142), (endo-) lysosomal activity was tested in G1 arrested cells with the DQ-Red BSA trafficking assay. DQ-Red BSA is a derivative of bovine serum albumin (BSA), which is conjugated to a fluorophore (and therefore quenched). Proteolysis of the BSA conjugates results in dequenching of the fluorophore and can be monitored by microscopy or flow cytometry. G1 arrested and control cells were fed with DQ-Red BSA and activation of the fluorophore was analyzed. Microscopy images as well as flow cytometry data showed a significant reduction of the fluorophore signal, in G1 arrested cells [Fig. 32 A, B]. Chloroquine and NH_4Cl were used as controls because both increase lysosomal pH and therefore inhibit activity of lysosomal hydrolases (125) (143) (144). The reduction of a fluorophore signal in G1 arrested cells clearly shows that proteolytic cleavage of the substrate was impaired, indicating impaired lysosomal activity.

In order to confirm this, endogenous levels of Cathepsin D were measured. Cathepsin D (CTSD) is an aspartic protease found in different forms in human cells. The first form is a diglycosylated precursor (pro-CTSD, 53 kDa) and mainly occurs in the Golgi complex. Once it reaches the endosome, the inhibitory pro-peptide is cleaved, and CTSD forms a single chain intermediate (48 kDa). Further processing to a double chained mature form (33 kDa) occurs in lysosomes (145). Western blot analysis of Cathepsin D revealed an accumulation of pro-CTSD and the intermediate form in G1 arrested cells, while the double chained mature form was slightly reduced [Fig. 32 C]. This shows reduced processing of proteases to lysosomes, which does not solely explain but at least contribute to the impaired lysosomal function.

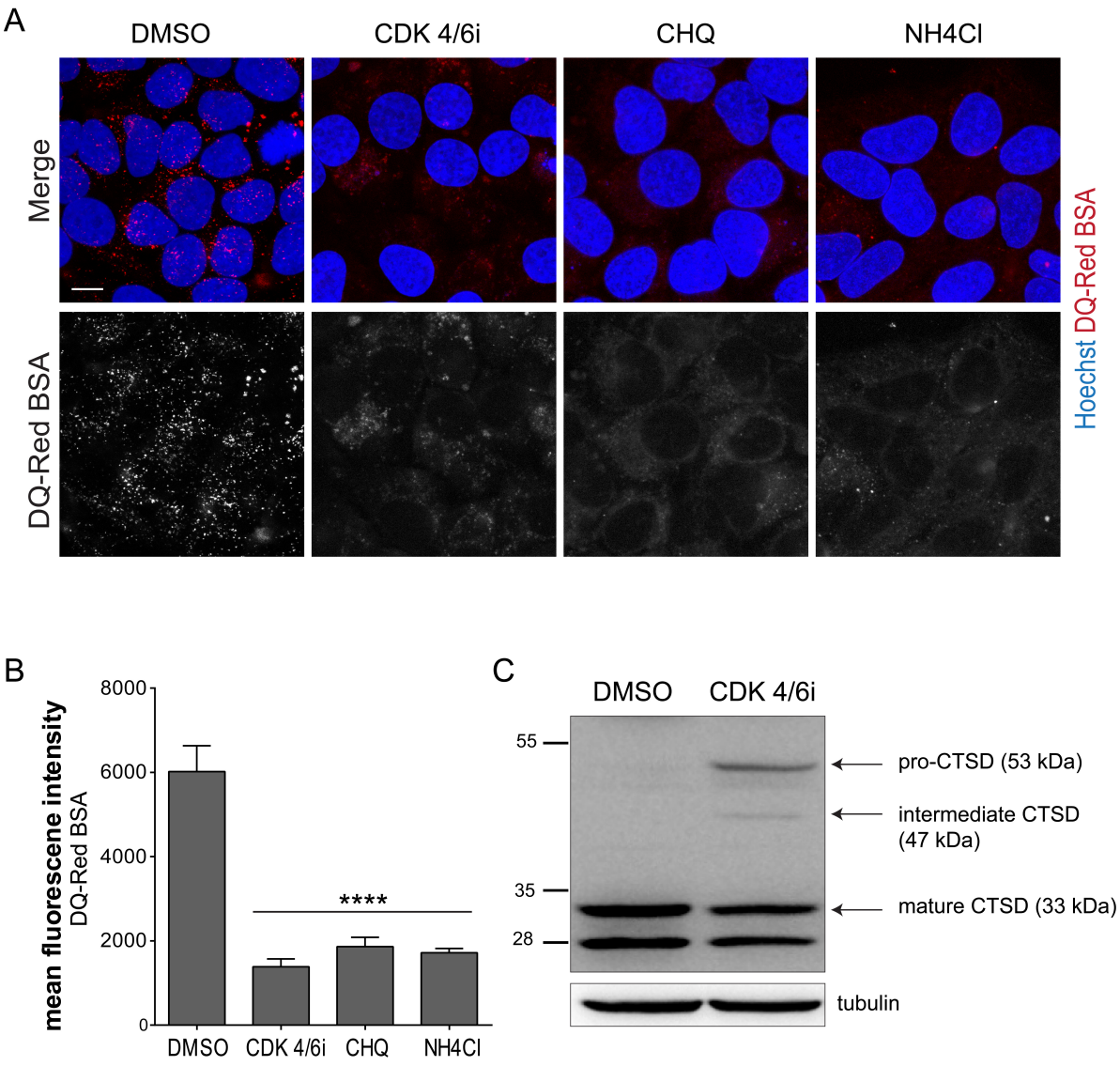

Fig. 32 Lysosomal activity is impaired in G1 arrested HeLa 229 cells

(A) Representative microscopy of HeLa 229 after addition of DQ-Red BSA for 5 hrs. Chloroquine (CHQ) and NH_4Cl were used as controls to inhibit lysosomal activity by raising lysosomal pH. DQ-Red BSA is quenched when fed to the cells and becomes fluorescent after hydrolytic cleavage in lysosomes, demonstrating lysosomal activity. Scale bar = 10 µm (B) Flow cytometry of HeLa 299 after addition of DQ-Red BSA for 5 hrs. Results are shown as mean ± s.e.m. of 5 individual experiments; unpaired t-test: ****p≤0.0001. (C) Representative Western blot for Cathepsin D. In G1 arrested cells the catalytically inactive precursor pro-Cathepsin D and the intermediate form can be found in addition to the mature form, which is slightly reduced. Tubulin is used as loading control.

2.3.3 Autophagy in G1 arrested HeLa 229 cells is compromised

Lysosomes are the final degradation machineries not only for endosomal cargo but also for autophagosomal content. Autophagosomes (AP) are formed after initiation of phagophores (PG) and subsequent elongation around the substrates. Fusion of APs with lysosomes leads to degradation of their intraluminal cargo and membrane structures. Upon activation of autophagy, LC-3B, a cytosolic marker protein, becomes lipidated to form LC-3B–phosphatidylethanolamine (LC-3B-PE or LC-3B II). LC-3B II is recruited to the PG membrane, where it remains associated with the AP until degradation. Afterwards, it is released into the cytoplasm again (LC-3B I). It is therefore used to label autophagocytic structures and to evaluate autophagocytic turnover in eukaryotic cells (22) (146).

Results so far showed reduced lysosomal activity in G1 arrested cells, which is why autophagosomal activity was assessed as well. Indeed, LC-3B staining showed a remarkable accumulation of APs in G1 arrested cells [Fig. 33 A]. However, it was not clear if the high number of APs was due to an increased initiation of autophagy and formation of APs or due to a block in degradation (or both). To address this, an autophagy flux assay was performed. In an autophagy flux assay the turnover of LC-3B II or more specifically, the amount of (lysosomal) degradation during a certain time period is determined (147). Therefore, the difference in amount of LC-3B-II is analyzed by Western blot before and after addition of CHQ. CHQ increases lysosomal pH and thus blocks degradation of autophagosomal content and membrane components, resulting in accumulation of LC-3B II.

Addition of CHQ to control cells for 3 hours blocked degradation of APs and led to a 5-fold increase of LC-3B II. This difference is indicative of the amount of autophagosomes that are delivered to lysosomes for degradation in that time (= basal autophagic activity) [Fig. 33 B]. Remarkably, LC-3B II levels in G1 arrested cells were already 15.5-fold higher before CHQ-treatment, confirming a strong accumulation of autophagosomes. After addition of CHQ to G1 arrested cells, LC-3B II levels did not increase significantly (1.2-fold), revealing that it was the final degradation step that was inhibited [Fig. 33 C]. If the high LC-3B II level would be caused by increased initiation of autophagy (e.g. due to starvation), treatment with CHQ would further increase LC-3B II

level. In addition, LC-3B I levels would be decreased. Of note, quantification of LC-3B I or of LC-3B II/ LC-3B I ratios is not recommendable, since antibodies are less sensitive to LC-3B I and rather tend to have a greater affinity to LC-3B II (147). Therefore, LC-3B I levels may vary and appear rather faint, depending on the antibody and the cell type and it is recommended to normalize LC-3B II to the housekeeping protein used (148).

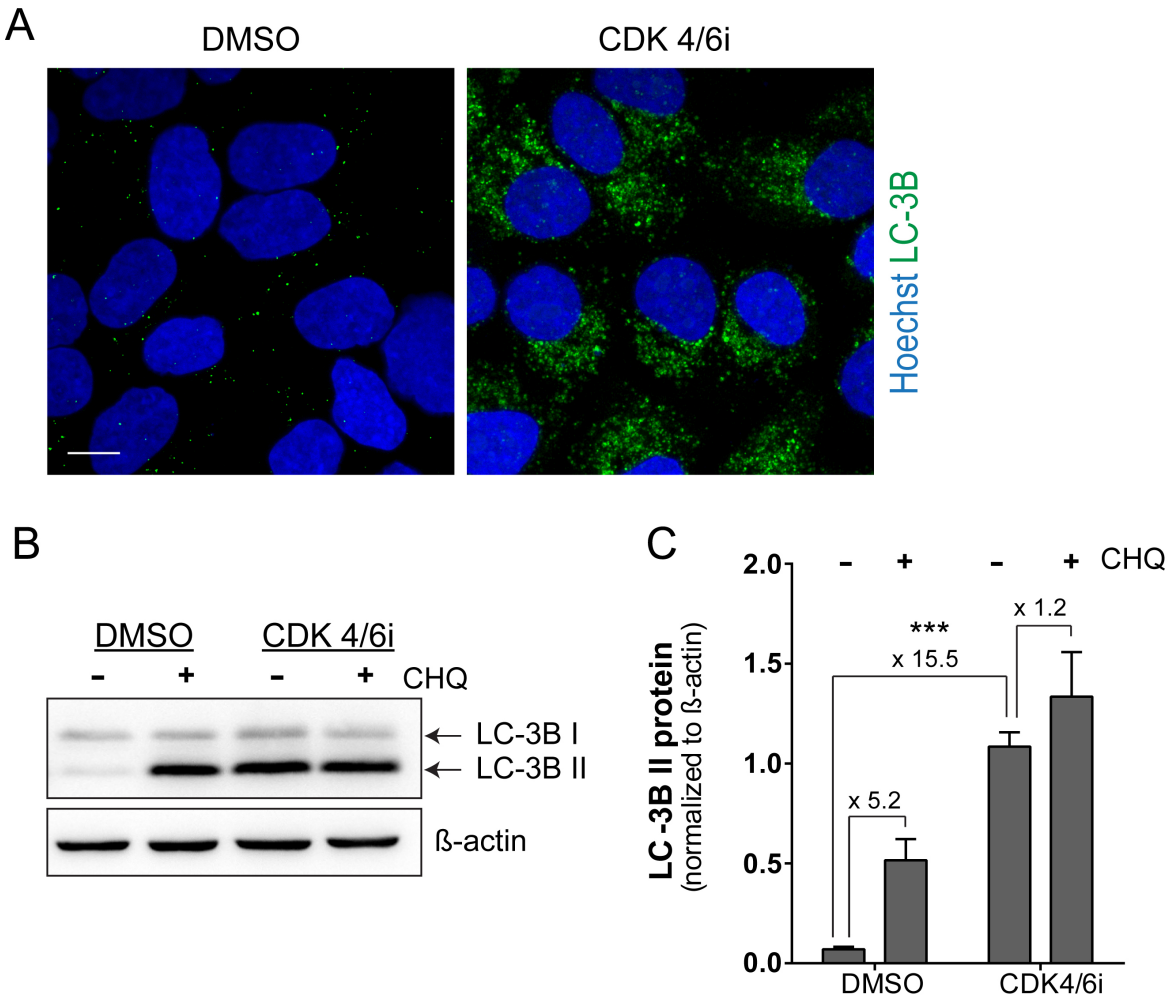

Fig. 33 Autophagy is compromised in G1 arrested HeLa 229 cells

(A) Representative microscopy images of HeLa 229. LC-3B antibody was used to label autophagosomes. (B) Western blot analysis of autophagy turnover. For each condition (control or G1 arrested) two wells were seeded. CHQ was added to one well for 3 hrs to inhibit lysosomal function and therefore degradation of autophagosomal content and membrane components, leading to accumulation of the conjugated form of LC-3B II. (C) Quantification of LC-3B II in control or G1 arrested cells after treatment with CHQ. Results are shown as mean ± s.e.m. of 5 individual experiments; two-way ANOVA: ***p≤0.001, Scale bar = 10 µm

2.3.4 The master regulator TFEB is activated in G1 arrested HeLa 229

The block of lysosomal degradation and strong accumulation of autophagosomes was an interesting phenomenon observed in G1 arrested host cells and initiated a closer assessment of the regulation of lysosomal biogenesis and autophagy. For both, the transcription factor EB (TFEB) plays an essential role. Under nutrient rich conditions and in the absence of stress TFEB is phosphorylated by mTORC1 and resides in the cytosol in an inactive state. Upon starvation or (lysosomal) stress, TFEB is dephosphorylated and rapidly translocates to the nucleus to activate transcription of genes related to lysosomal biogenesis and autophagy (31).

Immunofluorescence of TFEB in G1 arrested HeLa 229 cells, showed a significant translocation from the cytoplasm to the nucleus, which was comparable to the translocation after CHQ treatment that was used as control to induce lysosomal stress [Fig. 34 A]. TFEB of whole cell lysate of G1 arrested cells migrated slightly faster than TFEB of control cells, which was indicative of dephosphorylation as well [Fig. 34 B]. To confirm translocation of TFEB, nuclear and cytoplasmic fractions of control and G1 arrested cells were separated and analyzed by Western blot. Results showed that TFEB was in an inactive, cytoplasmic state in control cells, while G1 arrest or CHQ treatment caused activation and translocation of TFEB into the nucleus [Fig. 34 C]. Together these results show that upon lysosomal stress in G1 arrested cells, TFEB is activated and since it is a regulator of autophagy and lysosomal biogenesis, the translocation presumably contributes to the initiation of autophagosome formation.

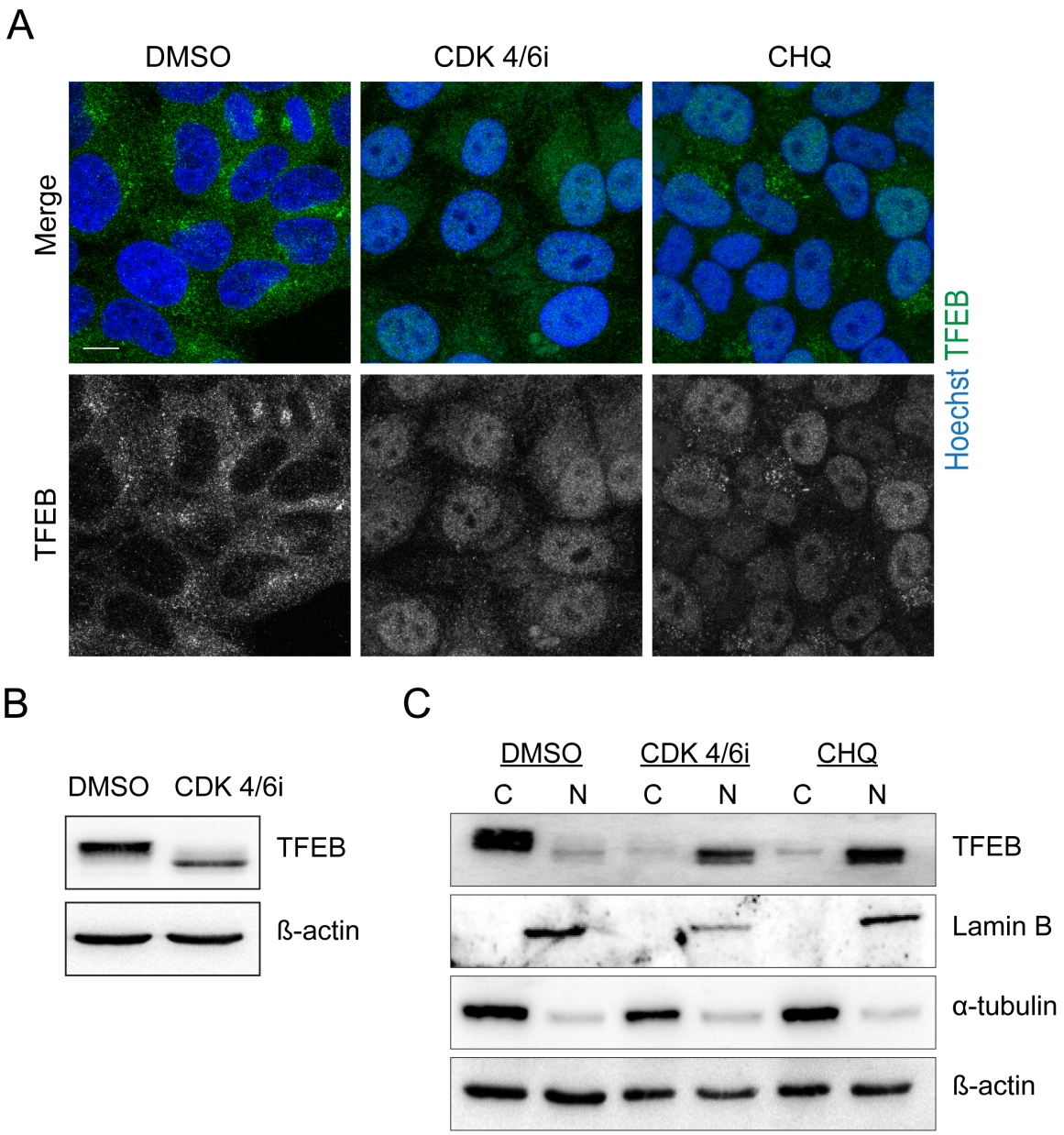

Fig. 34 Upon G1 arrest the transcription factor EB (TFEB) translocates to the nucleus

(A) Representative microscopy images of HeLa 229 treated with CDK4/6i (16 hrs) to induce G1 arrest or CHQ (3 hrs) to induce lysosomal stress. (B) Western blot analysis of TFEB in whole cell lysate. (C) Western blot for TFEB after separation of nuclear (N) and cytoplasmic (C) fractions of HeLa 229 cells. Lamin B is used as a marker for the nuclear fraction and α-tubulin as a marker for the cytosolic fraction. Scale bar = 10 µm

2.3.5 Autophagosomal and lysosomal activity is impaired in G1 arrested HCT8 cells

Results obtained in HeLa 229 revealed that lysosomal activity and autophagy flux is impaired in G1 arrested cells. In order to test whether the same phenomenon could be observed in HCT8, lysosomal and autophagosomal activity upon G1 arrest was assessed. Fluorescent labeling of Lamp1 revealed a strong accumulation of lysosomes with the same enlarged and accumulated appearance as in HeLa 229 [Fig. 35A]. Western blot analysis of Lamp1 confirmed that the overall amount of protein was comparable in control and G1 arrested cells [Fig. 35C]; however, Lamp1 migrated differently in SDS PAGE and appeared in a long smear [Fig. 35B]. The Lamp1 molecule has 18 N-linked glycosylation sites that are variably processed during trafficking from the ER via Golgi to lysosomes, resulting in a diffuse band in general (149). The even more diffuse appearance of Lamp1 in Western blot of G1 arrested HCT8, hinted at alterations in glycosylation during processing, which would eventually affect transport to and most likely functionality in lysosomes.

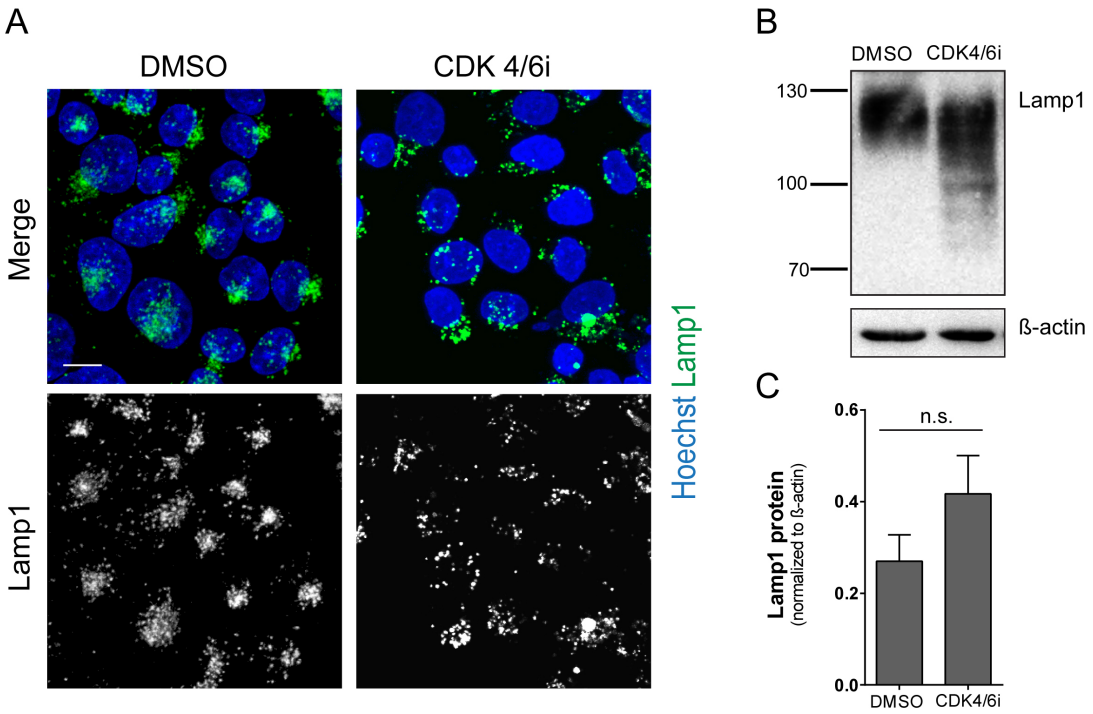

Fig. 35 Lamp1 distribution and processing is altered in G1 arrested HCT8 cells

(A) Representative images of HCT8 cells, lysosomes are labeled by Lamp1 immunofluorescence staining. (B) Western blot and (C) Quantification of Lamp1 in G1 arrested HCT8 cells. Results are shown as mean ± s.e.m. of 5 individual experiments. n.s. = non-significant. Scale bar = 10 µm

As expected, lysosomal activity in G1 arrested HCT8 was decreased, shown by reduced fluorescence of DQ-Red BSA by microscopy and flow cytometry analysis [Fig. 36 A, B]. Furthermore, pro-CTSD and more profoundly the intermediate form of CTSD accumulated upon G1 arrest, suggesting that processing of lysosomal proteins is impaired in HCT8 cells as well [Fig. 36 C].

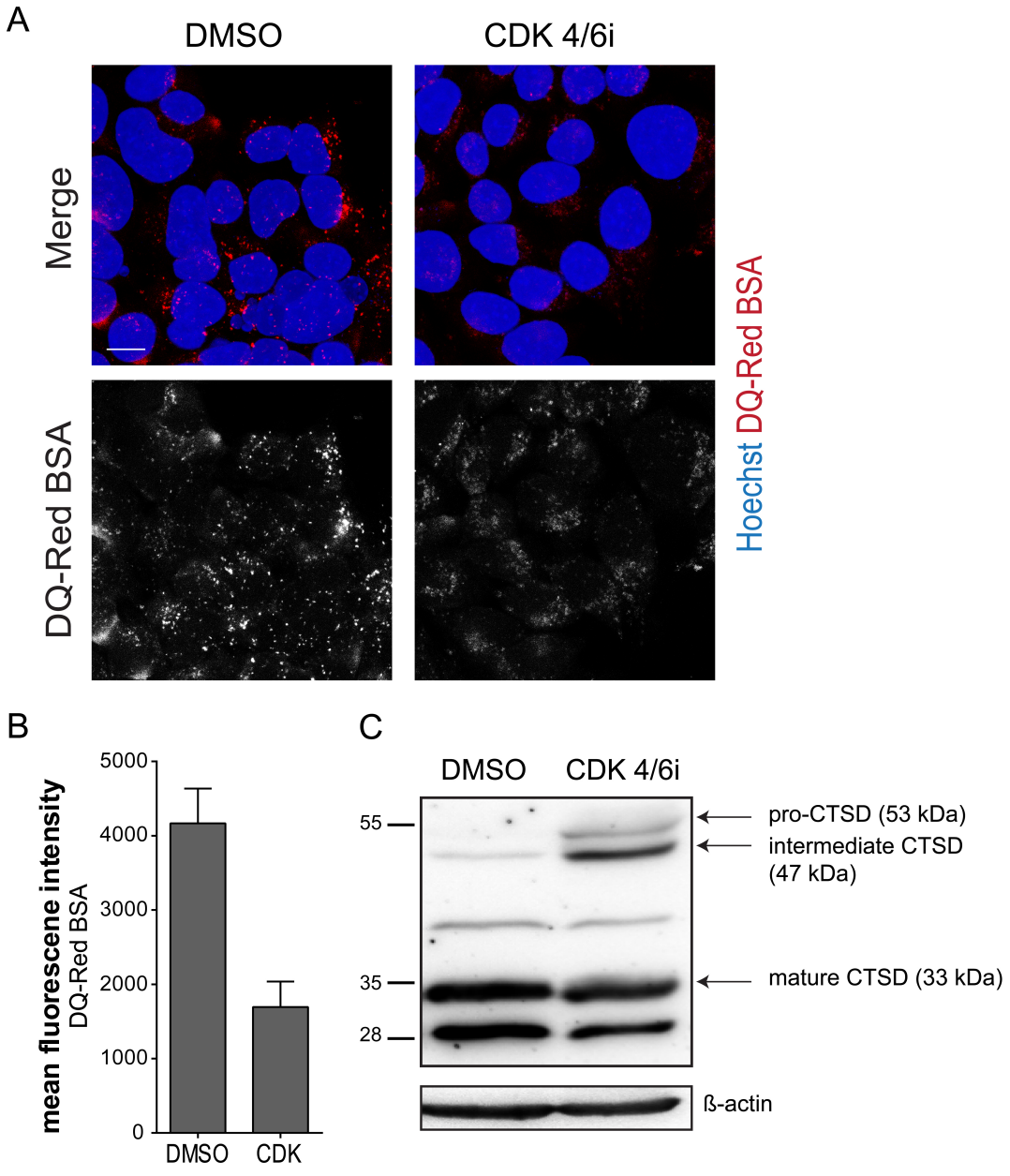

Fig. 36 Lysosomal activity is reduced in G1 arrested HCT8 cells

(A) Representative microscopy of HCT8 after addition of DQ-Red BSA for 5 hrs. DQ-Red BSA is quenched when fed to the cells and becomes fluorescent after hydrolytic cleavage in the lysosomes, representing lysosomal activity. (B) Flow cytometry of HCT8 after addition of DQ-Red BSA for 5 hrs. Results are shown as mean ± s.e.m. of 4 individual experiments (C) Representative Western blot for Cathepsin D. Scale bar = 10 µm

To investigate the effect of G1 arrest on autophagy in HCT8 cells, LC-3B staining was used and revealed a heavy accumulation of autophagosomes, similar to what was observed in HeLa 229 [Fig. 37 A]. Addition of CHQ to control HCT8 cells to analyze autophagy flux resulted in a 5.8-fold increase of LC-3B II, representing the formation of APs. G1 arrested HCT8 cells showed a 12.8-fold higher LC-3B II level. Blocking lysosomal degradation by CHQ did not increase this further, confirming that the final degradation steps were blocked in HCT8 [Fig. 37 B, C].

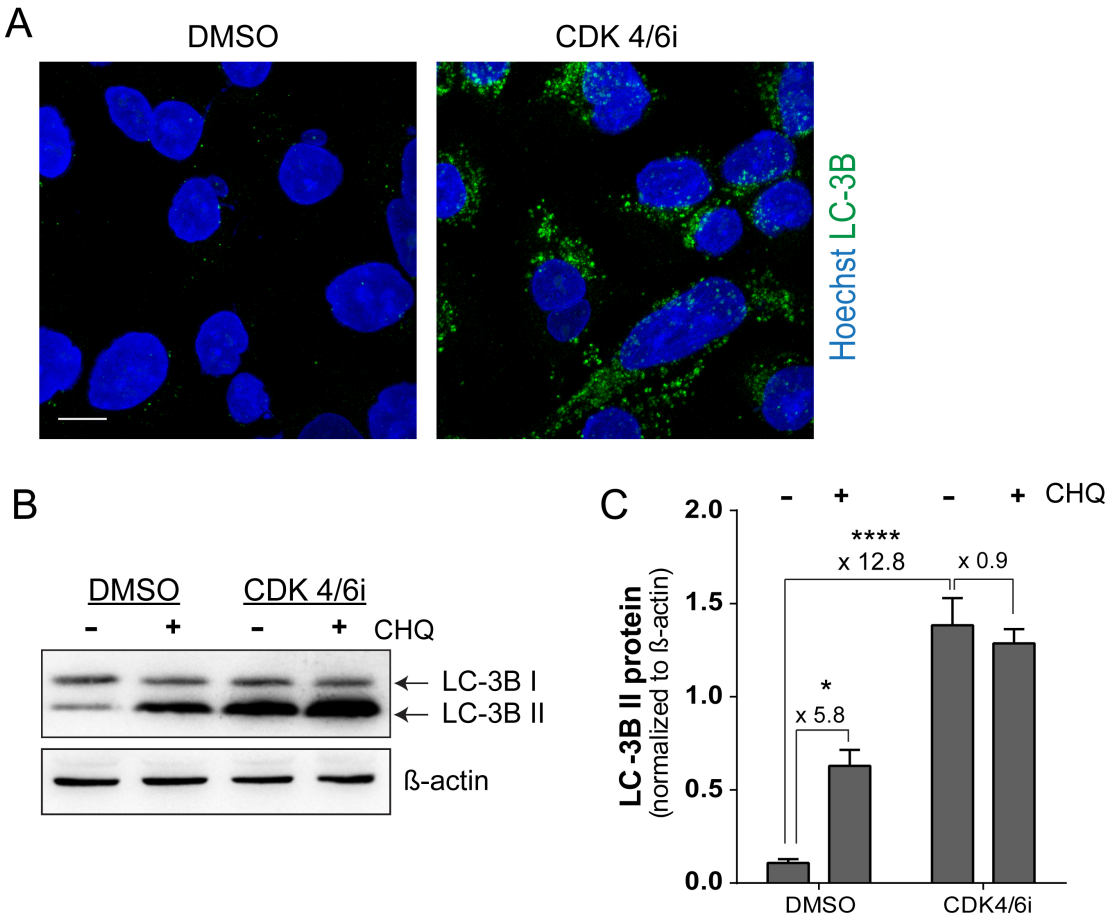

Fig. 37 Autophagy is compromised in G1 arrested HCT8 cells

(A) Representative microscopy images of HCT8. An LC-3B antibody was used to label autophagosomes. (B) Western blot analysis of autophagy flux. For each condition (control or G1 arrested) two wells were seeded. CHQ was added to one well for 3 hrs to inhibit lysosomal function and therefore degradation of autophagosomal content and membrane components, leading to accumulation of the conjugated form of LC-3B (LC-3B II). (C) Quantification of LC-3B II in control or G1 arrested cells after treatment with CHQ. Results are shown as mean ± s.e.m. of 5 individual experiments. two-way ANOVA: *p≤0.05, **p≤0.01, ***p≤0.001, ****p≤0.0001, Scale bar = 10 µm

2.3.6 Endolysosomal pH is ≤ 6.5 in G1 arrested HeLa 229

One hallmark of endosomal (and SCV) maturation is the gradual decrease of vesicle pH. While extracellular and cytoplasmic pH is neutral, luminal pH of endocytic organelles becomes increasingly acidic, specifically from 6.8 to 6.1 in EE, 6.0 to 4.8 in LE and approx. 4.5 in Lysosomes (15). Acidification of the system is gradual and mutually dependent on changes in membrane composition and recruitment of receptor proteins and organelle specific ligands, which in turn mediate fusion and fission with other endolysosomes. Eventually, activity of lysosomal hydrolases is optimal at pH 4.5-5.

Reduced activity of lysosomes, block of autophagosome turnover and reduced SPI-2 activation in *Salmonella* strongly suggested that acidification of the endosomal system was compromised in G1 arrested cells. In order to evaluate acidity of endosomal organelles various agents are available. Most commonly used are low molecular fluorescent dyes like Acridine orange (AO) or Lysotracker (LTR), despite their rather low sensitivity. AO is a metachromatic dye that shifts from green to red fluorescence in a concentration dependent manner in live cells. At neutral pH AO exists as a monomer and is membrane permeable. In low pH environment AO becomes protonated and the electric charge hinders AO from crossing organelle membranes again. Thus, acidic compartments concentrate Acridine Orange and the concentration dependent chromatic shift from green to red is correlated with the acidity of the organelle. LTR is a weak base linked to a fluorophore, that is only partially protonated (and hence membrane permeable) at neutral pH. Upon entry of acidic organelles it becomes increasingly protonated and thus trapped inside these vesicles. The concentration of the fluorophore, indicative of a low pH, can be monitored by microscopy (150)(151).

Unexpectedly, addition of LTR to G1 arrested cells resulted in fluorescence of intracellular vesicles, hinting towards an acidic pH [Fig. 38 A]. Bafilomycin A1, a known inhibitor of the v-ATPase (152) was used as control and completely abolished Lysotracker signals. In order to confirm these results, Acridine orange staining was applied. After addition of AO to live cells for 15 min, its intracellular concentration was evaluated by microscopy. Bafilomycin A1 was again used as control and results clearly showed that inhibition of the v-ATPase completely inhibited AO accumulation and

therefore no shift from green to red was observed. In contrast, G1 arrested cells concentrated AO inside their vesicles, resulting in a shift from green to red color [Fig. 38 B]. These results indicated that endolysosomal vesicles in G1 arrested cells were acidic. However, LTR and AO stainings only allow to state that vesicular pH is lower than 7.4. Determination of the actual pH and therefore a differentiation between early endosomes, late endosomes or lysosomes is hardly possible. Indeed, previous studies showed that LTR becomes already fluorescent at pH ≤ 6.5 resulting in labelling of early endosomes already (150). Also, Acridine orange becomes protonated in early endosomes (151) and thus allows labeling of the endolysosomal system without measuring the actual pH. Therefore, LTR and AO results show that the pH of the endosomal system is lower than that of the surrounding cytoplasm. However, it does not reflect the actual pH in the vesicles, and thus it is unclear whether the pH is acidic enough to activate lysosomal hydrolases or induce SPI-2 expression in SCVs.

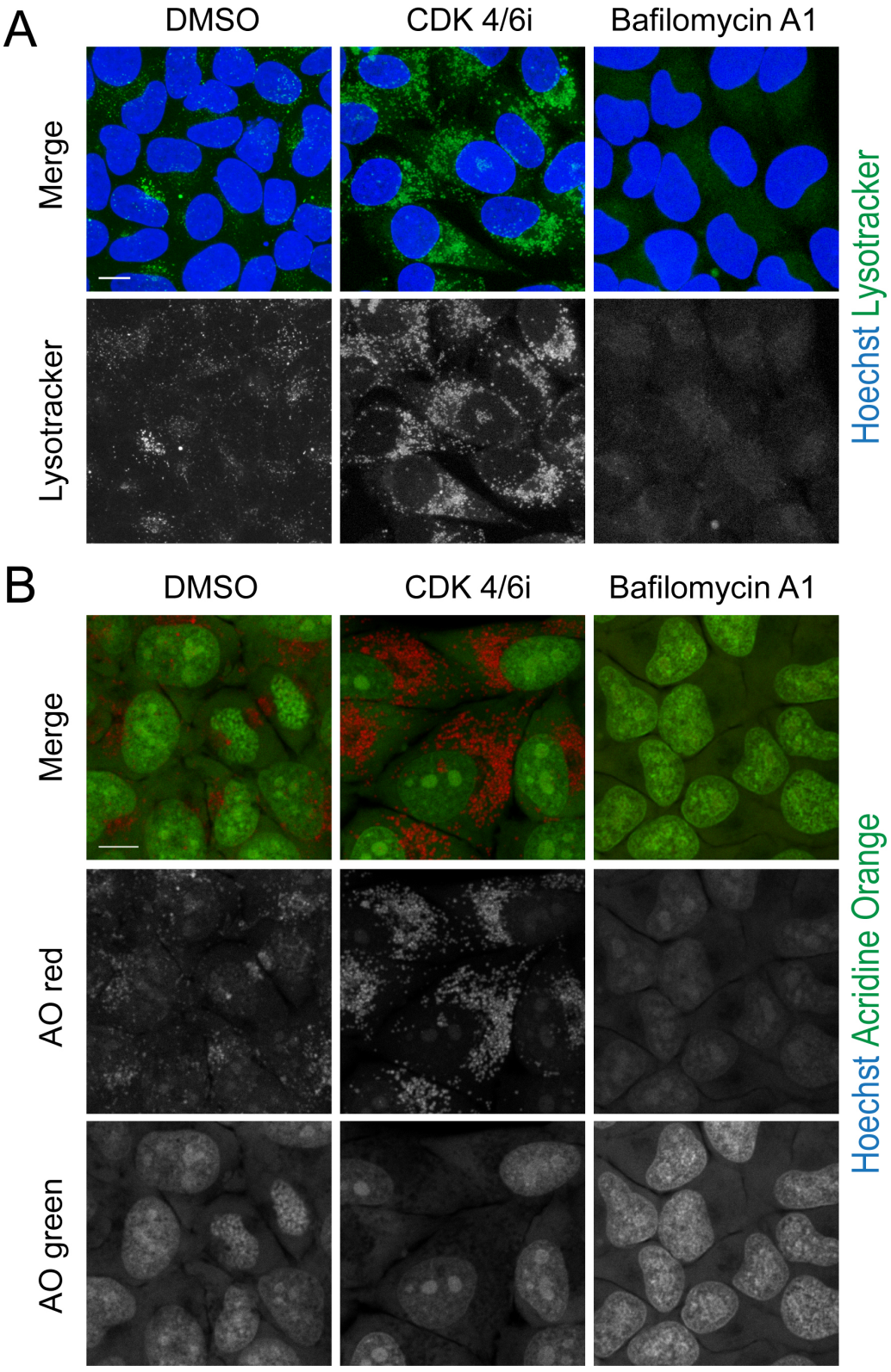

Fig. 38 Endolysosomal pH in G1 arrested cells is slightly acidic

(A) Representative images of Lysotracker staining in 229 cells. Bafilomycin, a v-ATPase inhibitor was used as positive control. LTR was applied for 2 hours before fixation. (B) Representative images of Acridine Orange staining in HeLa 229 cells. AO was added to the cells for 15 min and images were taken immediately without fixation. Scale bar = 10 µm

Together, these results reveal that upon G1 arrest endolysosomal trafficking is severely dysregulated. The cells accumulated enlarged vesicles that were unevenly distributed throughout the cell. Lysosomal activity was impaired and autophagy flux was blocked. Accumulation of non-degraded cargo caused lysosomal stress and induced translocation of TFEB, which contributed to initiation of autophagy as well as lysosomal biogenesis. Consequently, a large number of autophagosomes accumulated and synthesis of lysosomal proteins such as Cathepsin D was induced. However, proper processing of membrane (Lamp1) and luminal proteins (Cathepsin D) along the ER-Golgi-lysosome pathway was blocked or at least delayed. Measurement of endolysosomal pH revealed a mild acidification of the system; however it is not clear if acidification was strong enough to allow optimal activity of lysosomal hydrolases. This clearly shows that upon G1 arrest, endolysosomal trafficking is deregulated, which affects breakdown of cargo and processing of lysosomal proteins. Since maturation of SCVs is interconnected with endosomal trafficking, the data provide evidence that impaired SCV maturation in G1 arrested cells is caused by deregulation of the endosomal system.

2.4 Integrity of *Salmonella* containing vacuoles is compromised in G1 arrested cells

2.4.1 Acidification of the SCV is impaired in G1 arrested cells

Previous labeling of the endolysosomal system with fluorophores like Lysotracker or AO had revealed that the pH value is at least lower than that of the surrounding cytoplasm, without being sensitive enough to determine the actual pH in the different endolysosomal compartments. Thus, the pH might still be too high to enable activation of lysosomal hydrolases or to induce signaling for SPI-2 activation in SCVs. In order to determine to which extent SCVs acidify in G1 arrested cells, a different approach, based on previous studies (153) (154), was used. Therefore, *Salmonella* was coupled to FITC, a fluorophore that is quenched upon acidic pH. HeLa 229 cells were infected with Sal-FITC and with increasing acidification of SCVs the FITC signal should be quenched. At each time point cells were collected and FITC intensity was measured immediately in live cells. Subsequent equilibration of cells in buffer (+ ionophores) with pH 7.4 recovered the quenched FITC signal and the difference in fluorescence before and after equilibration was a measure for the acidity of SCVs [Fig. 39A]. Bafilomycin A1 was used as a control.

Measurement of pH_{SCV} revealed that acidification in control cells occurred rapidly within the first two hours of infection and the pH dropped progressively, reaching a plateau at 4 hpi. Interestingly, pH_{SCV} in G1 arrested and Bafilomycin A1 treated cells was higher than in mock treated cells at 0 hpi, hinting at alkalization of the cells. The high pH remained constant until 1 hpi, then decreased slightly, but remained at a level comparable to control cells at 0.5 hpi [Fig. 39B]. These results clearly show that acidification of the SCV is impaired in G1 arrested cells.

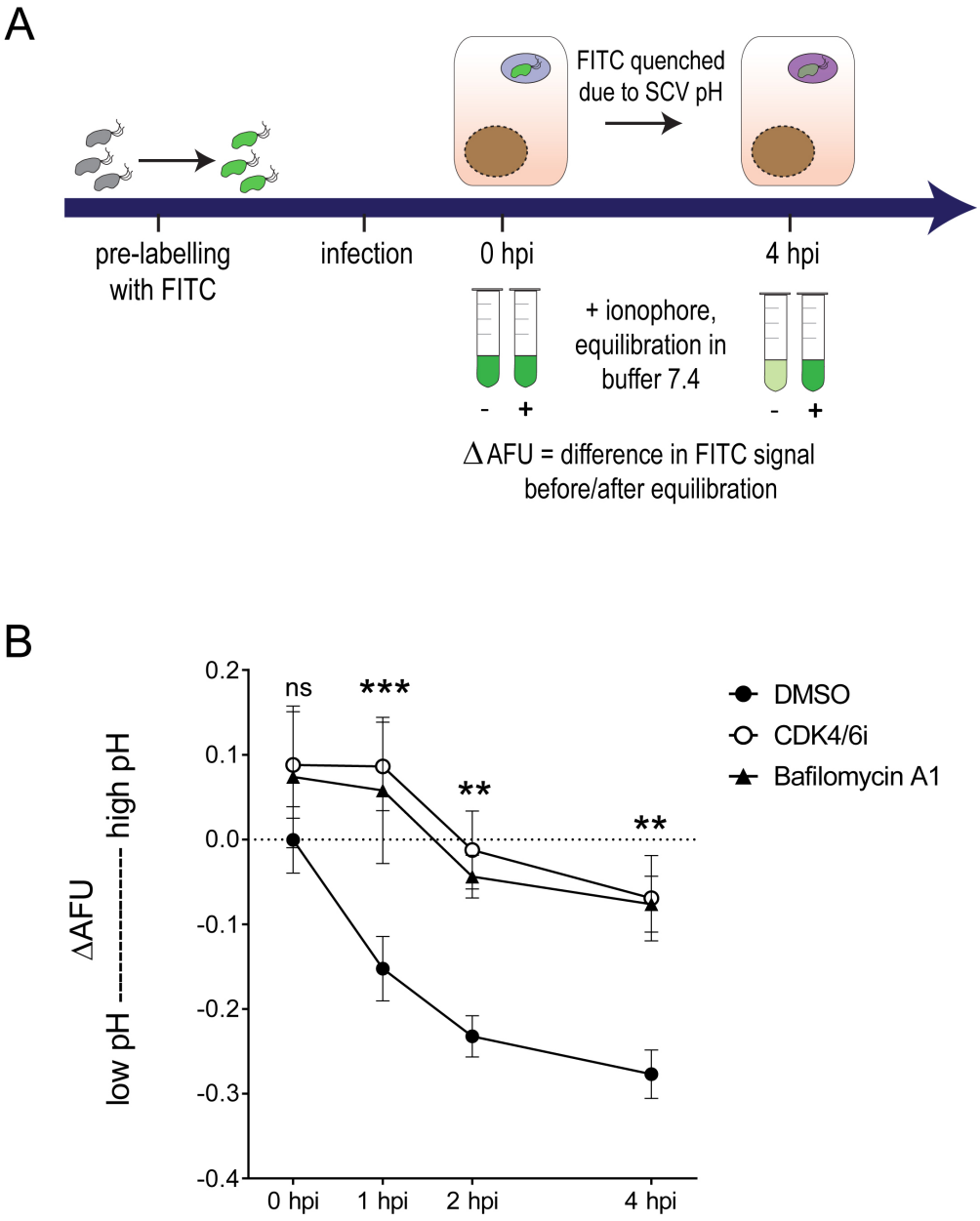

Fig. 39 The *Salmonella* containing vacuole does not acidify upon G1 arrest

(A) Experimental set up for measurement of pH_{SCV}. *Salmonella* was labeled with FITC and used to infect HeLa 229. At each time point cells were collected and intensity of FITC was determined. Upon acidification the signal was quenched. To recover the FITC signal, cells were equilibrated in buffer pH 7.4, supplemented with ionophores. (B) Acidification of SCVs in control or G1 arrested HeLa 229. As a control Bafilomycin A1 was used to inhibit acidification. Results are shown as mean ± s.e.m. of at least 6 individual experiments, each performed in duplicate; two-way ANOVA: **p≤0.01, ***p≤0.001, ns = non-significant

2.4.2 SCV maturation is stalled at an intermediate stage upon G1 arrest

Maturation of the SCV occurs in an endosome-like manner and depends on fusion with endolysosomal vesicles, which is triggered by secreted effector proteins from *Salmonella* that target certain host structures. Due to these fusion events, accompanied by gradual acidification, membrane components and intraluminal content (e.g. nutrients or ions) are provided and allow *Salmonella* to establish an intracellular protective niche in which it can replicate. The results above show that endosomal maturation and autophagy are dysregulated in a way that final degradation of cargo in lysosomes was blocked, even though the pH of the vesicular system dropped at least to ≤ 6.5. In addition, acidification of SCVs was not only delayed but almost completely abolished, resulting in reduced SPI-2 activation. In order to investigate consequences of impaired SCV maturation in more detail, HeLa 229 cells were infected with *Salmonella* and colocalization with early (EEA1) and late (Lamp1) endolysosomal markers, as well as exchange of endosomal cargo was determined.

Results revealed that the SCV quickly fused with early endosomes, resulting in accumulation of EEA1 on the SCV membrane in control and in G1 arrested cells. This confirmed that uptake and early steps of SCV formation were not inhibited [Fig. 40 A, D]. In control cells, EEA1 was gradually replaced by Lamp1, indicating fusion with late endosomes or lysosomes and thus conversion from an early to a late SCV within the first hour of infection. In contrast, *Salmonella* did not colocalize with Lamp1 in G1 arrested cells, showing that maturation of the SCV was stalled at an intermediate stage [Fig. 40 B, E]. In addition, removal of EEA1 from the SCV seemed to be slightly delayed upon G1 arrest. Since the *Salmonella* effector SopE has been shown to recruit Rab5 and thereby early endosomes to the early SCV (49) prolonged colocalization of SCVs with EEA1 is in agreement with previous findings that SopE degradation is delayed upon G1 arrest [Fig. 25, Fig. 27]. Gradual conversion from an early to a late *Salmonella* containing compartment was accompanied by activation of SPI-2 in mock-treat cells. The secreted effector proteins target various host structures and provide accessibility to endolysosomal content for *Salmonella*. The stalling of SCV maturation at an intermediate stage and lack of SPI-2 activation in G1 arrested cells suggested that

exchange of nutrients, ions and membrane components between endolysosomes and SCVs was reduced in G1 arrested cells. In order to test this, the host endolysosomal system was preloaded with fluorescently labelled dextran and cells were infected with *Salmonella*. A 60 min chase before infection ensured that the dextran reached late endosomal or lysosomal compartments. Results showed that both, control and G1 arrested cells, took up dextran, confirming that early steps in endocytosis were functional. In control cells, colocalization of *Salmonella* and dextran confirmed fusion and exchange of content, which is accompanied by acquisition of Lamp1. Upon G1 arrest, less than 10% of *Salmonella* colocalized with the dextran, confirming that only limited exchange of endosomal content has occurred [Fig. 39 C, F].

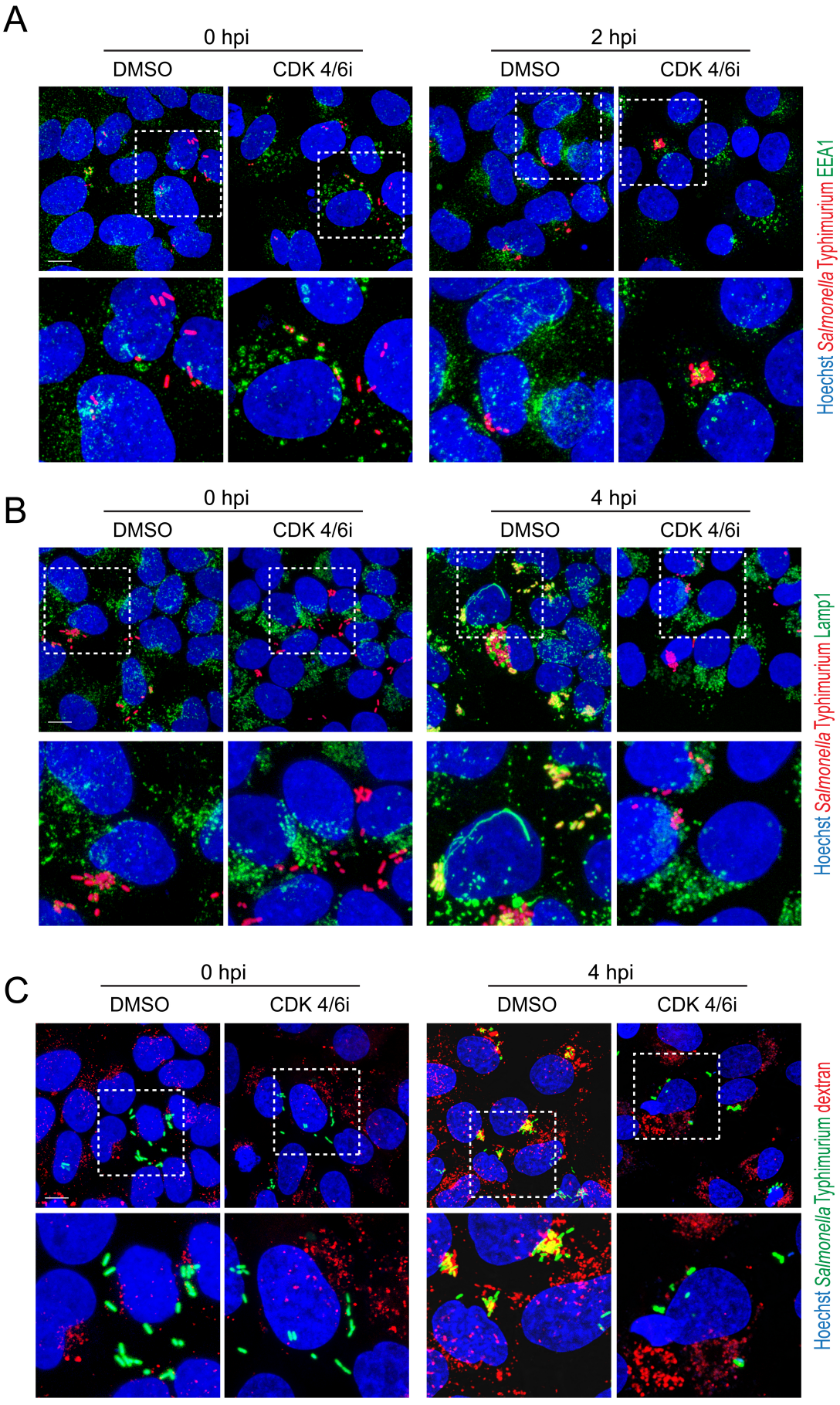

figure legend on next page

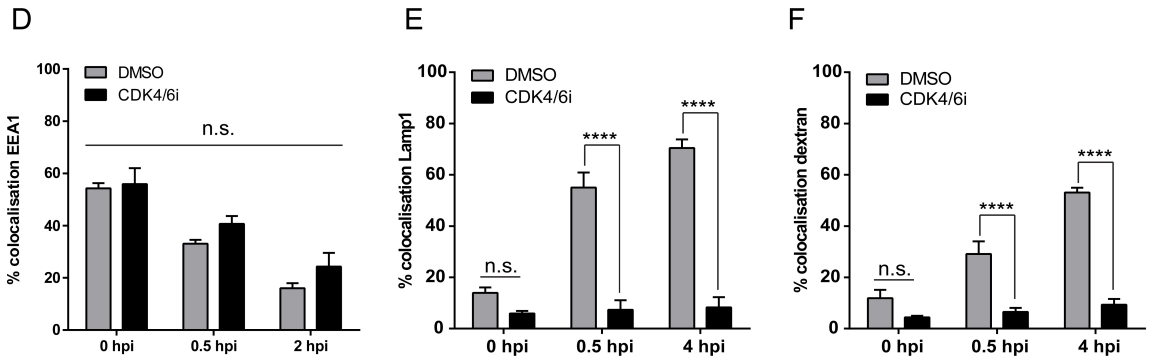

Fig. 40 SCV maturation is stalled at an intermediate stage

Representative images of HeLa 229 cells infected with *Salmonella* (MOI 25) and fluorescently labelled (A) EEA1, (B) Lamp1 or (C) preloaded with dextran 594. Lower panels show zoom of dashed square (D) Quantification of *Salmonella*-EEA1 colocalization. (E) Quantification of *Salmonella*-Lamp1 colocalization. (F) Quantification of *Salmonella*-dextran colocalization. For each condition the colocalization of intracellular *Salmonella* with the corresponding endolysosomal marker was analyzed in 30-50 infected HeLa 229 cells. Results are shown as mean ± s.e.m. of at least 4 individual experiments; two-way ANOVA: *p≤0.05, **p≤0.01, ***p≤0.001, ****p≤0.0001, n.s. = non-significant. Scale bar = 10µm

2.4.3 Integrity of the SCV is compromised in G1 arrested cells

So far colocalization experiments [Fig. 40], measurement of pH SCV [Fig. 39] and results from the CHQ resistance assay [Fig. 14] suggested that SCV integrity was compromised in G1 arrested cells and thus escape of *Salmonella* into the cytoplasm was promoted. In order to confirm this hypothesis galectin-3 was used as a marker for ruptured SCVs. Galectin-3 is a family member of ß-galactose-binding lectins. It is soluble and located in the cytoplasm of eukaryotic cells and has been shown to bind to N-glycans, which are usually found in the lumen of intracellular vesicles, but become exposed to the cytoplasm after lysis. Galactin-3 was therefore used as a marker for vacuolar rupture in infection with bacterial pathogens before (155) (156).

Indeed, infection of G1 arrested HeLa 229 cells resulted in more Galectin-3 decorated bacteria already at 0 hpi. At 0.5 hpi, 10-fold more bacteria colocalized with galectin-3, indicating rupture of SCVs and exposure of intraluminal proteins to the cytosol. In contrast, less than 2% of SCVs were galectin-3 positive in control cells, confirming proper integrity of their membranes [Fig. 41 A, B]. These results confirmed that the

nascent SCV was ruptured more easily and escape of *Salmonella* into the cytoplasm was supported upon G1 arrest.

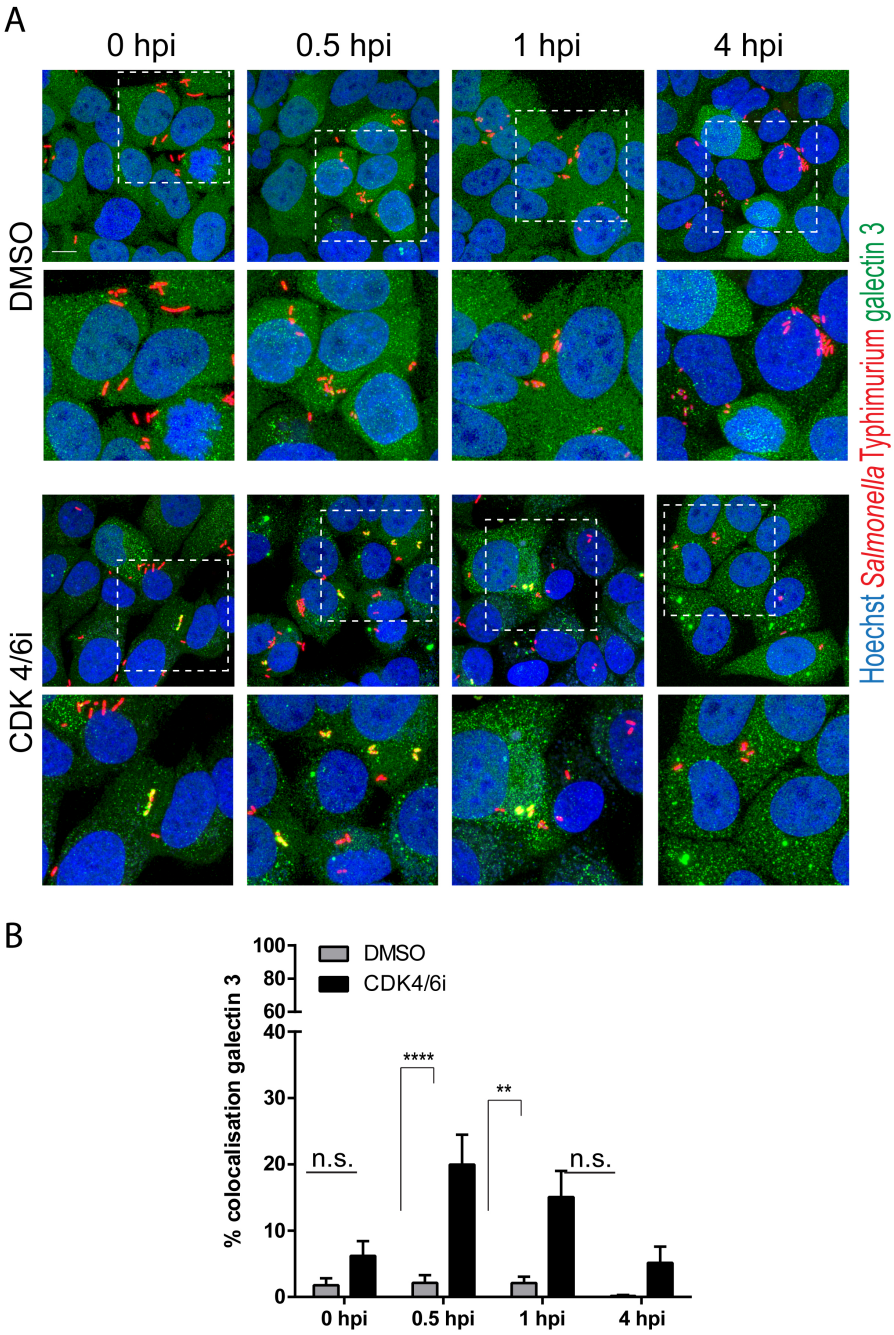

Fig. 41 Galectin-3, a marker for vacuolar lysis is recruited to the SCV in G1 arrested HeLa 229 cells

(A) Representative images for HeLa 229 cells infected with *Salmonella* (MOI 25). Galectin-3 is used as a marker for vacuolar lysis (B) Quantification of *Salmonella*-Galectin-3 colocalization. For each time point the colocalization of intracellular *Salmonella* and Galectin-3 was analyzed in 50 infected HeLa 229 cells. Results are shown as mean ± s.e.m. of 5 individual experiments; two-way ANOVA: **p≤0.01, ****p≤0.0001, n.s. = non-significant. Scale bar = 10 µm

2.5 Delay of G1-S cell cycle progression by miRNAs interferes with intracellular *Salmonella* replication

Treatment with cell cycle inhibitors like CDK4/6i or lovastatin blocked directly or indirectly proliferation of cells and resulted in an arrest in G1 phase of the cell cycle. Endolysosomal trafficking in these G1 arrested cells is compromised and maturation of the SCV, which depends on the interaction with the endosomal system, is consequently impaired. In order to solidify the link between the host cell cycle, its endosomal trafficking and SCV maturation, the effect of miRNAs, which arrest cells in G1 phase, was investigated. Previous studies have shown that many miRNAs are involved in regulation of the cell cycle and proliferation (5) (65), by either direct targeting of proteins involved in cell cycle regulation (e.g. Cyclin D1), or by interfering with other processes in the cell, which will eventually cause the cell to arrest. Interestingly, some of these miRNAs, miR-15a-5p, miR-16a-5p and miR-744-5p, were not only reported to arrest cells in G1 phase of the cell cycle (6) (157) (158) (159), but also to interfere with *Salmonella* infection at later time points (5). However, it is not clear if the replication defect observed is also related to impaired SPI-2 activation and compromised endosomal trafficking, as in CDK4/6i treated cells. To address this question, one member of the miR-15 family, namely miR-16a-5p, and miR-744-5p were overexpressed in HeLa 229 cells and the effect on *Salmonella* infection and SPI-2 activation was evaluated.

Cell cycle measurements after overexpression of miR-16a-5p and miR-744-5p revealed that miR-744-5p induced a strong G1 arrest, while the effect of miR-16a-5p on the cell cycle was hardly visible. To validate that miR-16a-5p was regulating the cell cycle, cells were transfected with the miRNAs and 36 hours later nocodazole was added for another 14 hrs to synchronize cells in G2/M phase. After nocodazole treatment, the majority of control cells were stalled in G2/M. Upon transfection with miR-16a-5p fewer cells had reached G2/M indicating a delay in cell cycle progression. Nocodazole treatment of miR-744-5p transfected cells hardly increased the G2/M fraction, undoubtedly showing that the cells did not proliferate but were arrested in G1 phase [Fig. 42 A, B]. This delay or arrest of cells also resulted in lower numbers of cells/well

after 48 hrs of transfection. Thus, for infection experiments with *Salmonella*, the number of bacteria added to the cells was adjusted to an MOI of 25 in all conditions. For CFU quantification, the amount of recovered bacteria was normalized to the corresponding input. As expected, arresting host cells in G1 (or delaying G1-S transition) reduced the number of intracellular bacteria already at 4 hpi, and at 20 hpi intracellular bacterial load was significantly reduced compared to control cells [Fig. 42 C]. In order to test for SPI-2 activation, transfected cells were infected with the *Salmonella* SPI-2 reporter strain and analyzed by microscopy and flow cytometry at 4 hpi. In cells transfected with the control miRNA ca. 58% of the intracellular *Salmonella* population was SPI-2 positive, while only 46% or 45% of the bacteria activated SPI-2 upon miR-16a-5p or miR-744-5p transfection, respectively [Fig. 42 D]. Although the differences in SPI-2 activation in transfected cells were less strong compared to treatment with the CDK4/6inhibitor (DMSO = 75%, CDK4/6i = 20%), the microscopy data clearly showed reduced SPI-2 activation after transfection with both cell cycle regulating miRNAs [Fig. 42 E]. Overall the results support the hypothesis that SPI-2 is not activated in G1 arrested host cells.

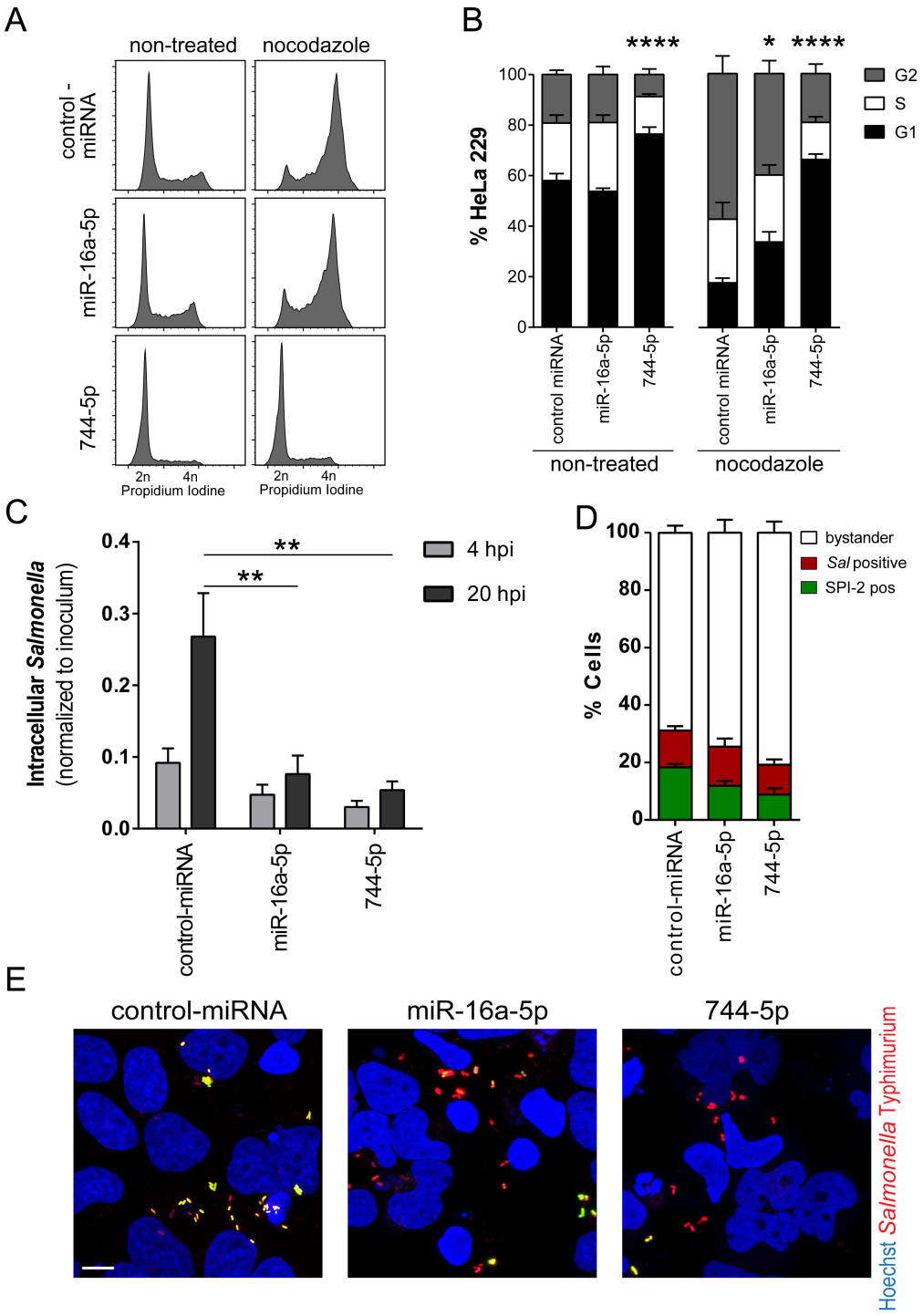

Fig. 42 MiRNA-induced delay of G1-S transition impairs intracellular replication of *Salmonella*

(A) Representative cell cycle profiles of HeLa 229 cells that were transfected with miR-16a-5p or miR-744-5p (left) and after additional treatment with nocodazole (right). (B) Quantification of HeLa 229 cells in different stages of cell cycle after transfection with miR-16a-5p or miR-744-5p, with or without nocodazole treatment. (C) CFU quantification after infection of transfected cells with *Salmonella* (MOI 25). Transfection with miR-16a-5p or miR-744-5p resulted in a different number of cells at the time of infection. Thus, to keep an MOI of 25, the bacterial input was adjusted accordingly. The recovered CFUs at each time point were normalized to each input. (D) Quantification of flow cytometry analysis of transfected cells after infection with the *Salmonella* reporter strain at 4 hpi. (E) Representative microscopy

figure legend continues on next page

images after transfection with control-miRNA, miR-16a-5p or miR-744-5p and infection with the *Salmonella* SPI-2 reporter strain at 4 hpi. Results are shown as mean ± s.e.m. of at least 4 individual experiments; two-way ANOVA: ** p≤0.001. Scale bar = 10 µm

2.5.1 Lysosomal trafficking is impaired by miRNAs that delay G1-S progression

Results so far revealed that arresting host cells in G1 phase by CDK4/6 inhibition caused dysregulation of endolysosomal trafficking, which consequently affected maturation of the SCV and intracellular *Salmonella* replication. Transfection with miR-16a-5p or miR-744-5p also delayed progression of cells from G1 to S and reduced intracellular *Salmonella* replication, which led to the assumption that endosomal trafficking must be affected in these cells as well. In order to test this, HeLa 229 cells were transfected with two members of the miR-15 family, miR-15a-5p and miR-16a-5p, as well as with miR-744-5p for 72 hrs. Lysosomal activity was assessed by DQ-Red BSA fluorescence by microscopy [Fig. 43 A] and flow cytometry [Fig. 43 D]. The reduced signal for all three miRNAs confirmed that lysosomal degradation of substrates was decreased upon G1 delay/arrest.

Nuclear translocation of TFEB was clearly visible in miR-15a-5p and miR-16a-5p transfected cells though less strong compared to CDK4/6i treated cells, which might be explained by a delay rather than a full arrest in G1 phase. Surprisingly, overexpression of miR-744-5p resulted in complete reduction of TFEB, indicating that it might be a miR-744-5p target [Fig. 43 B]. Western blot analysis confirmed a slight shift of TFEB upon overexpression of miR-15a-5p and miR-16a-5p, indicative for nuclear translocation, as well as the strong reduction of TFEB levels in cells transfected with miR-744-5p [Fig. 43 E]. Finally, Lamp1 protein levels were determined and results revealed a 1.8-fold reduction in miR-15a-5p and miR-16a-5p transfected cells, while Lamp1 is reduced 3-fold upon 744-5p transfection. The strong reduction of the Lamp1 protein level upon overexpression of miR-744-5p is most likely caused by the lack of transcriptional activation by TFEB [Fig. 43 C, F, and G].

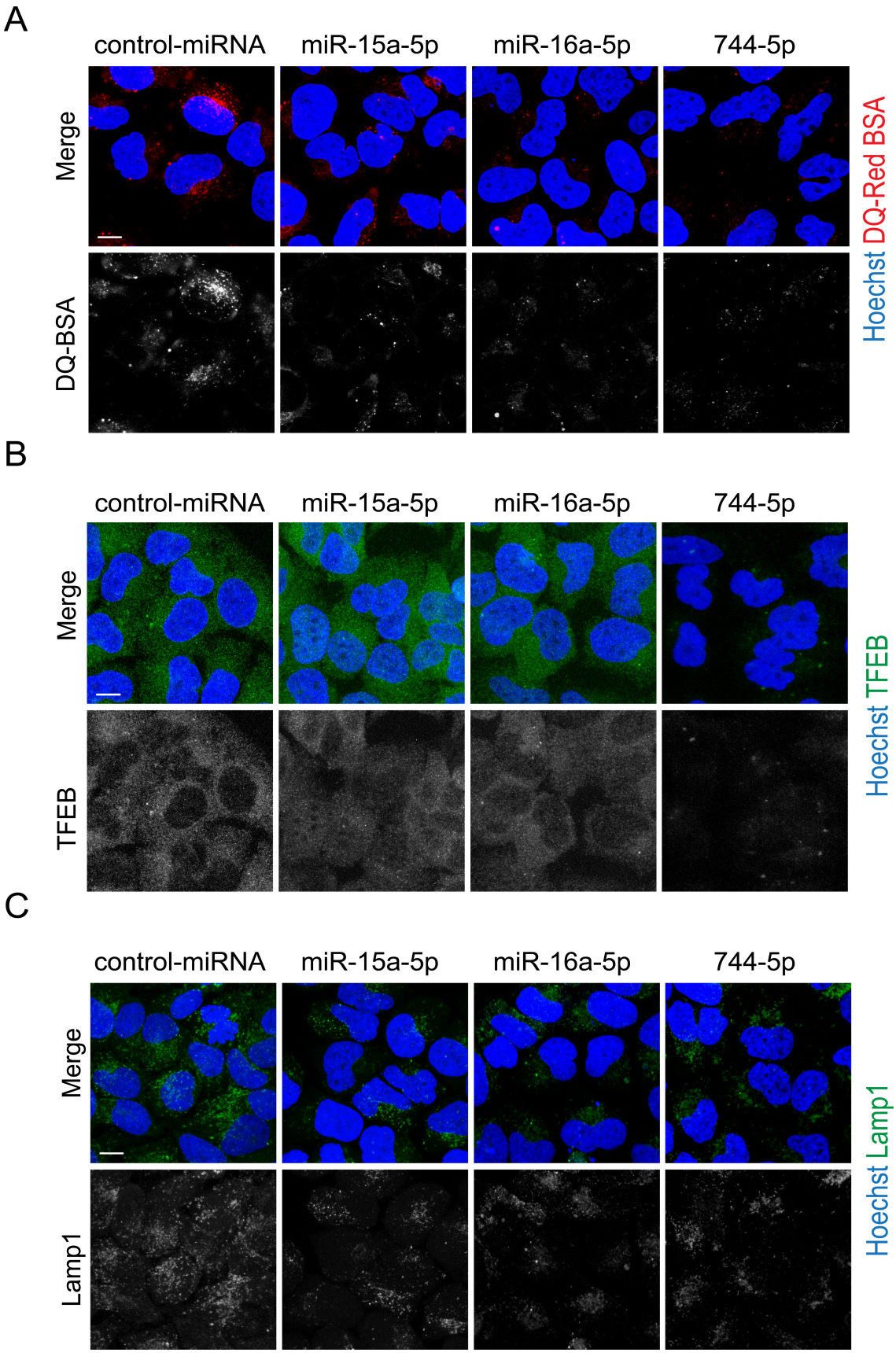

figure legend on next page

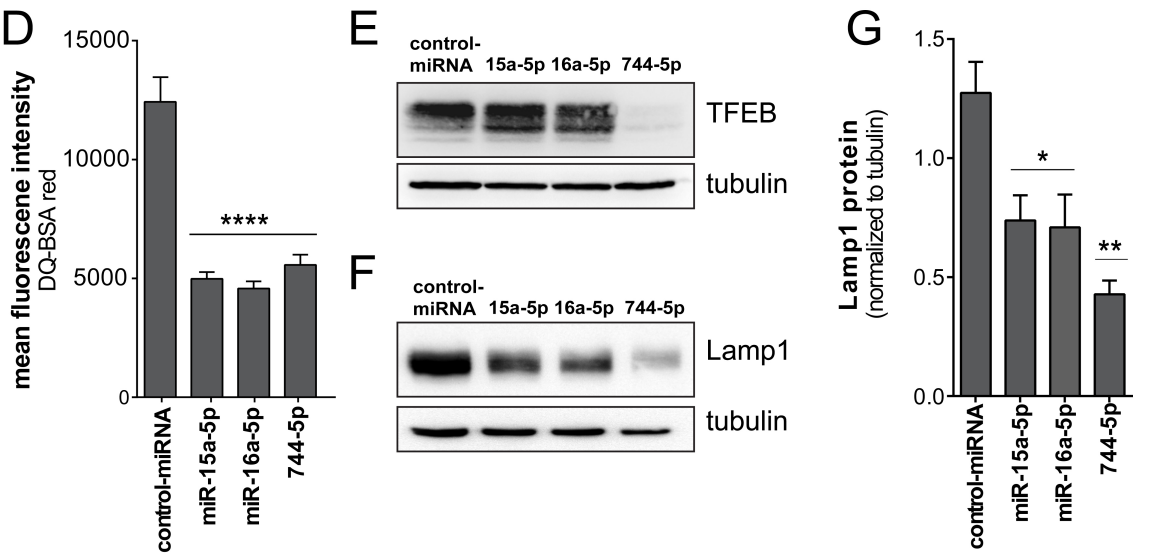

Fig. 43 Lysosomal activity in HeLa 229 cells after overexpression of miR-15a-5p, miR-16a-5p and miR-744-5p

(A) Representative microscopy after transfection with miR-15a-5p, miR-16a-5p and miR-744-5p and subsequent addition of DQ-Red BSA for 5 hrs. DQ-Red BSA is quenched when fed to the cells and becomes fluorescent after hydrolytic cleavage in the lysosomes, representing lysosomal activity. (B) Representative microscopy images of TFEB immunofluorescence staining in transfected HeLa 229 cells. (C) Representative microscopy of Lamp1 in transfected HeLa 229 cells. (D) Flow cytometry of transfected HeLa 229 cells after addition of DQ-Red BSA for 5 hrs. (E) Western blot of TFEB in whole cell lysate. Depending on its phosphorylation state TFEB migrates differently in SDS PAGE, i.e. dephosphorylated = inactive/ cytoplasmic (upper band) or phosphorylated = nuclear/active (lower band). (F) Western blot of Lamp1 in whole cell lysate. (G) Quantification of Lamp1 protein levels. Results are shown as mean ± s.e.m. of 3-5 individual experiments; one-way ANOVA: *p≤0.05, **p≤0.01, ***p≤0.001, ****p≤0.0001 Scale bar = 10 µm

Together, these results confirm that overexpression of miR-15a-5p, miR-16a-5p and miR-744-5p causes a delay or arrest of cells in G1 phase and that intracellular *Salmonella* replication is inhibited. Furthermore, it was shown that miRNA induced G1 delay/arrest also impairs SPI-2 activation. Eventually, investigation of endosomal trafficking revealed reduced lysosomal activation in cells transfected with miR-15a-5p, miR-16a-5p and miR-744-5p. Nuclear translocation (= activation) of TFEB was shown for members of the miR-15 family, whereas overexpression of miR-744-5p caused a severe reduction in TFEB and consequently of Lamp1 protein levels. Overall, the results confirm that delaying or arresting cells in G1 phase causes dysregulation of the endosomal trafficking and therefore has detrimental effects on SCV maturation.

2.6 Concluding remarks and model

Overall, the present study revealed that long-term replication of *Salmonella* in G1 arrested epithelial cells was impaired, while replication of *Shigella flexneri* was not affected. It was shown that the intracellular population of *Salmonella* changed from a vacuolar to a rather cytoplasmic lifestyle upon G1 arrest and depending on the host cell type *Salmonella* massively replicated inside the cytoplasm. In proliferating (control) cells nascent SCVs quickly acquired early endosomal markers. Within the first hour after invasion (0.5 hpi) continuous fusion with endolysosomes and exchange of fluid phase markers occurred [Fig. 40]. This sudden environmental change was sensed by *Salmonella* and triggered activation of the SPI-2 system [Fig. 21], which further enhanced interaction with the host endolysosomal system and stabilization of the vacuolar compartment. Upon G1 arrest of host cells, newly formed SCVs still acquired early markers, indicating fusion with early endosomes. Sustained expression of SPI-1 genes and reduced proteasomal degradation of the effector proteins promoted prolonged presence of the SPI-1 effector SopE and possibly enhanced recruitment of early endosomes. Recruitment of Galectin-3 confirmed damage and ruptures of vacuoles and, in combination with the chloroquine resistance assay, strongly supported the hypothesis of instable and leaky vacuoles. Furthermore, it was shown that due to their instable nature, SCVs did not acidify but *Salmonella* remained in a rather neutral compartment or even escaped into the cytosol. Consequently, an important environmental trigger for SPI-2 activation was missing and fusion events with late endosomes/lysosomes and thus recruitment of membrane proteins (e.g. Lamp1) or exchange of endosomal cargo was impaired. Together, these results reveal that the intracellular lifestyle of *Salmonella*, more specifically the decision between a vacuolar and a cytoplasmic lifestyle, was dependent on the cell cycle stage of the host.

Moreover, the present study showed that upon G1 arrest, cells accumulated endosomes and lysosomes to a higher extent than cycling cells. These organelles appeared enlarged, merged together and localized closer to the perinuclear region, while they were homogenously dispersed throughout the whole cytoplasm in control cells. The uneven distribution and vacuolization was indicative of alkalinization of the

endolysosomal system. Indeed, lysosomal activity and autophagy flux was significantly reduced upon G1 arrest, accompanied by delayed and/or altered processing of lysosomal proteins, like Cathepsin D, in HeLa 229 and HCT8 cells and possibly glycosylation of Lamp1 in HCT8. Presumably, this was triggered by the urgent need for lysosomal components and resulted in accelerated but therefore insufficient processing, which enhanced even more the dysfunctionality of lysosomes. Possibly, alterations of the membrane composition would have an impact on the assembly and function of the v-ATPase and thus acidification of lysosomes [Fig. 44].

In addition to the use of chemical inhibitors (CDK4/6i and lovastatin) to arrest cells in the G1 phase of the cell cycle, miRNAs, which have been shown to play important roles in cell cycle regulation, were used to confirm these findings. Overexpression of miR-16a-5p and miR-744-5p revealed that SPI-2 activation and subsequent intracellular replication of *Salmonella* was impaired in HeLa 229 cells. Furthermore, it was shown that lysosomal activity was reduced in cells delayed or arrested in G1 phase by miR-15a-5p, miR-16a-5p and miR-744-5p. Protein levels of Lamp1 were reduced and TFEB was activated by miR-15a-5p and miR-16a-5p, whereas overexpression of miR-744-5p caused a significant loss of TFEB. With this approach, it was confirmed that G1 delay/arrest causes deregulation of endolysosomal trafficking and that SPI-2 activation and intracellular replication of *Salmonella* is impaired.

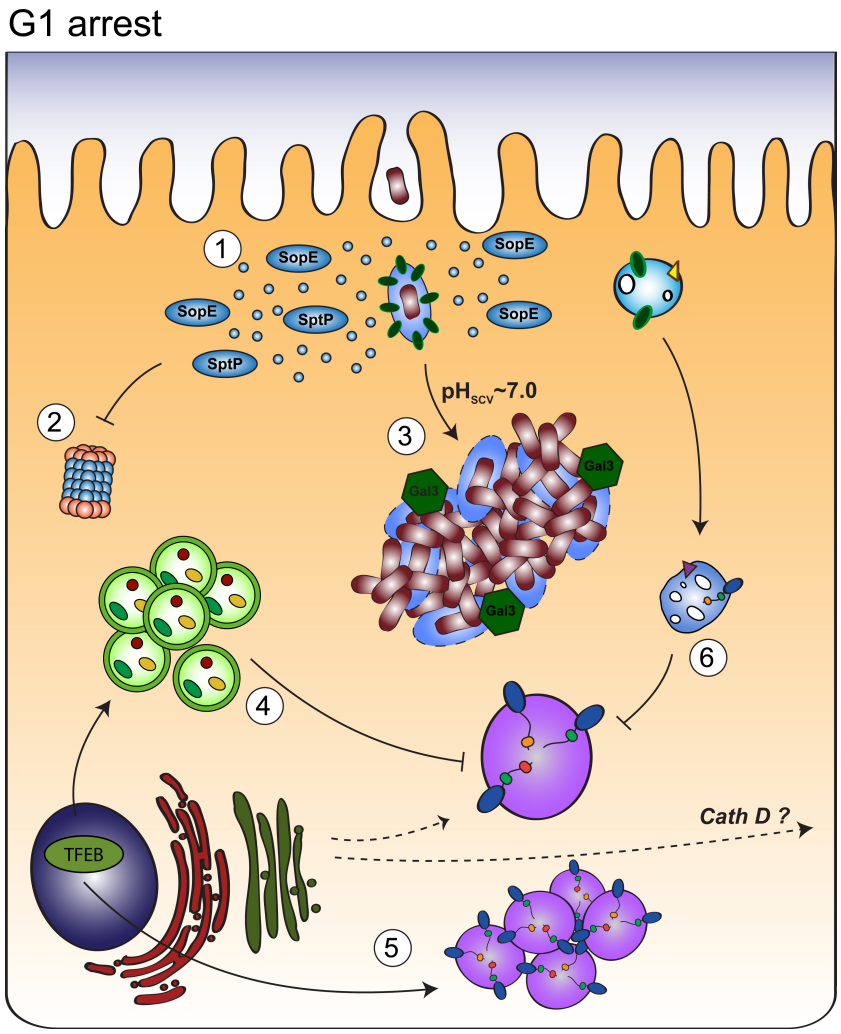

Fig. 44 Model of *Salmonella* infection in G1 arrested cells

The intracellular lifestyle of *Salmonella* is altered upon G1 arrest. 1. Sustained secretion of SPI-1 effectors cause prolonged recruitment of EEA1 and stall SCV maturation at an early and still vulnerable stage. 2. In addition, degradation of SPI-1 effectors by the host proteasome is reduced. 3. The nascent SCV becomes unstable and eventually *Salmonella* escapes into the cytoplasm or resides in leaky vacuoles, which do not acidify. Consequently activation of the SPI-2 system is impaired and necessary modifications to stabilize the SCV and fusion with the host endosomal system remain unaccomplished. Galectin-3, a host protein is recruited to damaged vacuoles in response. 4. Furthermore, lysosomal activity is impaired, causing activation of TFEB and increased autophagosome formation. Autophagy flux, however, is blocked, which in turn enhances TFEB signaling even more. 5. TFEB induced transcription of lysosomal genes increases synthesis and transport of hydrolases like Cathepsin D. Yet, processing of membrane or luminal proteins along the ER-Golgi-Lysosome axis was altered, presumably causing changes in glycosylation or even secretion of hydrolases to the extracellular space. 6. Activity of lysosomal hydrolases, as well as fusion with endosomes and autophagosomes is mutually dependent on the activity of the v-ATPase and absence of these events strongly indicates improper acidification of lysosomes.

3 Discussion

3.1 Intracellular lifestyle of *Salmonella* is altered upon G1 arrest of host cells

The intracellular lifestyle of the gastrointestinal pathogen *Salmonella* has been studied extensively for several decades and it was shown that *Salmonella* does not only induce uptake by epithelial cells but also modifies the nascent phagosome in order to ensure intracellular survival and to establish long-term infection (44). The set of virulence genes required for invasion and intracellular modifications are expressed in a timely coordinated manner, which shows that *Salmonella* senses and responds to the changes in the environment (42). The elaborate and specific targeting of particular host pathways by *Salmonella* secreted effector proteins show how well *Salmonella* has adapted to its mammalian host (55). On the other hand, host cells provide a dynamic environment with changing metabolic states, various nutrient availabilities and different cell cycle phases. Thus, *Salmonella* has evolved to specifically target particular host structures or processes and to respond rapidly to changes in the host environment.

Previous studies have shown that *Salmonella*, like many other pathogens, interferes with host cell cycle regulation and cause an arrest in G2/M phase (5) (123). Furthermore, *Salmonella* infection induced a faster G1-S phase transition and interestingly, long-term replication of *Salmonella* was inhibited in G1 arrested cells (5). In the present study, the effect of G1 arrest on the outcome of *Salmonella* infection was investigated in order to understand why *Salmonella* is not able to replicate in G1 arrested cells or if, and how, it adapts to this condition. Inhibition of CDK4/6 induced cell cycle arrest in G1 and resulted in a significant reduction of long-term *Salmonella* infection in various epithelial cell lines. Replication of another intracellular pathogen, *Shigella flexneri*, was not affected at any time, which shows that cell cycle dependent inhibition of replication is specific for *Salmonella* or its intracellular lifestyle. One prominent difference between both pathogens is the escape of *Shigella* from its

internalization vacuole, while the majority of intracellular *Salmonella* remain inside a vacuole for replication. Based on this, it was hypothesized that the maturation of the SCV was impaired in G1 arrested or quiescent cells, which was investigated in more detail.

3.1.1 To be or not to be cytoplasmic

For a long time *Salmonella* was considered to reside only inside a modified phagosome, called the SCV, in which it replicates (160). However, research during the last decades showed that the intracellular *Salmonella* population has a heterogeneous character. After uptake into a host cell, the nascent SCV might mature into a protective compartment that allows long-term replication. Alternatively, the SCV might be damaged and release of *Salmonella* into the cytosol of the host cell is possible (125) (126). Some of these damaged vacuoles are targeted by the autophagy machinery of the host and are sealed, which eventually re-directs these bacteria into the vacuolar pathway (48). The exact molecular mechanism(s) that decide(s) if *Salmonella* resides inside a vacuole or escapes into the cytoplasm are still not resolved but seem to be influenced by various pathogen- and host factors. Likewise some cells types, such as fibroblasts or macrophages are less permissive for cytosolic replication, whereas studies in epithelial cells showed that approximately 5-20 % of the intracellular population escapes from the vacuole and massively replicate inside the cytoplasm. This phenomenon is then called hyper-replication and was shown *in vitro* and *in vivo* (44) (126) (161).

The chloroquine resistance assay performed in the present study revealed that approximately 5-15% of *Salmonella* were cytoplasmic in control HeLa 229 or HCT8 cells, which is in agreement with previous findings (126). Upon G1 arrest however, this ratio changed dramatically and more than 75% of the population was CHQ resistant (and thus considered to be cytoplasmic) at 1 hpi in both cell lines. This is a remarkable reversion of the vacuolar : cytoplasmic population ratio and shows that *Salmonella* can adapt rapidly and replicate in the cytoplasm, once it is forced into it due to a compromised vacuole. Interestingly, HeLa 229 cells did not further support cytoplasmic replication, while in HCT8 and CCL2 cells the cytoplasmic fraction did replicate and

formed large intracellular bacterial cluster, similar to what has been described as hyper-replication in other studies (125). In addition, an increase of the vacuolar population in G1 arrested HCT8 cells from 1.6% at 1 hpi to 25% at 4 hpi hinted at a rescue of damaged vacuoles by the autophagy machinery, as described by Kreibich et al. (48).

Together, the results of the current study are in accordance with previous findings of a heterogeneous intracellular *Salmonella* population and showed for the first time that the cell cycle state of the host is an important factor influencing whether the intracellular *Salmonella* population becomes cytoplasmic or vacuolar. After invasion of fast proliferating host cells, such as the gastrointestinal epithelium, *Salmonella* becomes protected from the innate immune response in a vacuolar compartment that also provides nutrients. In addition, *Salmonella* delays proliferation of host cells by arresting them in G2/M, to avoid shedding of the epithelial layer and to ensure maintenance of the protective environment (123). Alternatively, if *Salmonella* invades an arrested or slow-proliferating cell, it is more likely to reach the host cytoplasm and quickly adapts to a cytoplasmic lifestyle. In a broader perspective, a cytoplasmic lifestyle in slow proliferating or even arrested host cells might be advantageous for overall spreading and dissemination of *Salmonella* into tissue, since the high bacterial load in the cytoplasm will be sensed by the host and induce a proinflammatory cytokine release, pyroptosis and cell lysis, by which bacteria are released into the extracellular space (125). Thus, the adaptive shift from a slow growing, vacuolar population in fast-proliferating host cells to a quickly growing, cytoplasmic population in arrested or slowly proliferating host cells, provides an advantage for *Salmonella* in spreading and overall host colonization.

The strict differentiation of bacterial pathogens into either vacuolar or cytoplasmic has been blurred for a few years already. Pathogens, like Mycobacteria that are considered to be vacuolar were shown to escape into the cytoplasm of macrophages and myeloid cells, as well (162) (163). On the other hand, *Francisella tularensis,* mainly considered to be cytoplasmic, re-enters a vacuolar pathway in mouse macrophages (164). *Shigella flexneri* and *Listeria monocytogenes*, bacteria that usually infect gastrointestinal cells

force their release into the cytoplasm (165). These data show that the intracellular fate of pathogens is adapted and depends on the host cell type. Moreover, it reveals that bacteria might not be restricted to only one host cell type, but adapt quickly to their environment. S. *aureus* for example, was shown to escape the vacuole in non-professional phagocytes, whereas it remains vacuolar in macrophages (166). The current study on *Salmonella* provides further evidence that it cannot only adapt to its particular host cell, but that it is actually the cell cycle state that contributes significantly to the decision whether the bacteria follow a vacuolar or cytoplasmic lifestyle.

3.1.2 SPI-1 activity of Salmonella in G1 arrested cells

Previous studies of cytoplasmic *Salmonella* populations revealed that these bacteria were mostly SPI-1 positive (126). The SPI-1 system is usually considered to be required for invasion, but is thought to contribute to vacuolar escape of *Salmonella* due to its pore-forming activity (167). Expression of the SPI-1 system is higher at late exponential growth phase and thus bacterial cultures at that stage are usually used for infection experiments (168). Previously, it was described that ΔSPI-1 mutants were also able to invade epithelial cells by hijacking invasion routes of WT *Salmonella* (169) and a recent study on the bi-stability of SPI-1 found that actually only 10-20% of a *Salmonella* population are SPI-1^{ON} , while the remaining bacteria are SPI-1^{OFF} and enter epithelial cells with help of SPI-1^{ON} bacteria (170). According to the authors, this relatively small number of bacteria seems to be sufficient to enable successful invasion of a *Salmonella* population. An increase of the SPI-1^{ON} fraction even reduced the invasion rate, although the molecular reason for this remains obscure. Interestingly, the described proportion of 10-20% SPI-1^{ON} bacteria is similar to the previously mentioned 5-20 % of cytoplasmic bacteria in epithelial cells and it is conceivable that the SPI-1^{ON} fraction that facilitates invasion is the same fraction that later escapes into the cytosol, while the SPI-1^{OFF} bacteria remain vacuolar. Upon G1 arrest of HeLa 229 and HCT8, intracellular *Salmonella* expressed more *sopE* and *sptP*, two effector proteins of the SPI-1 system. Given that SPI-1 activity destabilizes the nascent vacuole (48) and that SPI-1 activity is prolonged in G1 arrested cells, it would explain the increased proportion of cytoplasmic

Salmonella. Furthermore, the invasion efficiency of *Salmonella* depends on the strain (171), the growth phase (168) and the environmental condition (172), but also on the host cells type (173), and it was shown that *Salmonella* preferentially invades mitotic cells due to a different membrane cholesterol composition (47). With this in mind, one could speculate whether G1 arrested cells are "more attractive" for SPI-1^{ON} bacteria, which would result in an increase of the fraction of SPI-1^{ON} bacteria invading and subsequently escaping the nascent vacuole. On the other hand, an increase of the SPI-1^{ON} fraction, would lead to a reduction in the overall invasion rate, as described above. In the present study a slightly, yet not significantly, reduced number of intracellular bacteria was observed at 1 hpi in G1 arrested cells compared to control cells, which would be in agreement with this hypothesis. However, this requires further investigation and remains speculative for now.

3.1.3 Proteasomal degradation of bacterial effectors is delayed upon G1 arrest

Arresting cells in G1 phase resulted in reduced, though not completely abolished, degradation of the SPI-1 effectors SopE and SptP, which have previously been shown to be degraded by the host proteasome (51). In addition to the higher expression rate of *Salmonella* SPI-1 genes in G1 arrested cells, this might contribute to rupture of the nascent vacuole. Even though the here investigated effectors SopE and SptP were shown not to be responsible for vacuolar escape themselves (126) they can still be used as marker proteins for SPI-1 activity or the whole SPI-1 translocon apparatus, respectively. In G1 arrested cells degradation of the bacterial SPI-1 effectors SopE and SptP was less efficient and their presence and activity in host cells lengthened. This would have consequences on their target host pathways and might contribute to (i) stalling maturation of the SCV at an earlier stage e.g. by prolonged recruitment of Rab5/ early endosomes and (ii) rupture of the nascent vacuole and escape into the cytoplasm. Of note, the cell lines used in this study are immortal cancer cell lines and might have *per se* an increased proteasomal activity (39) (38) that could only be reduced and not completely abolished upon CDK4/6i treatment. It is conceivable that G1 arrest has a much stronger effect on proteasomal activity in primary cells and thus proteasomal degradation of SPI-1 effectors would be completely impaired and not only

reduced. *Salmonella* as an intracellular pathogen relies on host processes to establish a successful infection and the current study shows for the first time that cell cycle dependent regulation of this host process shapes the intracellular lifestyle of *Salmonella* and thus underline the importance of the host cell cycle for *Salmonella* infection. In previous studies reduced proteasomal activity contributed to increased lysosomal biogenesis (174) (175) and it is conceivable that in G1 arrested cells reduced proteasomal activity contributed to increased lysosomal biogenesis as well. However, this remains to be elucidated in future studies, while the current work focused on the implications of G1 arrest on the endolysosomal and autophagosomal pathway and its effect on the maturation of the *Salmonella* containing vacuole.

3.1.4 Galectin-3 recruitment confirms rupture of the SCV

Higher and prolonged SPI-1 activities, the presence of large bacterial clusters at 6 hpi in HCT8 and HeLa CCL2 cells and results from chloroquine resistance assays in G1 arrested cells, provided evidence for vacuolar escape and cytoplasmic replication. To confirm that SCVs are indeed damaged, presence of galectin-3 on SCVs was determined. Galectin-3 is a member of the family of β-galactoside-binding lectins, which are mainly localized in the cytosol (156). Galectins bind to glycans that are usually found on the extracellular cell surface or within the lumen of intracellular organelles and only become exposed to the cytosol upon disruption of organelle membranes by various stresses or pathogens. Binding of Galectins to unusually exposed glycans is considered to be a danger signal for the cell and triggers various cellular stress responses that are not yet fully elucidated (155). While it has been shown that Galectin-8 binding promotes autophagy (176), the consequence of Galectin-3 binding is not fully resolved. However, it was shown that Galectin-3 binds to damaged vacuoles of *Shigella flexneri* (156) and to bacterial phagosomes whose membranes were ruptured due to the pore forming activity of type three secretion systems (177). In G1 arrested cells, Galectin-3 was recruited to significantly more SCVs than in control cells, confirming that SCVs are more prone to damage and escape of bacteria into the cytosol was promoted. It is not clear if Galectin-3 recruitment induced a repair mechanism by the host and therefore rescues damaged SCVs, as it has been described for Galectin-8 (176), but it clearly

demonstrated that the early SCV membrane in G1 arrested cells is damaged, most likely by activity of the T3SS SPI-1.

Nonetheless, an additional factor influencing SCV membrane integrity in G1 arrested cells must be involved since only 15-20% of the *Salmonella* population (1 hpi HeLa) was fully decorated with Galectin-3, while in the chloroquine resistant assay almost 75% of the bacterial population was resistant and thus considered to be in the cytosol. Of note, quantification of Galectin-3 positive *Salmonella* was restricted to fully enclosed bacteria and did not consider bacteria with small dot-like Galectin-3 signals in order to reduce the risk of false-positive results. Furthermore, the mode of action of Chloroquine has to be taken into account. As described earlier, Chloroquine is trapped in acidic organelles and concentrations become increasingly bactericidal (127). In G1 arrested HeLa 229 cells, ca. 25% of the *Salmonella* population was killed by Chloroquine and were considered vacuolar. Approximately 20% of the bacteria were fully decorated with Galectin-3 and presumably escaped into the cytoplasm, while other bacteria were only partially decorated with Galectin-3 (resulting in ca. 50% Galectin-3 positive *Salmonella* – data not shown). This indicates that a large fraction of intracellular *Salmonella* in G1 arrested cells resides in a membrane enclosed compartment that did not acidify enough to accumulate Chloroquine in bactericidal concentrations. More specifically, it suggests that vacuoles were either leaky or their membrane composition, which is important for recruitment of the proton pumping v-ATPase, must have been compromised. Overall, it shows that in G1 arrested cells approximately 80% of *Salmonella* reside in the cytoplasm or in a compartment with a compromised vacuole.

3.1.5 Salmonella containing vacuole pH and v-ATPases

Acidification of SCVs usually starts within the first hour after invasion with fusion to early endosomes. Subsequently, fusion with late endosomes and lysosomes lead to an endosome-like maturation, including a gradual decrease in pH_{SCV}. To follow up on the previous findings pH_{SCV} was determined. While in control cells pH_{SCV} gradually decreased, it only dropped slightly at later time points in G1 arrested cells, comparable to what was observed in cells treated with Bafilomycin A1, an inhibitor of the v-ATPase (178) (179). This clearly confirmed that *Salmonella* did not reside in an acidic

compartment in G1 arrested cells; either due to vacuolar escape or insufficient acidification of (leaky) vacuoles or reduced fusion with endosomes. V-ATPases are large, complex proton pumps with a membrane spanning V_O and a cytosolic V_1 subunit and are, inter alia, responsible for acidification of eukaryotic organelles (15). Both subunits associate/ dissociate from each other in a dynamic, regulated and reversible fashion (180). However, the exact mechanism regulating their association and thus activity is only partially elucidated. So far, it is known that: (i) both subunits dissociate from each other upon glucose deprivation and starvation (181) (ii) v-ATPase abundance is cell type specific (15) (182) (iii) proton pumping efficiency varies between different isoforms of the V_O subunit (183) and (iv) specific lipid compositions of the membrane are required for generating active V_1 domains (180) (183). During maturation, endosomes gradually acidify, due to increased V_1/V_O ratios in late endosomes compared to early endosomes. Furthermore, the lipid environment, particularly the cholesterol and sphingolipid content of the membrane is crucial for proper activity (15) (180). The more fluid a membrane the faster V_1 dissociates and fewer protons are pumped, resulting in less acidification of the particular organelle. The more ridged the membrane the more stabilized is the V_1/V_O association. However, if membrane fluidity is too low and they become rather stiff, v-ATPase activity is blocked again, as shown by U18666A (a drug that leads to the accumulation of cholesterol in late endosomes) dependent cholesterol accumulation in a study by Lafourcade et al. (183). The role of the v-ATPase in membrane fusion events is still not clear. Earlier studies suggested that it regulates fusion together with SNARE proteins (184), or that it is not the presence of the V_1 subunit but rather the intraluminal pH facilitating fusion events (185), others claim that the v-ATPase is completely dispensable for fusion (186). While the current study did not aim at revealing new insights into the function and regulation of the v-ATPase, it clearly showed that acidification of the SCV in G1 arrested cells was impaired. A mild acidification to ≤ pH 6.5 of the endosomal system was however shown. Altogether, the lack of SCV acidification could have been caused either by reduced assembly of v-ATPase subunits, by reduced fusion with endosomes or because the majority of *Salmonella* had escaped from the SCV. Both processes are dependent on the protein and lipid composition of their membranes and strongly hinted at cell

cycle arrest-dependent changes of extra-and intracellular membranes. Future studies will have to determine whether the plasma and (nascent SCV) membranes of G1 arrested cells have a higher fluidity and thus rather loose V_1/V_O association (promoting membrane ruptures and low acidification) or if membrane fluidity is too low and hence v-ATPase activity is blocked (e.g. caused by cholesterol accumulation in lysosomes, which will be discussed later).

3.1.6 Reduced acidification impairs SPI-2 activation and vacuole maturation in G1 arrested cells

Acidification of the SCV is an important trigger for activation of the SPI-2 system of *Salmonella*. Studies in macrophages and epithelial cells had shown that the v-ATPase is recruited to SCVs within the first hour of infection and that SCVs gradually acidify to pH 5.0 (187) (188). Since acidification of SCVs did not occur in G1 arrested cells, it was hypothesized that SPI-2 activation was reduced. Indeed, by various methods it was proven that SPI-2 activation was impaired upon G1 arrest. A SPI-2 reporter confirmed that intracellular replication at 6 hpi (in CCL2 and HCT8) was SPI-2 independent. Interestingly, microscopy images of G1 arrested HCT8 revealed that some of the bacterial cluster still contained individual SPI-2 positive bacteria amongst a predominant SPI-2 negative population. Thus, in addition to a SPI-2 positive and a SPI-2 negative population a third, more heterogeneous fraction, was observed in FACS plots of G1 arrested HCT8 cells. This finding further supported the hypothesis that not all bacteria escaped into the cytoplasm, but some were either rescued or enclosed by a "leaky" membrane, over which no proper proton gradient could be established. Reduced expression levels of five selected SPI-2 genes and particularly of the response regulator *ssrB* suggested the absence of essential environmental changes and showed that inhibition of downstream signaling was blocked early. Finally, protein levels of SsrB and two other representative SPI-2 effectors clearly confirmed that activation of SPI-2 virulence genes and expression of SPI-2 effectors was reduced upon G1 arrest. Overall, these results support the hypothesis of leaky vacuoles in which acidification and SPI-2 expression was strongly reduced. As consequence of reduced SPI-2 activation, *Salmonella* effectors could not target host structures and enable modifications of the

SCV. Lysosomal markers like Lamp1, usually recruited within the first hour of infection, did not colocalize with *Salmonella* and also the exchange of fluid-phase markers such as fluorescently labelled dextran did not occur. This clearly demonstrated that SCVs did not recruit late endosomes/lysosomes or fused to exchange cargo. Still, *Salmonella* must initially have resided in a vacuolar compartment, since recruitment of EEA1 was not inhibited but rather prolonged. EEA1 and Rab5 are tethering partners and SopE targets Rab5, too. The prolonged presence of Rab5 and thus prolonged recruitment of EEA1 might have delayed exchange of Rab5 to Rab7 and therefore hold SCV maturation in an instable phase. This extended state of vacuole instability could additionally have promoted vacuolar escape of *Salmonella*.

Interestingly, a similar phenomenon of vacuolar instability in S-phase arrested cells has been observed in *Legionella pneumophila* infected cells (121). The authors observed that progression from G1 to S phase of *Legionella* infected cells is delayed. Concomitantly, Legionella failed to replicate in S-phase arrested cells, which was associated with the loss of the vacuole membrane barrier. A follow-up study on these results revealed that Legionella secretes translation inhibitors, which eventually target the host transcription machinery and induce degradation of Cyclin D1 (122).

3.1.7 Lovastatin induced G1 arrest impairs SCV maturation

Lovastatin, usually used to block cholesterol synthesis in cells, was used as an alternative method to arrest cells in G1 phase of the cell cycle. It has long been established to induce G1 arrest (138) (140), and lovastatin treatment of cells in the present study also resulted in strong cell cycle arrest. As expected, *Salmonella* long term infection was significantly reduced in HeLa 229, comparable to what has been observed after CDK4/6i treatment. Also SPI-2 expression was reduced, confirming that maturation of the SCV was impaired in G1 arrested cells. Lovastatin treatment of HCT8 cells resulted in a reduction of long term *Salmonella* infection as well (data not shown). This independent approach to arrest cells in G1 phase, confirmed that the course of *Salmonella* infection is dependent on the host cell cycle.

3.2 Endolysosomal and autophagosomal trafficking is dysregulated in G1 arrested cells

Maturation of the *Salmonella* containing vacuole heavily depends on the interaction with the endosomal system of the cell and corresponding trafficking pathways (189) (190). Since SCV maturation was impaired in G1 arrested cells, the question arose whether the endolysosomal system was altered upon G1 arrest and would thus have impaired vacuolar maturation and bacterial replication.

3.2.1 Endolysosomal trafficking is disturbed and lysosomes are inactive in G1 arrested cells

Investigation of G1 arrested host cells first and foremost revealed the accumulation of large intracellular vesicles with a lysosome-like electron dense structure. Subsequent labeling of marker proteins confirmed the endolysosomal nature of these vesicles. Surprisingly, the total amount of these proteins did not change significantly, but endolysosomes were unevenly distributed and appeared rather enlarged than evenly dispersed throughout the cytoplasm. Interestingly, similar phenotypes have been described upon lysosomal stress, alkalinization or in lysosomal storage disorders before, even though the exact molecular cause for these phenotypes remains unclear and speculative (26) (191) (192) (193) (194) (195). One aspect in common is a reduced activity or function of lysosomes. Assessing lysosomal activity in G1 arrested HeLa 229 and HCT8 cells indeed confirmed impaired degradation of cargo. This could have been caused by (i) a block of fusion of transport vesicles with lysosomes or (ii) misrouting of lysosomal hydrolases to the extracellular space or (iii) inactive hydrolases due to alkalinization of lysosomes. A block in cargo delivery to or fusion with lysosomes could be rather excluded, as the vesicles showed a very electron dense structure, which is typical for lysosomes harboring cytoplasmic and membranous components. Yet, final confirmation of impaired fusion with lysosomes remains to be done. More likely, lysosomes in G1 arrested cells accumulated cargo but were unable to degrade it. Degradation of cargo is facilitated by hydrolases that are still inactive when transported from the ER via Golgi towards lysosomes, where they become fully active due to the

acidic luminal pH. One of these hydrolases, Cathepsin D, was investigated and results revealed impaired processing upon G1 arrest. Protein levels of Golgi related precursors and intermediate forms were increased, whereas the mature form was slightly reduced. This could either be interpreted in a way that cells responded to the lack of degradation products by providing more Cathepsin D, and/or that the final processing in lysosomes was impaired and precursor and intermediate forms were "stuck" in trafficking, such that they accumulated. In addition, some preliminary results implied that Cathepsin D precursors were misrouted to the extracellular space (data not shown). Whether misrouting of hydrolases or inactivity (e.g. due to a lack of acidification) was responsible for reduced lysosomal activity needs to be clarified in future studies. The results clearly showed that in G1 arrested cells (i) endolysosomes were unevenly distributed and enlarged, (ii) lysosomal hydrolases were inactive and might have been misrouted to the extracellular space and (iii) breakdown of delivered cargo was blocked.

3.2.2 Autophagy flux is impaired upon G1 arrest

Since both, endosomal and autophagy pathways culminate in lysosomal degradation; autophagy capacity of G1 arrested cells was assessed as well. Chloroquine and NH_4Cl were used as controls as they are commonly used to study autophagy and autophagosome-lysosome fusion (22) (126) (196). Both drugs cause alkalinization of lysosomes and block turnover of membrane components and luminal proteins, though it is still under debate if this is due to impaired fusion of autophagosomes with lysosomes or if these organelles still fuse but degradation is blocked. In the present study G1 arrest caused a remarkable accumulation of autophagosomes in HeLa 229 and HCT8 cells, but autophagy turnover was significantly impaired. This, again, confirmed that lysosomal activity in G1 arrested cells was strongly impaired, most likely caused by alkalinization. Whether this already blocked fusion of autophagosomes with lysosomes or only degradation of delivered cargo could not be fully resolved. Preliminary colocalization data of LC-3B (= autophagosomes) and Lamp1 (=lysosomes) in G1 arrested HeLa 229 cells showed only 30% overlap, indicating reduced fusion (data not shown). However, the fast turnover and thus almost complete lack of autophagosomes

in control cells complicated a proper interpretation. Altogether, this provided additional evidence that lysosomes in G1 arrested cells were dysfunctional, resulting in impaired autophagy flux and accumulation of endosomal cargo.

Lysosomes are important for metabolic regulation and signaling in the cells. Upon lysosomal stress, breakdown of macromolecules is impaired and availability of amino acids, lipids or carbohydrates is reduced. In response, the transcription factor EB (TFEB) is released and translocates into the nucleus, where it activates transcription of genes necessary for lysosomal biogenesis and autophagy (31). The lack of lysosomal degradation products in G1 arrested HeLa 229 and HCT8 cells induced a significant nuclear translocation of TFEB and clearly confirmed that cells responded to lysosomal stress by initiating autophagosome formation and increased production of Cathepsin D. Yet, activation of the v-ATPase and therefore proper acidification seemed to be impaired, despite TFEB translocation. Interestingly, experiments in *ATP6ap2* knockout mice by Kissing et al. revealed that lack of the v-ATPase caused massive accumulation of autophagocytic vacuoles in hepatocytes, in spite of normal TFEB translocation, as well (197). This shows how crucial proper regulation and activity of the v-ATPase is and further supports the hypothesis of deregulated v-ATPase assembly and function in G1 arrested cells.

3.2.3 Lysosomal membrane composition and accumulation of cargo

Interestingly, Western blot analysis of Lamp1 in HCT8 cells revealed a different banding pattern even though the total amount of protein was not increased significantly. This suggests alterations in processing, more particularly in glycosylation, of Lamp1. Glycosylation of Lamp1 occurs in the Golgi apparatus and is important to protect the lysosomal membrane from self-digestion by luminal hydrolases; in fact 80% of a lysosomal membrane is decorated with Lamp1 and Lamp2 and thus provides a so-called protective glycocalix layer (195). In addition, Lamp1 facilitates Cholesterol export. While endosomes and the plasma membrane are quite rich in cholesterol and the cholesterol content is even increasing during maturation, it is exported from lysosomes and transported to the plasma membrane where it is recycled or exocytosed (198). How exactly export from lysosomes is facilitated is topic of research in several

labs and so far it has been shown that Niemann-Pick-Protein 1 (NPC1) and Niemann-Pick-Protein 2 (NPC2) are major players (199). Recently it was shown that Lamp1 provides a "bridge" between intraluminal cholesterol and the membrane standing NPCs in order to facilitate cholesterol transport (198). Mutations in NPCs are a well-known cause for a variety of lysosomal storage disorders that are characterized by cholesterol accumulation (200). Interestingly, electron microscopy images of these cells show a comparable accumulation of electron dense lysosomes as G1 arrested cells in the present study (201). Another important group of lysosomal storage disorders result in the so-called I-Cell disease or mucolipidosis, in which not only cholesterol but all kinds of lipids, proteins, carbohydrates or nucleic acids accumulate in lysosomes. Interestingly, the vesicles found in G1 arrested cells are also positive for Hoechst staining, a marker for nucleic acids (see brightfield images merge with Hoechst [Fig. 30]). I-Cell disease is caused by altered glycosylation of proteins in the Golgi, resulting in misrouting of lysosomal hydrolases to the extracellular space (202)(203). Upon the above mentioned clues it is possible to speculate whether glycosylation in the Golgi apparatus of G1 arrested cells is hampered. While glycosylation is important for function of certain Golgi proteins, it also functions a nutrient sensor for cells, since glycosylation of proteins increases/decreases dependent on glucose and amino acid availability (204). Particularly the Golgi proteins Grasp55/65 play an important role. Depletion of each of these proteins was shown to result in aberrant stacking of the Golgi and increased vesicle formation (205). In addition, processing of proteins in Grasp55/65 knockout cells had led to accelerated but insufficient processing of proteins. Eventually this resulted in misrouting of several proteins, including Cathepsin D, into the extracellular space (205). Furthermore, upon starvation Grasp55 was de-glycosylated and translocated from the Golgi to autophagosomes where it facilitated fusion by binding Lamp2 and LC-3B. When Grasp55 was depleted, autophagosomes were formed, but autophagy flux was impaired (204) (206). Therefore, glycosylation of lysosomal proteins, membranous or soluble, should be investigated in more detail in G1 arrested cells in order to investigate the mechanism behind lysosomal inactivity. The present study reveals that processing and trafficking of endolysosomal proteins is altered upon G1 arrest. These findings provide additional

information to the field of endolysosomal research and help to shed light on the link between cell cycle regulation and regulation of endosomal trafficking. Eventually, these results establish a link between cell cycle regulation and the outcome of *Salmonella* infection.

3.2.4 Autophagy and cellular metabolism of G1 arrested cells

Going into a quiescent or arrested state induces several changes in the metabolic network of cells, such that they maintain only basic metabolic function to enable a fast re-entry into the cell cycle. They slow down anabolic processes and switch towards catabolism (207). It has been observed that autophagy is increased in G_0/G1 arrested cells and interestingly the same pathways involved in autophagy initiation (e.g. mTOR pathway) were observed to channel cell cycle arrest (40) (208) (209). Although the interdependence of these processes is not fully resolved, research of last decades accumulated enough evidence to demonstrate that regulation of the cell cycle and regulation of metabolic processes are mutually dependent on each other (210). For that reason, results obtained in the present study have to be evaluated against this background as well. Upon G1 arrest endolysosomal and autophagosomal trafficking was dysregulated and lysosomal cargo was not degraded. On the other hand autophagosome formation was induced. This might be solely the result of lysosomal stress, but could additionally be influenced or even be triggered by the quiescent cell cycle state. As already mentioned, lysosomal stress induced dephosphorylation and translocation of TFEB to the nucleus. TFEB is regulated by mTORC1, a master regulator of cellular metabolism and growth. MTORC1 itself is regulated by (i) plasma membrane related factors (growth factors, cytokines, hormones) (211) (212), which will not be discussed here; (ii) lysosomal and/or mitochondrial stress (degradation or liberation of nutrients) as already discussed above (213) (214) or (iii) cytoplasm related factors (energy status) (215) (216) (217) (218). The energy status or availability of nutrients in the cytoplasm is sensed by AMPK (AMP-activated protein kinase). AMPK phosphorylates TSC, which in turn downregulates Rheb. Rheb eventually activates mTORC1. In cycling cells and under physiological conditions, AMPK levels are relatively low and thus phosphorylation of TSC is only marginal. Consequently, Rheb levels are

high. Since Rheb activates mTORC1 this results in phosphorylation (= inactivation) of TFEB. Upon nutrient starvation, AMPK levels increase. Hence, more TSC is phosphorylated and Rheb is strongly downregulated. Without Rheb, mTORC1 is not activated, TFEB becomes dephosphorylated and translocates into the nucleus as depicted below. A recent study provided further evidence of the interdependence of cell cycle and metabolic regulation. Lopez-Mejia et al. discovered that CDK4 does not only regulate cell cycle progression but inhibits AMPKα2, one of the two subunits of AMPK (219). This interesting finding implies that inhibition of CDK4 (as in quiescent/ G1 arrested cells) would lead to an increase in AMPK levels and more phosphorylation of TSC. The increased TSC activation would strongly inhibit Rheb function and thus less mTORC1 would be activated. Consequently, TFEB would be less phosphorylated and eventually translocate to the nucleus to induce lysosome biogenesis and autophagosome formation [Fig. 45].

Both, lysosomal stress and a possible increase in AMPK activity provide an explanation for TFEB translocation and subsequent autophagosome formation in G1 arrested cells. Still, the question remains why the actual degradation of cargo did not occur in G1 arrested cells. Further studies need to explore this in more detail and might provide more insight into regulation of metabolic pathways and their connection to the cell cycle. Interestingly, a recent study by Doronzo et al. provided new evidence for the interplay of cell cycle and autophagosomal regulation (220). The authors show that TFEB does not only initiate transcription of genes for lysosomal biogenesis and autophagy, but also binds to the promotor region of CDK4, thereby promoting cell cycle progression. This shows that CDK4 and TFEB are mutually influencing each other and thereby fine tune cell cycle and autophagosomal regulatory networks, which eventually affects the course of *Salmonella* infection.

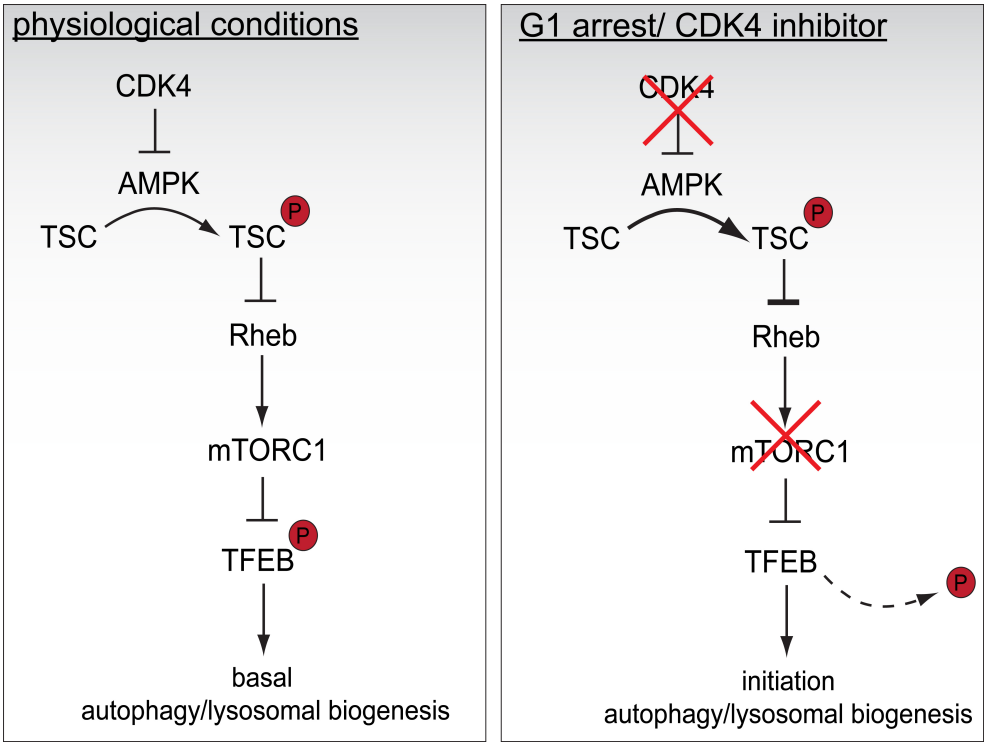

Fig. 45 CDK4 regulates autophagy and lysosomal biogenesis via the AMPK-TSC-TFEB axis

Under physiological conditions CDK4 reduces AMPK activity. AMPK phosphorylates (= activates) TSC, which in turn downregulates Rheb. Rheb activates mTORC1 and mTORC1 phosphorylates (=inactivates) TFEB. Therefore autophagosome formation and lysosomal biogenesis is kept in balance and cells maintain only basal levels. During G1 arrest (e.g. induced by CDK4 inhibition) AMPK levels increase and TSC is phosphorylated, leading to enhanced downregulation of Rheb. Subsequently, mTORC1 becomes deactivated and TFEB translocates to the nucleus resulting in increased initiation of autophagy and lysosomal biogenesis. CDK4 = Cyclin dependent kinase 4; AMPK = AMP-dependent kinase; TSC = Tuberous Sclerosis Complex; Rheb = Ras homolog enriched in brain; mTORC1 = mammalian/mechanistic target of rapamycin complex 1; TFEB = Transcription factor EB

3.3 Cell cycle arrest induced by miRNAs inhibits long-term infection by *Salmonella* Typhimurium

The CDK4/6 inhibitor and lovastatin are chemical drugs used to arrest cells in G1 before *Salmonella* infection. Both drugs are useful means to study the cell cycle dependent regulation of *Salmonella* infection, though they might be considered a non-physiological interference with cellular pathways. Thus, physiological regulators of the cell cycle and the effect on *Salmonella* infection were investigated. In this third approach miR-15a-5p, miR-16a-5p and miR-744-5p were overexpressed in HeLa 229 cells and results further confirmed the finding that cell cycle regulation, lysosomal biogenesis and thus the course of *Salmonella* infection are intertwined.

The present study revealed that TFEB, Lamp1 and lysosomal activity are significantly downregulated upon miR-744-5p overexpression, clearly showing the importance for miR-744-5p in overall regulation of autophagy and lysosomal processes. In addition, overexpression of miR-744-5p reduced the bacterial load already at 4 hpi and significantly decreased *Salmonella* infection at 20 hpi, which is in agreement with the reduced of SPI-2 activation. This strengthened the hypothesis that cell cycle dependent de-regulation of endolysosomal/ autophagosomal trafficking interfered with *Salmonella* infection.

MiR-744-5p was shown to regulate cell proliferation already in previous studies e.g. by targeting c-Myc, a component of the MAPK/ERK pathway, thereby acting as tumor suppressor (159). The same study observed that miR-744-5p is downregulated in human hepatocellular carcinoma cells, causing faster proliferation, while overexpression of miR-744-5p restored G1 accumulation. Similar data were obtained by Kleemann et al., who reported that miR-744-5p was downregulated in ovarian cancer cells and that overexpression of miR-744-5p had an pro-apoptotic effect on these cells (221). In contrast, a study by Zhang et al. observed an increase of miR-744-5p in tissue samples of patients with prostate cancer cells (222). After applying miR-744-5p inhibitors to these cancer cells, the authors observed less viable or more apoptotic cells, and a lower number of cell colonies, which led to their interpretation

that miR-744-5p promotes cell proliferation. Interestingly, the same study revealed that miR-744-5p targets LKB1 (liver kinase B1), a tumor suppressor. LKB1 is a serine/ threonine kinase that directly phosphorylates and activates AMPK (223) (224). Thus, by regulating LKB1, miR-744-5p would negatively regulate AMPK activity and eventually lysosomal biogenesis and autophagy. This finding is important, since it not only provides a link between miR-744-5p and regulation of the lysosomal pathway, but is also in agreement with the results obtained in the present study. As discussed before, CDK4/6i treatment caused strong activation of TFEB, presumably due to increased activation of AMPK [Fig. 45], while overexpression of miR-744-5p caused a loss of TFEB, LC-3 (data not shown) and reduced LAMP1 levels [Fig. 43]. This could be explained by the downregulation of LKB1 and consequently deactivation of AMPK by miR-744-5p. Without the regulatory effect of AMPK on mTORC1, TFEB would remain inactive and autophagy and lysosomal biogenesis were downregulated. Notably, RNA-sequencing results of cells transfected with miR-744-5p already suggested a regulatory role for miR-744-5p in autophagy trafficking and predicted LC-3B and ATP6V0A4, a subunit of the v-ATPase, to be a target (unpublished results lab). Overall, these data strengthen the hypothesis that cell cycle regulation, more particularly cell cycle arrest, and regulation of endolysosomal and autophagosomal trafficking are linked. Nevertheless, future studies need to evaluate this in more detail.

Further support was provided after overexpression of miR-15a-5p and miR-16a-5p, which directly target Cyclin D1 and thus delay cells in G1 phase (5) (6). In these cells, lysosomal activity was reduced, Lamp1 was downregulated and TFEB translocation was initiated, though less strong compared to treatment with CDK4/6i. Most likely, this was due to the milder effect on the cell cycle causing rather a delay in proliferation than a full arrest. While the role of miR-15a-5p and miR-16a-5p in cell cycle regulation has been studied, hardly anything is known about their role in regulation of endosomal or autophagosomal trafficking. A study on $CD4^+$ regulatory T cells (T_{reg}) revealed that miR-15b/16 regulate expression of *rictor* and *mtor*, genes encoding components of the mTOR signaling pathway, which is required for T_{reg} development and initiation (225). Interestingly, Rictor was shown to be directly regulated by miR-15a and miR-16 by another study, as well (226). In addition, the authors show that overexpression of miR-

15a/miR-16 or downregulation of Rictor by siRNAs results in G1 arrest and in induction of autophagy. Also, knockdown of Rictor resulted in reduced mTORC1 activity, which might have been the cause for induction of autophagy. Interestingly, the above mentioned study by Doronzo et al. did not only show that TFEB initiates transcription of CDK 4, but at the same time TFEB stimulated expression of the miR-15a/16-1 cluster, though it was not shown whether this is a direct or indirect effect (220). Nonetheless, this shows that TFEB plays a pivotal role in balancing or fine-tuning cell cycle progression by activating CDK4 and miR-15/16, which downregulate Cyclin D1 and thereby delay cell cycle progression. In the present study, TFEB was activated upon G1 arrest and thus additional evidence for a regulatory circuit of cell cycle and autophagosomal pathways is provided.

A third aspect, the impact on infection with *Salmonella* was investigated as well. Overexpression of miR-15a-5p and miR-16a-5p resulted in a delay, rather than an arrest in G1 phase. Thus, infection of miR-16a-5p transfected cells resulted in reduced, but not completely impaired SPI-2 activation at 4 hpi. Yet, the intracellular bacterial load was already reduced at 4 hpi and significantly decreased at 20 hpi. Suppression of autophagosomal/lysosomal processes was also less intense compared to CDK4/6i or miR-744-5p treated cells and goes alongside with a rather late interference with *Salmonella* infection, as observed by Maudet et al. (5). The authors have shown that upon miR-15a-5p and miR-16a-5p overexpression, SCV maturation progressed far enough to allow replication at 8 hpi but seemed to be interrupted afterwards, resulting in strongly reduced bacterial load at 20 hpi. In the present study, treatment with CDK4/6i or overexpression of miR-744-5p induced a full cell cycle arrest, not only a delay in proliferation, and consequently lysosomal activity was sufficiently suppressed, which compromised already early steps in SCV maturation.

3.4 Conclusion and Outlook

The present study shows that the intracellular lifestyle of *Salmonella* is altered upon G1 arrest of host cells. Proteasomal degradation is delayed and endolysosomal and autophagosomal trafficking is compromised. Processing of lysosomal proteins is insufficient and lysosomal activity and autophagy flux are impaired. The deregulation of these cellular signaling pathways affects maturation of the *Salmonella* containing vacuole (SCV) that is consequently stalled at an early, vulnerable stage. It is shown, that acidification of SCVs is impaired upon G1 arrest. Thus, an important environmental factor for the switch from SPI-1 to SPI-2 gene expression is missing and the SPI-2 system is not activated. As a result, targeting and modification of host cell structures by SPI-2 effectors e.g. recruitment of endolysosomal membrane proteins, like LAMP1, or exchange of endosomal cargo, is compromised. Finally, it was shown that SCV membrane integrity is compromised; the early SCV ruptures and bacteria are released into the cytoplasm. Depending on the host cell type, SPI-2 independent, cytoplasmic replication is promoted.

Proper maturation and function of both *Salmonella*-containing vacuoles and endolysosomes is dependent on gradual acidification and integrity of the surrounding membranes. Given that both are compromised in G1 arrested cells, the intracellular lifestyle of *Salmonella* is shifted towards vacuolar escape and cytoplasmic replication upon G1 arrest. Therefore, results of the current study on G1 arrested cells fit into the complex picture of intertwined lysosomal function, metabolic regulation and regulation of the cell cycle. It is shown that the intracellular lifestyle of *Salmonella* is strongly influenced, if not dependent, on the cell cycle state of host cells and that this effect is linked to deregulation of endosomal trafficking. While proliferating cells provide an environment that supports a vacuolar lifestyle, arrested cells represent a different cellular environment. Alterations of proteasomal and endolysosomal dynamics cause changes in the lipid and protein composition of cells. This impacts on the stability and, most importantly, on the acidification of the SCV. Instead of establishing a protective vacuolar niche, *Salmonella* escapes the vacuole and replicates in the cytosol. Altogether, cytoplasmic replication in resting cells might harm the individual host cell

but provide an overall advantage in spreading and tissue colonization of *Salmonella*. Therefore, the current study sheds light on the adaptive capacity of *Salmonella* and establishes a link between the intracellular *Salmonella* lifestyle and the host cell cycle state.

Future studies will need to show why SPI-1 expression is sustained in G1 arrested cells. One could speculate that G1 arrested cells selectively attract SPI-1^{ON} bacteria, e.g. due to an altered plasma membrane lipid composition. Also, the reason for reduced proteasomal activity needs to be unraveled, since the reduction of SPI-1 effector degradation contributed to stalling SCV maturation at an earlier stage. Additional methods need to be applied to decipher if fusion of autophagosomes and lysosomes in G1 arrested cells is blocked, which would also give more insight into fusion events between SCVs and endolysosomes. Since T3SS-induced damages of SCVs recruited galectin-3, it would be interesting to investigate consequences e.g. subsequent recruitment of the autophagy machinery or activation of innate immune responses and the impact on the *Salmonella* population. Furthermore, Golgi dynamics and the original cause for improper processing of lysosomal proteins and lipids needs to be studied in more detail to complete the understanding of lysosomal inactivity in G1 arrested cells. Also, possible alterations of the CDK-AMPK-TFEB signaling pathway should be addressed. Finally, it would be interesting to investigate if lifestyle of other intracellular bacteria that hijack the host endosomal system is also altered upon G1 arrest of host cells.

4 Materials and methods

4.1 Materials

4.1.1 Equipment and Instruments

Instrument	Manufacturer
Accuri™ C6 flow cytometer	BD Biosciences
Bio TDB-100, Dry block thermostat	Biosan
C1000 Touch™ Thermal Cycler	Bio-Rad
Centrifuge 5810	Eppendorf
CFX96 RealTime System	Bio-Rad
Confocal Leica TCS SP5 microscope	Leica
Eclipse TS100 Inverted Routine Microscope	Nikon
Electroporator MicroPulser	Bio-Rad
Eppendorf 5424 centrifuge	Eppendorf
Eppendorf 5424R centrifuge	Eppendorf
Eppendorf Research® plus 10, 20, 200, 1000	Eppendorf
FACSAria™ III sorter	BD Biosciences
Gel documentation system Gel iX Imager	Intas
Heraeus™ Multifuge™ X3 Centrifuge	Thermo Fisher
Horizontal electrophoresis systems PerfectBlue	PeqLab
Image Quant LAS 4000 imaging system	GE Healthcare
Impulse heat sealer	Geho
Incubator I	Memmert
Infinite® 200 PRO plate reader	Tecan
NanoDrop 2000 spectrophotometer	Perkin-Elmar
New Brunswick GALAXY 170S CO2 incubator	Eppendorf
Safe 2020 Class II Biological Safety Cabinets	Thermo Fisher
Shaker Duomax 1030	Heidolph
Shaker Unimax 100	Heidolph
Tank electroblotter WEB ™	PeqLab
Thermo-Shaker, TS-100C	Biosan
Vertical electrophoresis systems PerfectBlue Twin S	PeqLab

4.1.2 Consumables and commercial kits

Consumables	Manufacturer
Adhesive qPCR Seal	Sarstedt
Amersham Protan Blotting Membrane	GE Healthcare
Cell culture well-plates	Omnilab
Cell Scrapers	Fisher Scientific
Cell-culture flasks	Sarstedt
Coverslips round	Hartenstein
Coverslips squared	Laborhaus S. & Ö.
DMEM cell culture medium	Thermo Fisher Scientific
DNase I	NEB
dNTPs	Thermo Fisher Scientific
Fetal Bovine Serum	Biochrom
Hard-Shell® 96-Well PCR Plates	Bio-Rad
Inoculation loops	Omnilab
Lipofectamine RNAIMAX	Thermo Fisher Scientific
Microscope slides	Fisher scientific
Millex® Syringe Filter	Merk Millipore
Nitrocellulose membranes for Western blot 0.45 µm	GE Healthcare
NucleoSpin® Gel and PCR Clean-up	Machrey-Nagel
NucleoSpin® Plasmid EasyPure	Machrey-Nagel
Opti-MEM	Thermo Fisher Scientific
PageRuler™ Plus Prestained Protein Ladder	Thermo Fisher Scientific
Pasteur pipettes	Kimble
Phase Lock Gel tubes 2 ml	5 Prime
Pipette filter tips	Sarstedt
Pipette tips	Sarstedt
Protease Inhibitor Cocktail Tablets in EASYpacks	Roche
Random primers	Invitrogen
Reagent and centrifuge tubes 15, 50 ml	Sarstedt
RNaseOUT	Thermo Fisher Scientific
RPMI medium	Thermo Fisher Scientific
Safe-lock tubes 0.2 ml, 0.5 ml, 1.5 ml, 2.0 ml	Eppendorf
Serological pipettes	Sarstedt
Spectrophotometer cuvettes	Sarstedt
SsoAdvanced™ Universal SYBR® Green Supermix	Bio-Rad
Syringe sterile filters (0,22 µm)	Millex
Trypsin-EDTA (0.5%), no phenol red	Thermo Fisher Scientific
Tubing foil	Hartenstein
Whatman blotting paper	Albet LabScience

4.1.3 Chemicals

Chemicals	Manufacturer
1 Kb Plus DNA Ladder	NEB
100 mM DNTP Set	Thermo Fisher Scientific
2-Propanol (Isopropanol)	Roth
Agar agar	Becton Dickinson
Albumin Fraction V (BSA)	Roth
Ampicillin sodium salt	Roth
Chloramphenicol	Roth
Difco Agar	Merck
Dimethyl sulfoxide (DMSO)	Roth
EDTA	Roth
EGTA	Roth
Ethanol	Roth
Ethanol (absolute for analysis)	Laborhaus Scheller
Gentamycin	Sigma-Aldrich
GlycoBlue	Ambion
H_2O_2 30%	AppliChem
Kanamycin sulfate	Roth
Luminol	Sigma-Aldrich
Methanol	Roth
Milk powder (blotting grade)	Roth
M-MLV Reverse Transcriptase	Thermo Fisher Scientific
para-Formaldehyde	Sigma-Aldrich
p-Coumaric acid	Sigma-Aldrich
Propidium Iodide	Sigma-Aldrich
Random Primers	Thermo Fisher Scientific
RedSafe	ChemBio
RNAse A	Sigma-Aldrich
RNaseOut Recom. RNase Inhibitor	Thermo Fisher Scientific
Rotiphorese gel 40 (37.5:1)	Roth
SsoAdvanced Universal SYBR Green	Bio-rad
TEMED	Roth
Triton-X100	Sigma-Aldrich
Trizol	Thermo Fisher Scientific
TRIzol Reagent	Invitrogen
Trypticase Soy Broth	Becton Dickinson
Trypton / Pepton ex casein	Roth
Vectashield Mounting Medium	Biozol
Yeast broth Difco	BD
Yeast extract	Roth

4.1.4 Oligonucleotides

Stock Name	Sequence 5'-3'	Description
AE0001	ATGCTTTTCCCGTTATCCGG	Sense oligo for GFP
AE0002	GCGTCTTGTAGTTCCCGTCATC	Antisense oligo for GFP
AE0051	GACAGGATTGACAGATTG	Sense oligo for 18S
AE0052	ATCGGAATTAACCAGACA	Antisense oligo for 18S
AE0341	CCTGTACGCCAACACAGTGC	Sense oligo for human beta-actin
AE0342	ATACTCCTGCTTGCTGATCC	Antisense oligo for human beta-actin
AE1137	CCCCGTAATGCAGAAGAAGA	Sense oligo for mCherry
AE1138	GTGGAACAGTACGAACGCGCCGA	Antisense oligo for mCherry
AE1209	CATGGATGTGAACGTGAAAATC	Sense oligo for *Salmonella* SopD2
AE1210	AAGCGGTCTTGTTGAGATGG	Antisense oligo for *Salmonella* SopD2
AE1211	GACGGATGCATCACAACCAG	Sense oligo for *Salmonella* SteC
AE1212	CATGTAACCGATAGACTGTCCCA	Antisense oligo for *Salmonella* SteC
AE1213	GAGGTGCAAAATGCATTACGTA	Sense oligo for *Salmonella* SseC
AE1214	CTTTACGCGCTTTATCCTCCT	Antisense oligo for*Salmonella* SseC
AE1288	AATGCCTGTTGTGCATACGA	Sense oligo for *Salmonella* ssrB
AE1289	TTAGCACCTGCGGCTAAAGT	Antisense oligo for *Salmonella* ssrB
AE1290	AGCCAGACCCGTGAAGCTATAC	Sense oligo for *Salmonella* sopE
AE1291	AGAAAAGGCGCTATGTTGATCC	Antisense oligo for *Salmonella* sopE
AE1526	AATCTTAAAGGCGCTGTCCTT	Sense oligo for *Salmonella* pipB2
AE1527	TACTGTCGCCTAGTGATGTTCC	Antisense oligo for *Salmonella* pipB2
AE1528	TGTAGCCCGGTTCTCACAAT	Sense oligo for *Salmonella* sptP
AE1529	GCCGGCTTCTATTTTCTCAAG	Antisense oligo for *Salmonella* sptP

4.1.5 Cell lines

Cell line	Origin	Tissue	Disease
HeLa 229 (ATCC® CCL-2.1)	human	cervix	adenocarcinom
HCT-8 (ATCC®)	human	colon	ileocecal colorectal adenocarcinoma
HeLa (ATCC® CCL-2)	human	cervix	adenocarcinom

4.1.6 Antibodies

Primary antibodies

Name	Species	Conditions of use	Manufacturer	Catalogue #
Cathepsin D	Mouse	WB 1:300 (ON, 4°C + 2h RT)	Sigma-Aldrich	SAB4200767
EEA1	Mouse	IF 1:200 (ON, 4°C + 2h RT)	BD Biosciences	610457
galectin-3 (M3/38)	Rat	IF 1:50 (ON, 4°C + 2h RT)	Santa Cruz	sc-23938
LaminB1	Mouse	WB 1:300 (ON, 4°C + 2h RT)	Ssanta cruz	sc-374015
LAMP-1	Rabbit	IF 1:250 (1h, RT)	Novus Biologicals	NB120-19294
LAMP-1 (H4A3)	Mouse	IF 1:100 (ON, 4°C + 2h RT)	Santa Cruz	sc-20011
LC3B	Rabbit	WB 1:1000; IF 1:250 (ON, 4°C + 2h RT)	Sigma-Aldrich	L7543
Rab7	Rabbit	IF 1:100 (ON, 4°C + 2h RT)	Cell Signaling Technology	9367S
Rab7	Mouse	WB 1:300 (ON, 4°C + 2h RT)	Santa Cruz	sc-376362
Salmonella typhimurium0-4 [1E6]	Mouse	IF 1:1000 (2h RT)	abcam	ab8274
TFEB	Rabbit	WB 1:1000, IF 1:100 (ON, 4°C + 2h RT)	Cell Signaling Technology	4240
α-Tubulin	Mouse	WB 1:5000 (ON, 4°C + 2h RT)	Sigma-Aldrich	T6199
β-Actin	Mouse	WB 1:5000 (ON, 4°C + 2h RT)	Sigma-Aldrich	A2228

Secondary antibodies

Name		Conditions of use	Manufacturer	Catalogue #
Anti-Mouse IgG Alexa Flour 488	Donkey	1/250 (IF)	Thermo Fisher Scientific	A21202
Anti-Mouse IgG Alexa Flour 594	Chicken	1/250 (IF)	Thermo Fisher Scientific	A21201
Anti-Rabbit IgG Alexa Flour 488	Chicken	1/250 (IF)	Thermo Fisher Scientific	A21441
Anti-Rat IgG Alexa Flour 594	Chicken	1/250 (IF)	Thermo Fisher Scientific	A21471
HRP anti-Mouse IgG	Sheep	1/10000 WB	Amersham/GE Healthcare	NA931
HRP anti-Rabbit IgG	Donkey	1/10000 WB	GE Healthcare	NA934

4.1.7 Antibiotics

Antibiotic	Solvent	Working concentration
Ampicillin	H_2O	100 µg/ml
Chloramphenicol	Ethanol abs.	20 µg/ml
Kanamycin	H_2O	50 µg/ml
Gentamycin	-/-	10 and 50 µg/ml

4.1.8 MicroRNA mimics

Name	Manufacturer
cel-miR-231 (non-targeting 4)	Dharmacon, Thermo Scientific
hsa-miR-15a-5p	Dharmacon, Thermo Scientific
hsa-miR-16a-5p	Dharmacon, Thermo Scientific
hsa-miR-744-5p	Dharmacon, Thermo Scientific

4.1.9 Cell dyes

Name	Solvant	Stock	Working solution	Manufacturer	Catalogue
Alexa Fluor 594 dextran	H_2O	5 mg/ml	100 µg/ml for 15 hrs	Thermo Fisher Scientific	D22913
HCS CellMask™ Deep Red Stain	DMSO	-/-	1:10,000 for 1h	Thermo Fisher Scientific	H32721
DQ-Red-BSA	PBS	1 mg/ml	5 µg/ml for 5 hrs	Thermo Fisher Scientific	D1251
Hoechst 33342	-/-	-/-	1:5,000 for 20 min	Thermo Fisher Scientific	H3570
Lysotracker	DMSO	75 µM	75 nM for 2 hrs	Thermo Fisher Scientific	L7528
Acridine orange	PBS	1 mg/ml	26 µM for 15 min	Sigma-Adrich	A6014

4.1.10 Bacterial strains

Genotype	Species	antibiotic marker	Stock name	Reference/Source
pTet-GFP	S.Typhimurium SL1344	Str^R Cm^R	AE-035	Kai Papenfort, Jörg Vogel lab (JVO-5292)
SsaG-GFP; pFPV-mCherry	S.Typhimurium SL1344	Amp^R Cm^R	AE-231	This study [1,2]
pFPV-mCherry	S.Typhimurium SL1344	Amp^R	AE-236	This study [2]
SsrB-Flag	S.Typhimurium SL1344	Kan^R	AE-239	A.S., Jörg Vogel lab (JVO-758)
SopE-flag	S.Typhimurium SL1344	Kan^R	AE-266	Yanji Chao, Jörg Vogel lab (YC-0172)
SteC-flag	S.Typhimurium SL1344	Kan^R	AE-270	Yanji Chao, Jörg Vogel lab (JVO-10980)
SptP-Flag	S.Typhimurium SL1344	Kan^R	AE-281	This study
PipB2-Flag	S.Typhimurium SL1344	Kan^R	AE-284	Yanji Chao, Jörg Vogel lab (JVO-10959)
pXG-1 GFP	*Shigella flexnerii* M90T	Cm^R	AE-107	Caroline Tawk, Eulalio Lab

[1] plasmid provided by Yanji Chao,
[2] plasmid provided by Olivia Steele-Mortimer (Addgene plasmid # 20956)

4.1.11 Drugs

Name	Solvant	Stock	Working solution	Manufacturer	Catalogue
CDK4/6 inhib IV	DMSO	10mM	10µM/ 20 µM	Calbiochem	219492
Lysotracker	DMSO	75 µM	75 nM	Thermo Fisher Scientific	L7528
DQ-RED-BSA	PBS	1 mg/ml	5 µg/ml	Thermo Fisher Scientific	D1251
Nocodazole	DMSO	0,5mg/ ml	0,1ug/ml	Sigma-Aldrich	M1404
Thymidine	H_2O	100mM	2mM	Sigma-Aldrich	T1895
Bafilomycin A1	DMSO	100µM	100nM	Invivogen	tlr-baf
Chloroquine	H_2O	30mM	100µM	Sigma-Aldrich	C6628
NH_4Cl	H_2O	2M	20mM	Roth	5050.1
Monensin	EtOH	2 mM	50 mM	Sigma-Aldrich	M5273
Nigericin	EtOH	6 mM	10µM	Sigma-Aldrich	N7143

4.1.12 Media

Bacterial media

Lysogeny broth (LB) – Lennox ; liquid medium and LB Agar

- 5.0 g tryptone
- 2.5 g yeast extract
- 5.0 g NaCl
- 7.5 g agar (for LB agar)

add up to 500 ml H_2O.

Tryptic soy broth-Congo red agar

- 15 g TSB (BBL Trypticase Soy Broth)
- 0.05 g Congo Red
- 0.5 g Agar

add up to 500 ml H_2O.

Cell culture media

- Gibco™ DMEM, low glucose, GlutaMAX™ Supplement, pyruvate
- Gibco™ RPMI 1640 Medium, GlutaMAX™ Supplement, HEPES
- Gibco™ Opti-MEM™ I Reduced Serum Medium
- Fetal bovine serum

4.1.13 Buffers and Solutions

10x PHOSPHATE BUFFERED SALINE (PBS) 1L

2 g KCl

2.4 g KH_2PO_4

80 g NaCl

14.4 g Na_2HPO_4

1 x PBST (PBS-Tween 0.05%) 1 L

100 ml 10x PBS

900 ml mQ-H2O

5 mL 10% Tween

0.5 M EDTA, 500ml, filtered sterile (RNase free)

93.0 g EDTA

adjusted to pH to 8.0 with NaOH

0.5 M EGTA, 15 mL, filtered sterile (RNase free)

5.7g EGTA

adjusted to pH to 8.0 with NaOH

HEPES pH 7.0, 220 ml, 1M

119.15g HEPES

adjusted to pH to 7.0 with NaOH, stored at 4°C, dark

DTT – solution (1M)

7,71g DTT

50 mL mQ-H2O, filtered sterile

APS 10%

2.8g APS Ammonium persulfate pure

28 ml sterile mQ-H2O, aliquots stored at -20°C

WB 10x SDS running buffer 1L

30,275g Tris

144g Glycin

10g SDS

WB 10X Transfer buffer 1L

30g Tris

144g Glycin

Western blot developer solutions

Solution A:

50mg Luminol Sodium Salt

200mL TRIS-HCl (0.1 M, pH 8.8)

Adjusted to pH to 8.5 with HCl, stored at 4°C

Solution B:

11mg p-Coumaric acid

10mL DMSO, stored at RT, dark

NaOAc pH 5.2, 3M

49.2g NaOAc

200 ml mQ-H2O

adjusted to pH 5.2 with acetic acid, filtered sterile

LPM medium for *in-vitro* SPI-2 induction, pH 5.8 (227)

buffer	final concentration
MES	80mM
KCl	5mM
$(NH_4)_2SO_4$	7.5mM
K_2SO_4	0.5mM
glycerol	38mM (0.3% v/v)
casamino acids	0.1%
$MgCl_2$ hexahydrate	8µM
KH_2PO_4	337µM
L-Histidine	0.004%
TMC	1µg/ml

add up to 500ml mQ-H_20, adjust pH to 5.8 with 37% HCl, filtered sterile and stored at 4°C

LPM control medium for *in-vitro* SPI-2 induction, pH 7.0 (227)

buffer	final concentration
Tris-HCl	100mM
KCl	5mM
$(NH_4)_2SO_4$	7.5mM
K_2SO_4	0.5mM
glycerol	38mM (0.3% v/v)
casamino acids	0.1%
$MgCl_2$ hexahydrate	8µM
KH_2PO_4	337µM
L-Histidine	0.004%
TMC	1µg/ml

add up to 500ml mQ-H_20, adjust pH to 7.0 with KOH or HCl, filtered sterile and stored at 4°C

Hypotonic lysis buffer (HLB) for cell fractionation, pH 7.5

10 mM Tris-HCl

10 mM NaCl

3 mM MgCl2

0.3 % IGEPAL CA-630

1 mM DTT

1X protease inhibitors cocktail

1X DNase I buffer, pH 7.6

10 mM Tris-HCl

2.5 mM MgCl2

0.5 mM CaCl2

5X First-Strand buffer, pH 8.3

250 mM Tris-HCl

375 mM KCl

15 mM MgCl2

5x Protein loading buffer

15 g SDS pellets

46.95 mL Tris-HCl 1M (pH=6.8)

0.075 g Bromophenol blue

75 mL Glycerol 100%

11.56 g DTT

150 ml H2O

3x Laemmli sample buffer

36 ml Tris 1 M, pH 8

60 ml SDS 20 %

60 ml Glycerol 100 %

44 ml H2O

3.3. % (w/v) Bromophenol Blue

Ad 200 ml (store at RT)

1x Laemmli sample buffer

3.3 ml 3x SB

1 ml DTT, 1 M

5.7 m H2O, stored at 4°C

Equilibration buffer pH_{SCV}

140 mM NaCl

20mM KCl

1mM MgCl2

2mM CaCl2

10 mM HEPES pH 7.4

4.2 Experimental procedures

4.2.1 Cell culture and seeding

Human epithelial HeLa 229 (ATCC® CCL-2.1) and HeLa (ATCC® CCL-2) were cultured in DMEM. Human colon epithelial HCT-8 (ATCC®) were cultured in RPMI. Media were supplemented with 10% fetal bovine serum. Cells were maintained at 37°C in a 5% CO2 humidified atmosphere. For experiments with cell cycle inhibitory drugs different number of cells were seeded for mock or drug treatment, respectively to ensure a similar number of cells/well at time of infection. In 24-well plates $6x10^4$ cells for mock-treatment and $8x10^4$ cells/well for CDK4/6i or lovastatin treatment were seeded. In 6-well plates $2.5x10^5$ cells/ well for mock-treatment and $3.0x10^5$ cells/well for drug treatments were seeded.

4.2.2 Growth curves

Salmonella were streaked freshly on LB agar plates. An overnight culture was started from a single colony in 2 ml LB at 37˚C, 220rpm (12-14 h). The ON culture was diluted 1/10 in LB and 200 µl were transferred in 96-well transparent plates. Growth of bacteria was determined by measuring OD_{595nm} in a Tecan Infinite 200Pro plate reader for 17 hours at 37˚C, shaking.

4.2.3 Electroporation/Transformation

The *Salmonella* recipient strain was grown in 20 ml LB at 37°C, 220 rpm until OD_{600nm} 0.5. The culture was put on ice immediately and incubated for 30 min and shaken gently from time to time. Afterwards the culture was centrifuged for 20 min at 4°C, 4700 rpm and the pellet was resuspended in ca. 30 ml ice-cold mQ-H_2O for washing. The washing step was repeated two times, intermediate centrifugation was done for 10 min at 4°C, 4700 rpm. After decanting the supernatant the pellet was resuspended in the remaining 100-200 µl mQ-H_2O and transferred into a pre-cooled electroporation cuvette. 30-60µg plasmid DNA was added and the mixture was pulsed with 2.5KV for 5.5-6ms. Immediately 500µl pre-warmed LB medium was added and the bacteria were incubated for 1-2 hrs at 37°C, 220 rpm for recovery. After centrifugation for 2 min at

6000 rpm the supernatant was decanted and the pellet was resuspended in the remaining 50-100 µl LB. the suspension was plated onto LB plates with a selective antibiotic.

4.2.4 Treatment of cells

All drugs, dyes and the corresponding vehicles were added to 0.5 ml (24-well plate) or 2ml (6-well plate) culture medium. The medium of cells was exchanged with medium containing the drug/dye and cells were incubated at 37°C in a 5% CO2 humidified atmosphere for the designated time.

Cell cycle inhibition. CDK4/6i (10 µM for HeLa or 20 µM for HCT-8) was added 16 hrs prior collection or infection. During infection CDK4/6i was kept with the medium. Lovastatin was added 20 hrs prior infection and kept during infection. For all cell lines 20 µM lovastatin was used. Medium of control cells was supplemented with the corresponding amount of DMSO.

Lysosomal inhibition. 200 µM Chloroquine was to cells added for 3 hrs. Control cells were supplemented with the corresponding volume of H_2O. During DQ-Red BSA staining Chloroquine and NH_4Cl were added for 5 hrs, together with the dye. 100 nM Bafilomycin was added for 1 hr. The same volume of DMSO was added to control cells.

Lysosomal dyes. Lysotracker (75 nM) was added to live cells and incubated for 2 hrs before fixation. DQ-Red BSA (5µg/ml) was added for 5 hrs before fixation. Alexa 594-dextrans (100 µg/ml) were added for 15 hrs (pulse). The supernatant was removed and cells were washed 3x with culture medium, followed by a 1hr chase period. Acridine orange (10 µM) was added to live cells for 15 min. Confocal images were taken immediately from live cells.

4.2.5 Transfection

For reverse transfection of cells, 1.2 µl Lipofectamine RNAiMAX was added to 120 µl Opti-MEM® and incubated for 5 min at RT. Afterwards 40 µl miRNA mimic of a 500 nM stock (final concentration = 50 nM) was added to the Opti-MEM® -Lipofectamine solution, gently mixed by inverting the tube and incubated for 30 min at RT. 160 µl of the miRNA mix was transferred in the 24-well plate and 240 µl cell suspension was

added. For nocodazole treatment and subsequent cell cycle analysis $1.5x10^5$ cells were transfected with 50 nM miRNA mimics in a 12-well plate. On the second day, cells were detached with 5mM trypsin-EDTA and transferred in a 12-well plate. After 36 hours 0.1 µg/ml nocodazole or DMSO, respectively was added and cells were incubated for another 14 hrs. Afterwards the supernatant was collected and cells were detached directly by adding 5mM PBS-EDTA for 5-10 min without washing. Further processing for cell cycle analysis was done as described below.

4.2.6 Cell cycle analysis

Cells were washed and detached by incubating in 5mM PBS-EDTA for 5-10 min and pelleted at 4°C for 5 min, 850xg. After washing twice in ice-cold PBS, the pellet was carefully resuspended in 300 µl PBS. 800 µl ice-cold EtOH was dropwise added while vortexing. The samples were stored at -20°C for at least 16 hrs for fixation. Cells were pelleted (4°C for 5 min, 850xg), washed twice in ice-cold PBS and resuspended in 1 ml buffer H, supplemented with 0.2 mg/ml RNAseA and 50 µg/ml propidium iodine). Samples were covered with aluminum foil and incubated for 30 min at 37°C, 800 rpm in a Thermo-Shaker. Afterwards cells were pelleted (4°C for 5 min, 850xg), resuspended in PBS and immediately measured at the FACS Accuri C6. For quantification of the different cell cycle phases at least 10,000 cells were counted and the Dean-Jett-Fox model was applied. Analysis was done with the FlowJo© Enterprise Software from FlowJo, LLC.

4.2.7 Infection assays

Cells were seeded 2 days prior to the experiment. After 20-24 hrs cells were treated with drugs and incubated for another 16-20 hrs, unless stated otherwise. *Salmonella* were streaked freshly on LB agar plates. An overnight culture was started from a single colony in 2 ml LB at 37˚C, 220rpm (12-14 h). The ON culture was diluted 1/10 in 10ml LB and grown until an OD_{600nm} of 2.0 at 37˚C, 220rpm. 1 ml of the bacterial culture was centrifuged at 12,000rpm for 2min at RT, and resuspended in 1 ml cell culture medium. The culture was diluted further in cell culture medium to reach the required multiplicity

of infection (MOI). Therefore it was assumed that an OD600nm of 2.0 corresponds to $2x10^9$ bacteria/ml.

The supernatant of the cells was exchanged with the prepared bacterial suspension and centrifuged at 250xg for 10 min at RT, followed by 20 min incubation at 37˚C in 5% CO2 humidified atmosphere. The supernatant of cells was exchanged by medium containing 50 µg/ml of gentamycin and incubated again for 30 min at 37˚C, 5% CO2. This time point was depicted as time point 0 or 0 hpi. After 30 min the medium was exchanged again by medium containing 10 µg/ml gentamycin (0.5 hpi), which was kept until collection of cells for further analysis.

For *Shigella* infection only the following was changed: *Shigella* was streaked onto TSB/Congo Red agar plates. On the day of infection bacteria were grown until OD_{600nm} of 0.4 (corresponding to $4x10^8$ bacteria/ml). The cells with bacteria were centrifuged for 15 min at 2000xg and incubated for 15 min before exchanging medium with medium with gentamycin 50 µg/ml.

4.2.8 Flow cytometry

Cells were washed once with PBS and detached by incubating in 5mM PBS-EDTA for 5-10 min. Cells were pelleted at 4°C for 5 min, 850xg and washed twice in ice-cold PBS. For fixation 1 ml of PFA 4% was added dropwise to the cells while mild vortexing. Cells were incubated for 15 min at RT. The PFA was removed after centrifugation at 4°C for 5 min with 850xg. Cells were resuspended in ice-cold PBS and samples were measured immediately or stored at 4 °C in the dark. Analysis was done with the FlowJo© Enterprise Software from FlowJo, LLC.

4.2.9 Immunofluorescence and confocal microscopy

Cells were grown on glass coverslips and washed 3 times with PBS before fixation. Fixation was done by adding 4% paraformaldehyde (PFA) for 15 min at RT or ice-cold MeOH for 20 min at -20°C. PFA fixed cells were permeabilized with 0.5% Triton-X-100 in PBS for 1 hr and washed once in PBS. Blocking was performed for 30 min in 1% Bovine Serum Albumin (BSA) in PBS. Primary antibodies were diluted in blocking buffer and incubation was done overnight at 4°C plus 2 hrs at RT. Coverslips were then washed 3x

5 min with PBS. Secondary antibodies were diluted in blocking buffer and incubation was done for 2 hrs at RT. When indicated cells were incubated with CellMask™ for 1 hrs. After washing in PBS, coverslips were stained with Hoechst, washed in PBS again and mounted onto microscope slides in Vectashield mounting medium. Coverslips were sealed with transparent nail polish. Images were acquired with the Confocal Leica TCS SP5 microscope [40x Zoom 1.0 or 100x Zoom 2.0].

4.2.10 TEM

Cells were grown on glass coverslips and washed once with PBS before fixation in 2.5% glutaraldehyde in 0.1 M cacodylate buffer (pH 7.2). Fixation was done for 15 min at room temperature followed by 1.75 hrs at 4°C. Afterwards cells were washed 3x 5 min in cold 0.1 M cacodylate buffer (pH 7.2) and kept at 4°C until further processing. Preparation of fixed cells was done by Claudia Gehrig and Daniela Bunsen from the Imaging Core Facility at the Theodor-Boveri-Institute of Bioscience, University of Wuerzburg. Images were acquired by Dr. Ana Eulalio on a Zeiss EM10 TEM.

4.2.11 CFU assay

Cells were washed 3 times and lysed by adding 0.5 ml 0.1% Triton-X-100 in PBS. After incubation for 5-15 min, cells were collected by scraping. Dilutions of the lysate were made in 500 µl PBS, vortexed, and plated on LB agar plates using glass beads and incubated at 37°C ON. Colonies were counted and calculated according to the dilution factor, for total number of bacteria/well.

4.2.12 Chloroquine resistance assay

Chloroquine resistance assays were performed as described previously (143). Briefly, 2 wells per condition were seeded and infected with *Salmonella* as described in infection assays. 200 µM Chloroquine or water respectively was added to the cells for 1 hour. After three gently washes, cells were further processed for CFU quantification and the ratio of total population/Chloroquine resistant bacteria was determined.

4.2.13 RNA isolation, cDNA synthesis and qRT-PCR

RNA isolation. Cells were washed once with PBS. 500 µl TRIzol was added for 5-15 min and cells were scratched off the well to support lysis. 100 µl chloroform were added to the lysate and the mixture was mixed by shaking thoroughly for 15 sec. The lysate was centrifuged for 10 min at 12,000 rpm at 4°C, and the top aqueous phase was transferred into a new tube. 400 µl isopropanol and 1 µl Glycoblue was added, mixed briefly and incubated at -20°C for >20 min for RNA precipitation. Samples were inverted again and centrifuged at 21,130xg rpm for >20 min and washed 3 times with 85% Ethanol absolute. The pellet was dried and resuspended in RNase-free water. The RNA was stored at -20°C. RNA concentrations were determined using NanoDrop2000.

cDNA synthesis. 500 ng of total RNA in 12.5 µl of RNase-free was used for complementary DNA (cDNA) synthesis. 2.5 µl of mix 1 was added to the RNA and incubated at 37°C for 10 min for DNase treatment. Afterwards 1.5 µl EDTA (0.05 M) was added and incubated for another 10 min at 75°C to denaturate DNase. For reverse transcription 7.5 µl of mix 2 was added and samples were incubated for 5 min at 65°C. Subsequently mix 3 was added and samples were incubated for 2 min at 37°C. Finally 0.5 µl M-MLV reverse transcriptase was added and samples were incubated in a thermal cycler according to the described program.

Mix 1:

- 1.5 µl 10X DNase I buffer
- 0.5 µl of RNaseOUT
- 0.5 µl of DNase I

Mix 2:

- 2 µl dNTP mix 10 mM
- 2 µl random primers (1:20 dilution of the stock)
- 3.5 µl H_2O

Mix 3:

- 8 µl 5X First-Strand buffer
- 4 µl DTT 0.1 M
- 2 µl H_2O

Program C1000 Touch:

- 25°C for 10 min
- 30°C for 50 min
- 75°C for 15 min

Quantitative real-time PCR. The cDNA was diluted 1:5 and 1-2 µl were used for qRT-PCR. 9 µl of the qRT-PCR mix was pipetted into 96-well plates, sealed with PCR plate seal, and centrifuged at 1500xg for 1 min at RT. The qRT-PCR was read on the CFX96 Touch™ Real-Time PCR Detection System from Biorad with the described protocol.

qRT-PCR mix:

- 3 µl H_2O
- 1 µl primer mix 18 µM
- 5 µl SsoAdvanced™ Universal SYBR® Green Supermix

Protocol CFX96:

- Step1 95°C for 3 min
- Step2 95°C for 10 min
- Step3 59°C for 60 sec, repeat step2-3 40 times

4.2.14 Nuclear and cytoplasmic cell fractionation

Fractionation was done as described previously (228). $2.5x10^5$ cells were seeded in 6-well plates 2 days prior to the experiment. Cells were incubated with DMSO/CDK for 16hrs. CHQ was added for 3 hours. Cells were detached by incubating in 5mM PBS-EDTA for 5-10 min and washed 2 times in ice-cold PBS at 4˚C. The cells were resuspended in 400 µl of ice-cold hypotonic lysis buffer (HLB), and incubated on ice for 12 min with gentle pipetting. The lysate was centrifuged at 800g for 5 min at 4˚C. The supernatant was kept as the cytosolic fraction by adding 90 µl of 5X protein loading buffer (PL). The pelleted nuclei were washed 3 times in 800 µl HLB with 5 min incubation on ice each, pipetting and vortexing, and centrifuged at 150 g for 2 min at 4˚C. The nuclei were resuspended in 200 µl (1/2 the volume of the cytoplasmic

fraction) lysis buffer, with 1mM DTT and 1X protease inhibitors cocktail, and 40 µl 5X PL. (modified from Gagnon et al, 2014).

4.2.15 SDS PAGE and Western blot

SDS PAGE. Cells were washed 3 times with PBS and detached by incubating in 5mM PBS-EDTA for 5-10 min. Cells were pelleted at 4°C for 5 min, 850xg and washed once in ice-cold PBS. Afterwards the pellet was resuspended in 100-200µl Laemmli sample buffer and stored at -20°C until further processing. After thawing, samples were sonicated with 3 pulses á 5 sec, incubated at 95°C for 5 min to denature proteins and quick-chilled on ice. After a quick spin down samples were loaded on freshly prepared polyacrylamide gels. Depending on the protein size 8-12% separating gels and 4% stacking gels were used. Initially 15mA per gel were applied and later increased to 25 mA for separation.

Western blot. Proteins were transferred onto a nitrocellulose membrane by wet blotting in a tank electro blotter at 4°C for 2 hrs at 215 mA. Protein gels, nitrocellulose membranes as well as Whatmann paper were equilibrated in MeOH transfer buffer before stacking. After transfer membranes were washed briefly in PBST and blocked in blocking buffer for 1 hr. Subsequently membranes were incubated with primary antibodies (diluted in blocking buffer) at 4°C overnight on a platform shaker. After additional 2 hours incubation at RT membranes were washed three times (5 min each in PBST) and incubated with secondary antibodies, also diluted in blocking buffer, for 1 hour. Primary antibody dilutions were used up to three times, while secondary antibody dilutions were prepared fresh every time. Afterwards blots were washed three times in PBST and the membrane was developed using chemiluminescence detection solution. Image acquisition was done with the ImageQuant LAS 4000 system and blots were quantified with image J.

4.2.16 pH determination SCV

pH measurement of intracellular *Salmonella*/SCV was done as previously described (153). *Salmonella* was grown until OD_{600nm} 1.9 and 1 ml was washed once in sterile PBS. The pellet was resuspended in 1 ml freshly prepared FITC solution (0.1 mg/ml in PBS)

and incubated shaking in the dark at 37°C for 1 hr. Bacteria were washed 3-5 times with 2ml PBS to remove residual FITC. Afterwards bacteria were resuspended in cell culture medium. Cells were infected with MOI 250 as usual. For collection cells were washed once with PBS and detached by incubating in 5mM PBS-EDTA for 5-10 min. Cells were pelleted at 4°C for 5 min, 850xg, washed once and resuspended in 1 ml equilibration buffer. Two aliquots of 500 µl were prepared and either incubated with 50 µM monensin+10 µM nigericin or the same volume of EtOH shaking in the dark at 37°C for 15 min. Cells were transferred on ice and FITC fluorescence was immediately measured at the FACS Accuri C6. To determine the number of intracellular bacteria the AFU (= arbitrary fluorescence units) was used according to the following formula: AFU = (MFI FITC of infected cells * % of infected cells). The difference in AFU (ΔAFU) in samples treated with and without monensin, normalized to the invasion rate, was used as to determine the pH_{SCV} according to the formula ΔAFU = ($AFU_{-ionophore}$ − $AFU_{+ ionophore}$) / $AFU_{+ ionophore}$) The lower/more negative the ΔAFU values, the more acidic is the pH.

4.2.17 *in-vitro* SPI-2 induction in LPM medium

Salmonella were streaked freshly on LB agar plates. An overnight culture was started from a single colony in 2 ml LB at 37˚C, 220rpm (12-14 h). The ON culture was diluted 1/10 in 10ml LB and grown until an OD_{600nm} of 2.0 at 37˚C, 220rpm. 2x 1ml bacteria were pelleted, washed twice in sterile PBS and first resuspended in 2x1ml of LPM medium(pH 7.0 or 5.8 respectively). Subsequently the bacteria were diluted 1/50 in 10 ml LPM medium (pH 7.0 or 5.8 respectively), supplemented with DMSO or CDK4/6i. Bacteria were grown until OD_{600nm} of 0.3 and collected in TRIzol for RNA isolation.

4.2.18 Statistical analysis

All data are presented as mean ± standard error of the mean (s.e.m.) of at least five independent experiments, unless indicated differently in the figure legends. Statistical analysis was performed using Prism Software (GraphPad). For statistical comparison of datasets from two conditions, two-tailed Student's t-test was used; for data from three or more conditions, two-way ANOVA was used. P-values ≤ 0.05 or lower were considered significant.

5 References

1. Schmitz S (2011) Zellbiologische Grundlagen. *Der Experimentator: Zellkultur* (Spektrum Akademischer Verlag, Heidelberg), pp 13–38.

2. Daignan-Fornier B, Sagot I (2011) Proliferation/Quiescence: When to start? Where to stop? What to stock? *Cell Div* 6(1):20.

3. Sherr CJ, Bartek J (2017) Cell Cycle–Targeted Cancer Therapies. *Annu Rev Cancer Biol* 1(1):41–57.

4. Vermeulen K, Van Bockstaele DR, Berneman ZN (2003) The cell cycle: a review of regulation, deregulation and therapeutic targets in cancer. *Cell Prolif* 36:131–149.

5. Maudet C, et al. (2014) Functional high-throughput screening identifies the miR-15 microRNA family as cellular restriction factors for Salmonella infection. *Nat Commun* 5:4718.

6. CAI C-K, et al. (2012) miR-15a and miR-16-1 downregulate CCND1 and induce apoptosis and cell cycle arrest in osteosarcoma. *Oncol Rep* 28(5):1764–1770.

7. Alberts B, et al. (2008) *Molecular biology of the cell* (Garland Science). 5th Ed. [Accessed November 16, 2018].

8. Pollard TD, Earnshaw WC, Lippincott-Schwartz J, Johnson G (2017) *Cell biology* (Elsevier). 3rd Ed.

9. Skotheim JM, Di Talia S, Siggia ED, Cross FR (2008) Positive feedback of G1 cyclins ensures coherent cell cycle entry. *Nature* 454(7202):291–296.

10. Otto T, Sicinski P (2017) Cell cycle proteins as promising targets in cancer therapy. *Nat Rev Cancer* 17(2):93–115.

11. Williams GH, Stoeber K (2012) The cell cycle and cancer. *J Pathol* 226:352–364.

12. Knudsen ES, Witkiewicz AK (2017) The Strange Case of CDK4/6 Inhibitors:

Mechanisms, Resistance, and Combination Strategies. *Trends in Cancer* 3(1):39–55.

13. Soni R, et al. (2001) Selective in vivo and in vitro effects of a small molecule inhibitor of cyclin-dependent kinase 4. *J Natl Cancer Inst* 93(6):436–46.

14. Merckmillipore Cdk4/6 Inhibitor IV - CAS 359886-84-3 - Calbiochem CAS 359886-84-3 | 219492. [Accessed November 26, 2018].

15. Huotari J, Helenius A (2011) Endosome maturation. *EMBO J* 30(17):3481–3500.

16. Doherty GJ, McMahon HT (2009) Mechanisms of Endocytosis. *Annu Rev Biochem* 78(1):857–902.

17. Zerial M, McBride H (2001) Rab proteins as membrane organizers. *Nat Rev Mol Cell Biol* 2:107–119.

18. Law F, et al. (2017) The VPS34 PI3K negatively regulates RAB-5 during endosome maturation. *J Cell Sci* 130(12):2007–2017.

19. Zeigerer A, et al. (2012) Rab5 is necessary for the biogenesis of the endolysosomal system in vivo. *Nature* 485(7399):465–70.

20. Poteryaev D, Datta S, Ackema K, Zerial M, Spang A (2010) Identification of the switch in early-to-late endosome transition. *Cell* 141(3):497–508.

21. Ungermann C, Langosch D (2005) Functions of SNAREs in intracellular membrane fusion and lipid bilayer mixing. *J Cell Sci* 118:3819–28.

22. Klionsky DJ, et al. (2016) Guidelines for the use and interpretation of assays for monitoring autophagy (3rd edition). *Autophagy* 12(1):1–222.

23. Dikic I, Elazar Z (2018) Mechanism and medical implications of mammalian autophagy. *Nat Rev Mol Cell Biol* 19(June):349–364.

24. Bento CF, et al. (2016) Mammalian Autophagy : How Does It Work ? *Annu Rev Biochem* 85:685–716.

25. Klionsky DJ (2018) MAP1A/BLC3? Now I am really confused. *Autophagy* 14(12):2033–2034.

26. Xu H, Ren D (2015) Lysosomal Physiology. *Annu Rev Physiol* 77:57–80.

27. Luzio JP, Hackmann Y, Dieckmann NMG, Griffiths GM (2014) The Biogenesis of Lysosomes and Lysosome-Related Organelles. *Cold Spring Harb Perspect Biol* 6:1–18.

28. Settembre C, Ballabio A (2014) Lysosome: Regulator of lipid degradation pathways. *Trends Cell Biol* 24(12):743–750.

29. Perera RM, Zoncu R (2016) The Lysosome as a Regulatory Hub. *Annu Rev Cell Dev Biol* 32:223–253.

30. Carroll B, Dunlop EA (2017) The lysosome: a crucial hub for AMPK and mTORC1 signalling. *Biochem J* 474:1453–1466.

31. Napolitano G, Ballabio A (2016) TFEB at a glance. *J Cell Sci* 129(13):2475–2481.

32. Luzio JP, Pryor PR, Bright NA (2007) Lysosomes: Fusion and function. *Nat Rev Mol Cell Biol* 8:622–632.

33. Wolf DH, Hilt W (2004) The proteasome: a proteolytic nanomachine of cell regulation and waste disposal. *Biochim Biophys Acta* 1695:19–31.

34. Ciechanover A (2005) Proteolysis: from the lysosome to ubiquitin and the proteasome. *Nat Rev Mol Cell Biol* 6:79–87.

35. Enenkel C (2014) Proteasome dynamics. *Biochim Biophys Acta - Mol Cell Res* 1843(1):39–46.

36. Zhang T, et al. (2017) Proteome-wide modulation of degradation dynamics in response to growth arrest. *Proc Natl Acad Sci U S A* 114(48):E10329–E10338.

37. Lenos KJ, Vermeulen L (2016) Cancer stem cells don't waste their time cleaning-low proteasome activity, a marker for cancer stem cell function. *Ann Transl Med* 4(24):519.

38. Kumatori A, et al. (1990) Abnormally high expression of proteasomes in human leukemic cells. *Proc Natl Acad Sci U S A* 87:7071–5.

39. Crawford LJ, Walker B, Irvine AE (2011) Proteasome inhibitors in cancer therapy. *J Cell Commun Signal* 5:101–10.

40. Legesse-Miller A, et al. (2012) Quiescent fibroblasts are protected from proteasome inhibition–mediated toxicity. *Mol Biol Cell* 23(18):3566–3581.

41. Schulte M, Hensel M (2016) Models of intestinal infection by Salmonella enterica : introduction of a new neonate mouse model [version 1; referees: 2 approved]. *F1000Research* 5((F1000 Faculty Rev)):1498.

42. Haraga A, Ohlson MB, Miller SI (2008) Salmonellae interplay with host cells. *Nat Rev Microbiol* 6:53–66.

43. Schleker S, et al. (2013) The current Salmonella – host interactome. *Proteomics Clin Appl* 6:117–133.

44. Castanheira S, García-del Portillo F (2017) Salmonella Populations inside Host Cells. *Front Cell Infect Microbiol* 7:1–12.

45. Hume PJ, Singh V, Davidson AC, Koronakis V (2017) Swiss Army Pathogen: The Salmonella Entry Toolkit. *Front Cell Infect Microbiol* 7:1–13.

46. Fredlund J, et al. (2018) The entry of Salmonella in a distinct tight compartment revealed at high temporal and ultrastructural resolution. *Cell Microbiol* 20(4):1–13.

47. Santos AJM, Meinecke M, Fessler MB, Holden DW, Boucrot E (2013) Preferential invasion of mitotic cells by Salmonella reveals that cell surface cholesterol is maximal during metaphase. *J Cell Sci* 126(14):2990–2996.

48. Kreibich S, et al. (2015) Autophagy proteins promote repair of endosomal membranes damaged by the Salmonella type three secretion system 1. *Cell Host Microbe* 18(5):527–537.

49. Mukherjee K, Parashuraman S, Raje M, Mukhopadhyay A (2001) SopE Acts as an Rab5-specific Nucleotide Exchange Factor and Recruits Non-prenylated Rab5 on Salmonella-containing Phagosomes to Promote Fusion with Early Endosomes. *J Biol Chem* 276(26):23607–23615.

50. Madan R, Krishnamurthy G, Mukhopadhyay A (2008) *SopE-Mediated Recruitment of Host Rab5 on Phagosomes Inhibits Salmonella Transport to Lysosomes* ed Deretic V (Humana Press, Totowa, NJ). 445th Ed. doi:10.1007/978-1-59745-157-4_27.

51. Kubori T, Galán JE (2003) Temporal regulation of *Salmonella* virulence effector function by proteasome-dependent protein degradation. *Cell* 115:333–42.

52. McEwan DG, et al. (2015) PLEKHM1 regulates salmonella-containing vacuole biogenesis and infection. *Cell Host Microbe* 17:58–71.

53. Dandekar T, et al. (2015) Salmonella — how a metabolic generalist adopts an intracellular lifestyle during infection. *Front Cell Infect Microbiol* 4:1–11.

54. McGourty K, et al. (2012) Salmonella inhibits retrograde trafficking of mannose-6-phosphate receptors and lysosome function. *Science (80-)* 338(6109):963–967.

55. Jennings E, Thurston TLM, Holden DW (2017) Salmonella SPI-2 Type III Secretion System Effectors: Molecular Mechanisms And Physiological Consequences. *Cell Host Microbe* 22:217–231.

56. Liss V, et al. (2017) Salmonella enterica Remodels the Host Cell Endosomal System for Efficient Intravacuolar Nutrition. *Cell Host Microbe* 21(3):390–402.

57. Knuff K, Finlay BB (2017) What the SIF Is Happening—The Role of Intracellular Salmonella-Induced Filaments. *Front Cell Infect Microbiol* 7(335). doi:10.3389/fcimb.2017.00335.

58. Dandekar T, Fieselmann A, Popp J, Hensel M (2012) Salmonella enterica: A surprisingly well-adapted intracellular lifestyle. *Front Microbiol* 3:1–11.

59. Garmendia J, Beuzón CR, Ruiz-Albert J, Holden DW (2003) The roles of SsrA-SsrB and OmpR-EnvZ in the regulation of genes encoding the Salmonella typhimurium SPI-2 type III secretion system. *Microbiology* 149:2385–2396.

60. Lee AK, Detweiler CS, Falkow S (2000) OmpR Regulates the Two-Component System SsrA-SsrB in Salmonella Pathogenicity Island 2. *J Bacteriol* 182(3):771–781.

61. Fass E, Groisman EA (2009) Control of Salmonella pathogenicity island-2 gene expression. *Curr Opin Microbiol* 12:199–204.

62. Löber S, Jäckel D, Kaiser N, Hensel M (2006) Regulation of Salmonella pathogenicity island 2 genes by independent environmental signals. *Int J Med Microbiol* 296:435–447.

63. Bartel DP (2018) Metazoan MicroRNAs. *Cell* 173(1):20–51.

64. Barca-Mayo O, Richard Lu Q (2012) Fine-tuning oligodendrocyte development by micrornas. *Front Neurosci* 6(FEB):1–7.

65. Aguilar C, Mano M, Eulalio A (2019) MicroRNAs at the Host–Bacteria Interface: Host Defense or Bacterial Offense. *Trends Microbiol* 27(3):206–218.

66. Maudet C, Mano M, Eulalio A (2014) MicroRNAs in the interaction between host and bacterial pathogens. *FEBS Lett* 588(22):4140–4147.

67. Jovanovic M, Hengartner MO (2006) miRNAs and apoptosis: RNAs to die for. *Oncogene* 25:6176–6187.

68. Quiat D, Olson EN (2013) MicroRNAs in cardiovascular disease : from pathogenesis to prevention and treatment. *J Clin Invest* 123(1):11–18.

69. Adams BD, Kasinski AL, Slack FJ (2014) Aberrant regulation and function of microRNAs in cancer. *Curr Biol* 24(16):R762–R776.

70. Belair C, et al. (2011) Helicobacter pylori interferes with an embryonic stem cell micro RNA cluster to block cell cycle progression. *Silence* 2(1):1–16.

71. Zhang Z, et al. (2008) miR-21 plays a pivotal role in gastric cancer pathogenesis and progression. *Lab Investig* 88(12):1358–1366.

72. Li N, et al. (2012) Increased miR-222 in H. pylori-associated gastric cancer correlated with tumor progression by promoting cancer cell proliferation and targeting RECK. *FEBS Lett* 586(6):722–728.

73. Tan X, Tang H, Bi J, Li N, Jia Y (2018) MicroRNA-222-3p associated with Helicobacter pylori targets HIPK2 to promote cell proliferation, invasion, and inhibits apoptosis in gastric cancer. *J Cell Biochem* 119(7):5153–5162.

74. Meyer TF, et al. (2010) Helicobacter pylori Induces miR-155 in T Cells in a cAMP-Foxp3-Dependent Manner. *PLoS One* 5(3):e9500.

75. Koch M, Mollenkopf H-J, Klemm U, Meyer TF (2012) Induction of microRNA-155 is TLR- and type IV secretion system-dependent in macrophages and inhibits DNA-damage induced apoptosis. *Proc Natl Acad Sci* 109(19):E1153–E1162.

76. Ramírez-Lázaro MJ, et al. (2012) microRNA profiling in duodenal ulcer disease caused by Helicobacter pylori infection in a Western population. *Clin Microbiol Infect* 18(8):E273–E282.

77. Zou Q, et al. (2009) Induction of microRNA-155 during Helicobacter pylori Infection and Its Negative Regulatory Role in the Inflammatory Response . *J Infect Dis* 200(6):916–925.

78. Wang W, et al. (2013) Let-7b Is Involved in the Inflammation and Immune Responses Associated with Helicobacter pylori Infection by Targeting Toll-Like Receptor 4. *PLoS One* 8(2):e56709.

79. Matsushima K, et al. (2011) MicroRNA signatures in Helicobacter pylori-infected gastric mucosa. *Int J Cancer* 128(2):361–370.

80. Rothchild AC, et al. (2016) MiR-155–regulated molecular network orchestrates cell fate in the innate and adaptive immune response to Mycobacterium tuberculosis. *Proc Natl Acad Sci* 113(41):E6172–E6181.

81. Jana K, et al. (2015) MicroRNA 17-5p regulates autophagy in Mycobacterium tuberculosis -infected macrophages by targeting Mcl-1 and STAT3 . *Cell Microbiol* 18(5):679–691.

82. Chen Z, et al. (2015) Inhibition of autophagy by MiR-30A induced by Mycobacteria tuberculosis as a possible mechanism of immune escape in human macrophages. *Jpn J Infect Dis* 68(5):420–424.

83. Jo E-K, et al. (2015) MicroRNA-125a Inhibits Autophagy Activation and Antimicrobial Responses during Mycobacterial Infection. *J Immunol* 194(11):5355–5365.

84. Rao R, Nagarkatti P, Nagarkatti M (2014) Staphylococcal Enterotoxin B-Induced MicroRNA-155 Targets SOCS1 To Promote Acute Inflammatory Lung Injury. *Infect Immun* 82(7):2971–2979.

85. Ramirez HA, et al. (2018) Staphylococcus aureus Triggers Induction of miR-15B-5P to Diminish DNA Repair and Deregulate Inflammatory Response in Diabetic Foot Ulcers. *J Invest Dermatol* 138(5):1187–1196.

86. Sunkavalli U, et al. (2017) Analysis of host microRNA function uncovers a role for miR-29b-2-5p in Shigella capture by filopodia. *PLOS Pathog* 13(4):e1006327.

87. Schnitger AKD, et al. (2011) Listeria monocytogenes infection in macrophages induces vacuolar-dependent host miRNA response. *PLoS One* 6(11). doi:10.1371/journal.pone.0027435.

88. Izar B, Mannala GK, Mraheil MA, Chakraborty T, Hain T (2012) MicroRNA response to listeria monocytogenes infection in epithelial cells. *Int J Mol Sci* 13(1):1173–1185.

89. Schulte LN, Eulalio A, Mollenkopf HJ, Reinhardt R, Vogel J (2011) Analysis of the host microRNA response to Salmonella uncovers the control of major cytokines by the let-7 family. *EMBO J* 30(10):1977–1989.

90. Sharbati S, Sharbati J, Hoeke L, Bohmer M, Einspanier R (2012) Quantification

and accurate normalisation of small RNAs through new custom RT-qPCR arrays demonstrates Salmonella-induced microRNAs in human monocytes. *BMC Genomics* 13(1). doi:10.1186/1471-2164-13-23.

91. Ahmad SM, et al. (2015) Salmonella Engages Host MicroRNAs To Modulate SUMOylation: a New Arsenal for Intracellular Survival. *Mol Cell Biol* 35(17):2932–2946.

92. Carvajal A, et al. (2018) Regulatory role of microRNA in mesenteric lymph nodes after Salmonella Typhimurium infection. *Vet Res* 49(1):1–12.

93. Chen Q, et al. (2017) Involvement of microRNAs in probiotics-induced reduction of the cecal inflammation by Salmonella typhimurium. *Front Immunol* 8(JUN):1–13.

94. Bao H, et al. (2015) Genome-wide whole blood microRNAome and transcriptome analyses reveal miRNA-mRNA regulated host response to foodborne pathogen Salmonella infection in swine. *Sci Rep* 5(July):1–12.

95. El-Aouar Filho RA, et al. (2017) Heterogeneous Family of Cyclomodulins: Smart Weapons That Allow Bacteria to Hijack the Eukaryotic Cell Cycle and Promote Infections. *Front Cell Infect Microbiol* 7:208.

96. Nougayrède J-P, Taieb F, De Rycke J, Oswald E (2005) Cyclomodulins: bacterial effectors that modulate the eukaryotic cell cycle. *Trends Microbiol* 13(3):103–10.

97. Pérès SY, et al. (1997) A new cytolethal distending toxin (CDT) from Escherichia coli producing CNF2 blocks HeLa cell division in G2/M phase. *Mol Microbiol* 24(5):1095–1107.

98. Koch A, Mizrahi V (2018) Mycobacterium tuberculosis. *Trends Microbiol* 26(6):555–556.

99. Cumming BM, et al. (2017) Mycobacterium tuberculosis arrests host cycle at the G1/S transition to establish long term infection. *PLoS Pathog* 13(5):1–29.

100. Oswald E, Nougayrède JP, Taieb F, Sugai M (2005) Bacterial toxins that modulate host cell-cycle progression. *Curr Opin Microbiol* 8(1):83–91.

101. Chiou CC, Chan CC, Kuo YP, Chan EC (2003) Helicobacter pylori inhibits activity of cdc2 kinase and delays G2/M to G1 progression in gastric adenocarcinoma cell line. *Scand J Gastroenterol* 38(2):147–152.

102. Fehri LF, et al. (2009) Helicobacter pylori-induced modification of the histone H3 phosphorylation status in gastric epithelial cells reflects its impact on cell cycle regulation. *Epigenetics* 4(8):577–586.

103. Cerda-Opazo P, et al. (2017) Helicobacter pylori Induced Phosphatidylinositol-3-OH Kinase/mTOR Activation Increases Hypoxia Inducible Factor-1α to Promote Loss of Cyclin D1 and G0/G1 Cell Cycle Arrest in Human Gastric Cells. *Front Cell Infect Microbiol* 7(March). doi:10.3389/fcimb.2017.00092.

104. Vare D, et al. (2012) Neisseria gonorrhoeae infection causes DNA damage and affects the expression of p21, p27 and p53 in non-tumor epithelial cells . *J Cell Sci* 126(1):339–347.

105. von Papen M, Oosthuysen WF, Becam J, Claus H, Schubert-Unkmeir A (2016) Disease and carrier isolates of Neisseria meningitidis cause G1 cell cycle arrest in human epithelial cells. *Infect Immun* 84(10):2758–2770.

106. Oosthuysen WF, Mueller T, Dittrich MT, Schubert-Unkmeir A (2016) Neisseria meningitidis causes cell cycle arrest of human brain microvascular endothelial cells at S phase via p21 and cyclin G2. *Cell Microbiol* 18(1):46–65.

107. Pombinho R, et al. (2014) Listeria monocytogenes induces host DNA damage and delays the host cell cycle to promote infection. *Cell Cycle* 13(6):928–940.

108. Samba-Louaka A, et al. (2014) Listeria monocytogenes Dampens the DNA Damage Response. *PLoS Pathog* 10(10). doi:10.1371/journal.ppat.1004470.

109. Rault L, et al. (2013) Staphylococcus aureus-Induced G2/M Phase Transition Delay in Host Epithelial Cells Increases Bacterial Infective Efficiency. *PLoS One*

8(5):e63279.

110. Deplanche M, et al. (2016) Staphylococcus aureus Lpl Lipoproteins Delay G2/M Phase Transition in HeLa Cells. *Front Cell Infect Microbiol* 6(December):1–12.

111. Iwai H, et al. (2007) A Bacterial Effector Targets Mad2L2, an APC Inhibitor, to Modulate Host Cell Cycling. *Cell* 130(4):611–623.

112. Nougayréde J-P, et al. (2006) Escherichia coli induces DNA Double-Strand Breaks in eukaryotic cells. *Science (80-)* 313:848–852.

113. Nougayrède J-P, Oswald E, Taieb F, Watrin C, Samba-Louaka A (2006) Escherichia coli cyclomodulin Cif induces G 2 arrest of the host cell cycle without activation of the DNA-damage checkpoint-signalling pathway. *Cell Microbiol* 8(12):1910–1921.

114. Marches O, et al. (2002) Type III Secretion-Dependent Cell Cycle Block Caused in HeLa Cells by Enteropathogenic Escherichia coli O103. *Infect Immun* 69(11):6785–6795.

115. He X, et al. (2017) Host cell interactions of outer membrane vesicle-associated virulence factors of enterohemorrhagic Escherichia coli O157: Intracellular delivery, trafficking and mechanisms of cell injury. *PLOS Pathog* 13(2):e1006159.

116. Escoubas J-M, et al. (2009) Cycle Inhibiting Factors (CIFs) Are a Growing Family of Functional Cyclomodulins Present in Invertebrate and Mammal Bacterial Pathogens. *PLoS One* 4(3):e4855.

117. McCormack RM, Lyapichev K, Olsson ML, Podack ER, Munson GP (2015) Enteric pathogens deploy cell cycle inhibiting factors to block the bactericidal activity of Perforin-2. *Elife* 4(September2015):1–22.

118. Korbsrisate S, et al. (2014) Analysis of the Prevalence, Secretion and Function of a Cell Cycle-Inhibiting Factor in the Melioidosis Pathogen Burkholderia pseudomallei. *PLoS One* 9(5):e96298.

119. Whitehouse CA, et al. (1998) Campylobacter jejuni cytolethal distending toxin causes a G2-phase cell cycle block. *Infect Immun* 66(5):1934–1940.

120. Balsara ZR, Misaghi S, Lafave JN, Starnbach MN (2006) Chlamydia trachomatis infection induces cleavage of the mitotic cyclin B1. *Infect Immun* 74(10):5602–5608.

121. Jesús-Díaz DA de, Connor Murphy B, Sol A, Marion Dorer A, Isberg RR (2017) Host Cell S Phase Restricts Legionella. 8(4):1–18.

122. Isberg RR, et al. (2019) Legionella pneumophila translocated translation inhibitors are required for bacterial-induced host cell cycle arrest. *Proc Natl Acad Sci* 116(8):3221–3228.

123. Mesa-Pereira B, Medina C, Camacho EM, Flores A, Santero E (2013) Novel Tools to Analyze the Function of Salmonella Effectors Show That SvpB Ectopic Expression Induces Cell Cycle Arrest in Tumor Cells. *PLoS One* 8(10):1–16.

124. Durkin CH, Holden DW, Santos AJM, Helaine S, Boucrot E (2016) Clustered Intracellular Salmonella enterica Serovar Typhimurium Blocks Host Cell Cytokinesis. *Infect Immun* 84(7):2149–2158.

125. Knodler LA (2015) Salmonella enterica: living a double life in epithelial cells. *Curr Opin Microbiol* 23:23–31.

126. Knodler LA, Nair V, Steele-Mortimer O (2014) Quantitative assessment of cytosolic Salmonella in epithelial cells. *PLoS One* 9(1). doi:10.1371/journal.pone.0084681.

127. Slater AFG (1993) Chloroquine: Mechanism of Drug Action and Resistance in Plasmodium Falcipar Um. *Pharmac Ther* 57:203–235.

128. Killackey SA, Sorbara MT, Girardin SE (2016) Cellular Aspects of Shigella Pathogenesis: Focus on the Manipulation of Host Cell Processes. *Front Cell Infect Microbiol* 6:38.

129. Waterman SR, Holden DW (2003) Microreview Functions and effectors of the Salmonella pathogenicity island 2 type III secretion system. *Cell Microbiol* 5(8):501–511.

130. Chakravortty D, Rohde M, Jäger L, Deiwick J, Hensel M (2005) Formation of a novel surface structure encoded by Salmonella Pathogenicity Island 2. *EMBO J* 24(11):2043–2052.

131. Westermann AJ, et al. (2016) Dual RNA-seq unveils noncoding RNA functions in host-pathogen interactions. *Nature* 529(7587):496–501.

132. Kröger C, et al. (2013) An infection-relevant transcriptomic compendium for Salmonella enterica serovar Typhimurium. *Cell Host Microbe* 14:683–695.

133. Espinosa E, Casadesús J (2014) Regulation of Salmonella enterica pathogenicity island 1 (SPI-1) by the LysR-type regulator LeuO. *Mol Microbiol* 91(6):1057–69.

134. Lee AK, Detweiler CS, Falkow S (2000) OmpR regulates the two-component system SsrA-SsrB in Salmonella pathogenicity island 2. *J Bacteriol* 182(3):771–781.

135. Friebel A, et al. (2001) SopE and SopE2 from Salmonella typhimurium Activate Different Sets of RhoGTPases of the Host Cell. *J Biol Chem* 276(36):34035–34040.

136. Sharpe LJ, Brown AJ (2013) Controlling cholesterol synthesis beyond 3-hydroxy-3-methylglutaryl-CoA reductase (HMGCR). *J Biol Chem* 288(26):18707–15.

137. Endo A (2010) A historical perspective on the discovery of statins. *Proc Jpn Acad Ser B Phys Biol Sci* 86(5):484–93.

138. Wu J-R, Gilbert DM (2000) Lovastatin arrests CHO cells between the origin decision point and the restriction point. *FEBS Lett* 484(2):108–112.

139. Jakóbisiak M, Bruno S, Skierski JS, Darzynkiewicz Z (1991) Cell cycle-specific effects of lovastatin. *Proc Natl Acad Sci* 88(9):3628–32.

140. Keyomarsi K (1996) Synchronization of mammalian cells by Lovastatin. *Methods*

Cell Sci 18(2):109–114.

141. CH C, et al. (2018) Lysosome enlargement during inhibition of the lipid kinase PIKfyve proceeds through lysosome coalescence Christopher. *J Cell Sci* 131(10):pii: jcs213587.

142. Johnson DE, Ostrowski P, Jaumouillé V, Grinstein S (2016) The position of lysosomes within the cell determines their luminal pH. *J Cell Biol* 212(6):677–92.

143. Du J, et al. (2016) The type III secretion system apparatus determines the intracellular niche of bacterial pathogens. *Proc Natl Acad Sci* 113(17):4794–4799.

144. Yan X, Ye T, Hu X, Zhao P, Wang X (2016) 58-F, a flavanone from Ophiopogon japonicus, prevents hepatocyte death by decreasing lysosomal membrane permeability. *Sci Rep* 6(May):1–15.

145. Vidoni C, Follo C, Savino M, Melone MAB, Isidoro C (2016) The Role of Cathepsin D in the Pathogenesis ofHuman Neurodegenerative Disorders. *Med Res Rev* 36(5):845–870.

146. Loos B, du Toit A, Hofmeyr J-HS (2014) Defining and measuring autophagosome flux—concept and reality. *Autophagy* 10(11):2087–96.

147. Yoshii SR, Mizushima N (2017) Monitoring and measuring autophagy. *Int J Mol Sci* 18(9):1–13.

148. Jiang P, Mizushima N (2015) LC3- and p62-based biochemical methods for the analysis of autophagy progression in mammalian cells. *Methods* 75:13–18.

149. Novus Biologicals LAMP-1/CD107a Antibody (6E2) (NBP2-25155). [Accessed December 3, 2018].

150. Pierzynska-Mach A, Janowski PA, Dobrucki JW (2014) Evaluation of acridine orange, LysoTracker Red, and quinacrine as fluorescent probes for long-term tracking of acidic vesicles. *Cytom Part A* 85(8):729–737.

151. Thomé MP, et al. (2016) Ratiometric analysis of acridine orange staining in the

study of acidic organelles and autophagy. *J Cell Sci*:jcs.195057.

152. Mauvezin C, Neufeld TP (2015) Bafilomycin A1 disrupts autophagic flux by inhibiting both V-ATPase-dependent acidification and Ca-P60A/SERCA-dependent autophagosome-lysosome fusion. *Autophagy* 11(8):1437–1438.

153. Grosz M, et al. (2014) Cytoplasmic replication of Staphylococcus aureus upon phagosomal escape triggered by phenol-soluble modulin α. *Cell Microbiol* 16(4):451–465.

154. Lam T-T, et al. (2010) Phagolysosomal integrity is generally maintained after Staphylococcus aureus invasion of nonprofessional phagocytes but is modulated by strain 6850. *Infect Immun* 78(8):3392–3393.

155. Weng IC, et al. (2018) Cytosolic galectin-3 and -8 regulate antibacterial autophagy through differential recognition of host glycans on damaged phagosomes. *Glycobiology* 28(6):392–405.

156. Paz I, et al. (2010) Galectin-3, a marker for vacuole lysis by invasive pathogens. *Cell Microbiol* 12(4):530–544.

157. Liu Q, et al. (2008) miR-16 family induces cell cycle arrest by regulating multiple cell cycle genes. *Nucleic Acids Res* 36(16):5391–5404.

158. Bueno MJ, Malumbres M (2011) MicroRNAs and the cell cycle. *Biochim Biophys Acta - Mol Basis Dis* 1812(5):592–601.

159. Lin F, et al. (2014) Decrease expression of microRNA-744 promotes cell proliferation by targeting c-Myc in human hepatocellular carcinoma. *Cancer Cell Int* 14(1):1–9.

160. Garcia-del Portillo F, Finlay BB (1995) Targeting of Salmonella typhimurium to vesicles containing lysosomal membrane glycoproteins bypasses compartments with mannose 6-phosphate receptors. *J Cell Biol* 129(1):81–97.

161. Laughlin RC, et al. (2014) Spatial Segregation of Virulence Gene Expression

during Acute Enteric Infection with Salmonella enterica serovar Typhimurium. *MBio* 5(1):1–11.

162. Simeone R, et al. (2012) Phagosomal Rupture by Mycobacterium tuberculosis Results in Toxicity and Host Cell Death. *PLoS Pathog* 8(2):e1002507.

163. van der Wel N, et al. (2007) M. tuberculosis and M. leprae Translocate from the Phagolysosome to the Cytosol in Myeloid Cells. *Cell* 129(7):1287–1298.

164. Chong A, Celli J (2010) The francisella intracellular life cycle: Toward molecular mechanisms of intracellular survival and proliferation. *Front Microbiol* 1(DEC):1–12.

165. Fredlund J, Enninga J (2014) Cytoplasmic access by intracellular bacterial pathogens. *Trends Microbiol* 22(3):128–137.

166. Moldovan A, Fraunholz MJ (2019) In or out: Phagosomal escape of Staphylococcus aureus. *Cell Microbiol* (July 2018):1–9.

167. Hansen-Wester I, Hensel M (2001) Salmonella pathogenicity islands encoding type III secretion systems. *Microbes Infect* 3(7):549–559.

168. Steele-Mortimer O, et al. (2009) Induction of Salmonella pathogenicity island 1 under different growth conditions can affect Salmonella-host cell interactions in vitro. *Microbiology* 156(4):1120–1133.

169. Lorkowski M, Felipe-López A, Danzer CA, Hansmeier N, Hensel M (2014) Salmonella enterica invasion of polarized epithelial cells is a highly cooperative effort. *Infect Immun* 82(6):2657–2667.

170. Sánchez-Romero MA, Casadesús J (2018) Contribution of SPI-1 bistability to Salmonella enterica cooperative virulence: insights from single cell analysis. *Sci Rep* 8(1):14875.

171. Carney LJ, et al. (2011) Differences in Salmonella enterica serovar Typhimurium strain invasiveness are associated with heterogeneity in SPI-1 gene expression.

Microbiology 157(7):2072–2083.

172. Ellermeier JR, Slauch JM (2007) Adaptation to the host environment: regulation of the SPI1 type III secretion system in Salmonella enterica serovar Typhimurium. *Curr Opin Microbiol* 10(1):24–29.

173. Manon R, et al. (2012) The Different Strategies Used by Salmonella to Invade Host Cells. *Salmonella - Distrib Adapt Control Meas Mol Technol*. doi:10.5772/29979.

174. Kocaturk NM, Gozuacik D (2018) Crosstalk Between Mammalian Autophagy and the Ubiquitin-Proteasome System. *Front Cell Dev Biol* 6(October):1–27.

175. Nam T, Han JH, Devkota S, Lee and HW (2017) Emerging paradigm of crosstalk between autophagy and the ubiquitin-proteasome system. *Mol Cells* 40(12):897–905.

176. Thurston TLM, Wandel MP, Von Muhlinen N, Foeglein Á, Randow F (2012) Galectin 8 targets damaged vesicles for autophagy to defend cells against bacterial invasion. *Nature* 482(7385):414–418.

177. Feeley EM, et al. (2017) Galectin-3 directs antimicrobial guanylate binding proteins to vacuoles furnished with bacterial secretion systems. *Proc Natl Acad Sci U S A* 114(9):E1698–E1706.

178. Huss M, Wieczorek H (2009) Inhibitors of V-ATPases: old and new players. *J Exp Biol* 212(3):341–346.

179. Marqueta J, et al. (1991) Bafilomycin A1, a Specific Inhibitor of Vacuolar-type H+-ATPase, Inhibits Acidification and Protein Degradation in Lysosomes of Cultured Cells. *J Biol Chem* 26(15):17707–17712.

180. Vavassori S, Mayer A (2014) A new life for an old pump: V-ATPase and neurotransmitter release. *J Cell Biol* 205(1):7–9.

181. McGuire CM, Forgac M (2018) Glucose starvation increases V-ATPase assembly

and activity in mammalian cells through AMP kinase and phosphatidylinositide 3-kinase/Akt signaling. *J Biol Chem* 293(23):9113–9123.

182. Cotter K, Stransky L, McGuire C, Forgac M (2015) Recent Insights into the Structure, Regulation, and Function of the V-ATPases. *Trends Biochem Sci* 40(10):611–622.

183. Lafourcade C, Sobo K, Kieffer-Jaquinod S, Garin J, van der Goot FG (2008) Regulation of the V-ATPase along the endocytic pathway occurs through reversible subunit association and membrane localization. *PLoS One* 3(7). doi:10.1371/journal.pone.0002758.

184. Wang D, et al. (2014) Ca^{2+}-Calmodulin regulates SNARE assembly and spontaneous neurotransmitter release via v-ATPase subunit V0a1. *J Cell Biol* 205(1):21–31.

185. Kawai A, Uchiyama H, Takano S, Nakamura N, Ohkuma S (2007) Autophagosome-lysosome fusion depends on the pH in acidic compartments in CHO cells. *Autophagy* 3(2):154–157.

186. Kissing S, et al. (2015) Vacuolar ATPase in phagosome-lysosome fusion. *J Biol Chem* 290(22):14166–14180.

187. Steele-Mortimer O, Meresse S, Gorvel JP, Toh BH, Finlay BB (1999) Biogenesis of Salmonella typhimurium-containing vacuoles in epithelial cells involves interactions with the early endocytic pathway. *Cell Microbiol* 1(1):33–49.

188. Rathman M, Sjaastad MD, Falkow S (1996) Acidification of phagosomes containing Salmonella typhimurium in murine macrophages. *Infect Immun* 64(7):2765–2773.

189. Drecktrah D, Knodler LA, Howe D, Steele-Mortimer O (2007) Salmonella trafficking is defined by continuous dynamic interactions with the endolysosomal system. *Traffic* 8(3):212–225.

190. Liss V, Hensel M (2015) Take the tube: Remodelling of the endosomal system by

intracellular Salmonella enterica. *Cell Microbiol* 17(5):639–647.

191. Boustany R-MN (2013) Lysosomal storage diseases—the horizon expands. *Nat Rev Neurol* 9(10):583–598.

192. Fraldi A, et al. (2010) Lysosomal fusion and SNARE function are impaired by cholesterol accumulation in lysosomal storage disorders. *EMBO J* 29(21):3607–3620.

193. Lu Y, et al. (2013) Two pore channel 2 (TPC2) inhibits autophagosomal-lysosomal fusion by alkalinizing lysosomal pH. *J Biol Chem* 288(33):24247–24263.

194. Seranova E, et al. (2017) Dysregulation of autophagy as a common mechanism in lysosomal storage diseases. *Essays Biochem* 61(6):733–749.

195. Schwake M, Schröder B, Saftig P (2013) Lysosomal Membrane Proteins and Their Central Role in Physiology. *Traffic* 14(7):739–748.

196. Miyagawa K, et al. (2016) Lipid-Induced Endoplasmic Reticulum Stress Impairs Selective Autophagy at the Step of Autophagosome-Lysosome Fusion in Hepatocytes. *Am J Pathol* 186(7):1861–1873.

197. Kissing S, et al. (2017) Disruption of the vacuolar-type H+-ATPase complex in liver causes MTORC1-independent accumulation of autophagic vacuoles and lysosomes. *Autophagy* 13(4):670–685.

198. Li J, Pfeffer SR (2016) Lysosomal membrane glycoproteins bind cholesterol and contribute to lysosomal cholesterol export. *Elife* 5(September2016):1–16.

199. Samie MA, Xu H (2014) Lysosomal exocytosis and lipid storage disorders. *J Lipid Res* 55(6):995–1009.

200. Yu D, et al. (2014) Niemann-pick disease type C: Induced pluripotent stem cell-derived neuronal cells for modeling neural disease and evaluating drug efficacy. *J Biomol Screen* 19(8):1164–1173.

201. Tang Y, Leao IC, Coleman EM, Broughton RS, Hildreth JEK (2009) Deficiency of

Niemann-Pick Type C-1 Protein Impairs Release of Human Immunodeficiency Virus Type 1 and Results in Gag Accumulation in Late Endosomal/Lysosomal Compartments. *J Virol* 83(16):7982–7995.

202. Coutinho MF, Prata MJ, Alves S (2012) Mannose-6-phosphate pathway: A review on its role in lysosomal function and dysfunction. *Mol Genet Metab* 105(4):542–550.

203. Marschner K, Kollmann K, Schweizer M, Braulke T, Pohl S (2011) A key enzyme in the biogenesis of lysosomes is a protease that regulates cholesterol metabolism. *Science* 333(6038):87–90.

204. Zhang X, et al. (2018) GRASP55 Senses Glucose Deprivation through O-GlcNAcylation to Promote Autophagosome-Lysosome Fusion. *Dev Cell* 45(2):245–261.e6.

205. Bekier ME, et al. (2017) Knockout of the Golgi stacking proteins GRASP55 and GRASP65 impairs Golgi structure and function. *Mol Biol Cell* 28(21):2833–2842.

206. Zhang X, Wang Y (2015) GRASPs in Golgi Structure and Function. *Front cell Dev Biol* 3(January):84.

207. Mathiassen SG, De Zio D, Cecconi F (2017) Autophagy and the Cell Cycle: A Complex Landscape. *Front Oncol* 7(March):1–16.

208. Leeman DS, et al. (2018) Lysosome activation clears aggregates and enhances quiescent neural stem cell activation during aging. *Science* 359(6381):1277–1283.

209. Azzopardi M, Farrugia G, Balzan R (2017) Cell-cycle involvement in autophagy and apoptosis in yeast. *Mech Ageing Dev* 161:211–224.

210. Neufeld TP (2012) Autophagy and cell growth - the yin and yang of nutrient responses. *J Cell Sci* 125(10):2359–2368.

211. Bond P (2016) Regulation of mTORC1 by growth factors, energy status, amino

acids and mechanical stimuli at a glance. *J Int Soc Sports Nutr* 13(1):1–11.

212. Meo-Evoli N, et al. (2015) V-ATPase: a master effector of E2F1-mediated lysosomal trafficking, mTORC1 activation and autophagy. *Oncotarget* 6(29):28057–28070.

213. Raben N, Puertollano R (2016) TFEB and TFE3: Linking Lysosomes to Cellular Adaptation to Stress. *Annu Rev Cell Dev Biol* 32(1):255–278.

214. Peña-Llopis S, et al. (2011) Regulation of TFEB and V-ATPases by mTORC1. *EMBO J* 30(16):3242–3258.

215. Kim YM, et al. (2015) MTORC1 phosphorylates UVRAG to negatively regulate autophagosome and endosome maturation. *Mol Cell* 57(2):207–218.

216. Zhou J, et al. (2013) Activation of lysosomal function in the course of autophagy via mTORC1 suppression and autophagosome-lysosome fusion. *Cell Res* 23(4):508–523.

217. Roczniak-Ferguson A, et al. (2012) The transcription factor TFEB links mTORC1 signaling to transcriptional control of lysosome homeostasis. *Sci Signal* 5(228). doi:10.1126/scisignal.2002790.

218. Pena-Llopis S, Brugarolas J (2011) TFEB A novel mTORC1 effector implicated in lysosome biogenesis, endocytosis and autophagy. *Cell Cycle* 10(23):3987–3988.

219. Lopez-Mejia IC, Lagarrigue S, Giralt A, Hardie DG (2017) CDK4 Phosphorylates AMPKα2 to Inhibit Its Activity and Repress Fatty Acid Oxidation. *Mol Cell* 68:336–349.

220. Chiabotto G, et al. (2018) TFEB controls vascular development by regulating the proliferation of endothelial cells. *EMBO J* 38(3):e98250.

221. Schneider EM, et al. (2018) MiR-744-5p inducing cell death by directly targeting HNRNPC and NFIX in ovarian cancer cells. *Sci Rep* 8(1):1–15.

222. Zhang M, Li H, Zhang Y, Li H (2019) Oncogenic miR-744 promotes prostate cancer

growth through direct targeting of LKB1. *Oncol Lett* 17(2):2257–2265.

223. Shackelford DB, Shaw RJ (2010) The LKB1-AMPK pathway: metabolism and growth control in tumor suppression. *Nat Rev Cancer* 9(8):563–575.

224. Alexander A, Walker CL (2011) The role of LKB1 and AMPK in cellular responses to stress and damage. *FEBS Lett* 585(7):952–957.

225. Singh Y, Garden OA, Lang F, Cobb BS (2015) MicroRNA-15b/16 Enhances the Induction of Regulatory T Cells by Regulating the Expression of Rictor and mTOR. *J Immunol* 195(12):5667–5677.

226. Huang N, et al. (2015) MiR-15a and miR-16 induce autophagy and enhance chemosensitivity of Camptothecin. *Cancer Biol Ther* 16(6):941–948.

227. Coombes BK, Brown NF, Valdez Y, Brumell JH, Finlay BB (2004) Expression and secretion of Salmonella pathogenicity island-2 virulence genes in response to acidification exhibit differential requirements of a functional type III secretion apparatus and SsaL. *J Biol Chem* 279(48):49804–49815.

228. Tawk CS (2017) The role of host-stress in the infection by the bacterial pathogen Shigella flexneri. Dissertation (Julius-Maximilians-Universität Würzburg).

Curriculum vitae

List of Publications

Manuscripts

Tawk, C.; Nigro, G.; Lopes, I.; Aguilar, C.; Lisowski, C.; Mano, M.; Sansonetti, P.; Vogel, J.; Eulalio, A. ***Stress-induced host membrane remodeling protects from infection by non-motile bacterial pathogens.*** EMBO J. (2018) doi 10.15252/embj.201798529

Aguilar, C[#]; Cruz, AR[#]; Maudet, C; Lopez, IR; Sunkavalli, U; Silva, RJ; Sharan, M; Lisowski, C; Zaldivar-Lopez, S; Garrido, J; Giacca, M; Mano, M; Eulalio, A. ***Functional screenings reveal different requirements for host microRNAs in Salmonella and Shigella infection.*** in revision

Lisowski, C.; Eulalio, A. ***Compromised endolysosomal trafficking during G1 arrest of host cells impairs maturation of the Salmonella containing vacuole***. in preparation

Attended conferences

3rd Mol Micro meeting 2014

07.-09.05. 2014 University of Würzburg

EUREKA - Symposium 2016

12.-13.10.2016 University of Würzburg

Talk: The role of miRNAs in host-*Salmonella* infection

Microbiology and Infection 2017

Annual Conference of the Association for General and Applied Microbiology (VAAM)

05.-08.03.2017 Würzburg

Talk: Maturation of the *Salmonella* containing vacuole depends on the host cell cycle

EUREKA - Symposium 2017

11.-12.10.2017 University of Würzburg

Poster presentation

Affidavit

I hereby confirm that my thesis entitled *Maturation of the Salmonella containing vacuole is compromised in G1 arrested cells* is the result of my own work. I did not receive any help or support from commercial consultants. All sources and/or materials applied are listed and specified in the thesis.

Furthermore, I confirm that this thesis has not yet been submitted as part of another examination process neither in identical nor in similar form.

Würzburg,

Clivia Lisowski

Eidesstattliche Erklärung

Hiermit erkläre ich an Eides statt, die Dissertation *Die Reifung der Salmonella-enthaltenden Vakuole ist kompromittiert in G1-arretiereten Wirtszellen* eigenständig, d.h. insbesondere selbständig und ohne Hilfe eines kommerziellen Promotionsberaters angefertigt und keine anderen als die von mir angegebenen Quellen und Hilfsmittel verwendet zu haben.

Ich erkläre außerdem, dass die Dissertation weder in gleicher noch in ähnlicher Form bereits in einem anderen Prüfungsverfahren vorgelegen hat.

Würzburg, den

Clivia Lisowski